Title
Computational Investigations of Pd-Catalyzed C–H Functionalization Reactions

Author
Bay, Katherine Lynn

Publication Date
2020

Peer reviewed|Thesis/dissertation

UNIVERSITY OF CALIFORNIA

Los Angeles

Computational Investigations of Pd-Catalyzed C–H Functionalization Reactions

A dissertation submitted in partial satisfaction of the requirements for the degree Doctor of Philosophy in Chemistry

by

Katherine Lynn Bay

2020

ABSTRACT OF THE DISSERTATION

Computational Investigations of Pd-Catalyzed C–H Functionalization Reactions

by

Katherine Lynn Bay

Doctor of Philosophy in Chemistry

University of California, Los Angeles, 2020

Professor Kendall N. Houk, Chair

The use of an inert C–H bond towards the generation of a functional group is advantageous, as these bonds are the most abundant chemical moieties in organic molecules. A one-step conversion of a C–H bond to the desired functionality reduces the number of synthetic steps, which in turn minimizes the use of costly reagents, solvent, and time. Selective activation of a particular C–H bond in an organic molecule where C–H bonds are ubiquitous, however, is a challenging task. Among the most challenging aspects of developing robust C–H functionalization methodologies is identifying catalyst and reagent combinations capable of site-selective as well as stereoselective reactions. Therefore, directed C–H bond functionalization using a directing group and a suitable transition metal is of current interest.

Palladium complexes are highly selective and have shown efficiency in various areas of organic synthesis, which make palladium catalysts particularly useful in the field of C–H functionalization. Palladium is incredibly powerful for the construction of carbon–carbon and carbon–heteroatom bonds by C–H activation of aryl and alkyl groups. Palladium-catalyzed ligand-directed C–H functionalization is a key goal towards the synthesis of complex multifunctional substrates.

Understanding the mechanism and origins of stereoselectivity of palladium-catalyzed C–H functionalization reactions is essential to progress this field. The collaboration between experiment and computations has provided a deeper mechanistic understanding and insight than any of the isolated techniques can provide. Kinetics and isolation of intermediates provide information on mechanistic pathways, while computations can provide details of both structures and energetics in specific steps in the whole catalytic cycle. Computations have become vital to elucidate structures of molecules, mechanisms, and selectivities of reactions. Due to the rapid development of hardware, software, and theoretical methods, computational chemistry has evolved into a very powerful and routine tool to study complex mechanisms. The work in this thesis has stemmed from several collaborations through the NSF Center for Selective C–H Functionalization (CCHF), which is comprised of synthetic methodologists, physical organic chemists, catalyst developers, enzymologists, computational chemists, and several partners in the pharmaceutical industry.

Various methods are employed in the chapters described in this dissertation. Theoretical chemical models along with quantum mechanical (QM) calculations help unravel complex chemical reactions into many components that influence chemical reactivity and selectivity. Density functional theory (DFT) is used to characterize ground state geometry, conformational analysis, transition state geometry, molecular orbitals, and reorganization energies. Each chapter of this dissertation demonstrates that QM calculations can help predict and explain the complexities of chemical phenomena involving Pd-catalyzed C–H functionalization reactions. In an effort to forge an expanding synergism between experiment and computations for the future development of C–H functionalization reactions, this work aims to:

1. Predict reaction kinetics towards catalyst speciation both on and off the catalytic cycle.
2. Unveil mechanistic details of various Pd-catalyzed C–H functionalization reactions.
3. Elucidate the origins of stereoselectivity to lend insight into future ligand and catalyst design.

Motivated by the potential of understanding C–H functionalization transformations in order to promote the development of new reactions, this thesis focuses on using computational methods to understand systems of relevance to C–H activation using palladium as a catalyst. Early projects aim to use computations to make proposed models for nonlinear effects to serve as a meaningful mechanistic probe for predicting reaction kinetics (Chapters 1-2). The second section delves into elucidating the mechanisms as well as the role of various substrates, ligands, and oxidants, particularly silver (I) acetate, on how each particular reaction is performed (Chapters 3-6). Later in this thesis, the focus diverges to highlight the elucidation of an enantioselective γ-C–H functionalization where stereoselectivity arises from attractive aryl–aryl interactions (Chapter 7).

The dissertation of Katherine Lynn Bay is approved.

Neil K. Garg

Alexander M. Spokoyny

Paula L. Diaconescu

Kendall N. Houk, Committee Chair

University of California, Los Angeles

2020

Table of Contents

List of Schemes

List of Figures

List of Tables

Acknowledgements

I must first thank my PhD advisor, Professor Kendall N. Houk. Over the last four years, he has steadily guided my research projects, through which I have learned an immense amount. He is an advisor from and with whom I have learned, and I am grateful for all the times when we would sit down and think through problems together. I am thankful to forever be a Houkie and to help push back the frontiers of science.

I would also like to acknowledge the professors who comprise my thesis committee. Professor Neil Garg for not only being one of my first research advisors at UCLA but for also giving me professional advice as I begin my independent career in academia. The rotation during fall quarter of my first year was difficult but I thank the members of the Garg lab who graciously welcomed me, taught me, and challenged me during that time. Professor Paula Diaconescu and her class on organometallic chemistry was a huge part of my decision to invest my PhD in researching Pd-catalyzed C–H activation reactions. Professor Alex Spokoyny has been an excellent collaborator with whom I have enjoyed lively discussions of his boron cluster degradation pathways with him and his students. I thank these committee members for the part that they each played in the creation of this dissertation.

My mentors throughout my undergraduate career have played integral roles in helping me decide to pursue a PhD in chemistry. Dr. Iraj Parchamazad who not only opened my eyes to the beauty of organic chemistry, but also entrusted me with a research project early in my undergraduate career. Dr. Ricardo Morales, one of the best chemistry professors I had during my time at the University of La Verne, who showed me by example what hard work looks like, and always bore a smile and encouraging words when I did not know which career path to take. Professor William Jenks from Iowa State University who took me under his wing to teach me the ins and outs of organic synthesis. Dr. Jagadeesh Kolattor who walked side-by-side with me to get anhydrous solvent, run EPR's, and how to setup my first column. Professor Brian Stoltz from

Caltech, a mentor who was a huge inspiration to me to pursue a PhD. After several meetings in his office outlining the pros and cons of pharmacy school vs a PhD in chemistry, he played a major role in my decision to go to graduate school. Dr. Seojung Han, a mentor who took me under her wing and taught me not only science but also the trials and tribulations of graduate life. Professor Matthew Gaunt and Dr. Aaron Trowbridge from the University of Cambridge, mentors who challenged me with hard questions, putting me at the board to explain concepts to them, and never letting me slide by.

The older lab members in the Houk group welcomed me with lots of laughter, sarcasm, and advice. Dr. Yun-Fang Yang, whose work laid the foundation of much of this thesis, was my mentor who taught me from the beginning through each command line and the setup of each calculation. She has always served in my mind as a vision of a strong female scientist who not only can publish in amazing journals but also who is an amazing mother to two beautiful daughters. I am thankful for her invitation of allowing me to give a research talk to her newly established group of mostly female graduate students at Zhejiang University in Hangzhou, China – she will always be an inspiration to me. Dr. Xiangyang Chen who has been the best co-worker in helping me solve difficult chemical puzzles throughout various project collaborations. My friends who comprise of the BB-D3 gang: Dr. Marc Garcia Borràs who is a great encourager and coffee mate, Dr. Jason Fell who never ceased to miss a coffee break opportunity, Dr. Adam Simon for being the machine learning expert and who always had an answer to my many chemistry questions, and Kersti Caddell Haatveit who has been a great friend and conference buddy throughout the PhD program.

The Bobo Gang friends who I began and continue this journey with: Gina Lee and Monica Pengshung. We have shared an apartment where our three lives that meshed into one all the way in the San Fernando Valley. Gina, my kind-hearted friend and lab mate who would get a boba with me way too many times to count throughout each week. I am grateful that throughout the years, we have been aligned in our ideologies and have kept each other

grounded through thick and thin. Monica, my number one homie for life who has made me laugh and has been such a huge supporter of mine throughout graduate school. Both coming from similar backgrounds, I will always remember our heart-to-heart conversations during our long, traffic-filled commute with fondness. Gina and Monica have been my forever study partners, listening to Disney music as we slogged through our problem sets during our first year of graduate school together. I definitely would not have gotten through it all if it was not for their relentless encouragement. Marcus Jellen, honorary Bobo Gang member, who is a walking encyclopedia of all MOF-, gear-, and macrocycle-related chemistry, and has been a very supportive friend since the beginning.

My undergraduate friends who have stuck by my side since day one – thank you. Nicole Miller, a friend with whom I can never stop laughing but can also share my deepest thoughts and conversations. If chemistry was a touring band group, she'd be in the front row of my every concert. Jamie Sato, a friend who is so many things, wholehearted supporter, sage in life, keeps me grounded, and a reminder of all things important going on in my life.

To my amazing high school friends – Joanna Liao, Ellison Chen, Connie Chen, and Sally Chung. From being fresh-faced teenagers a part of Destination Imagination to tackling all the ins and outs of adulthood, we have been through so many chapters of life together. Through countless brunch gatherings over the years, they all have inspired me to reach any seemingly unattainable goal without ever looking back and for that, thank you.

My brother Joshua whose drive and desire to be creative has inspired me. My mother and father, each of whom are different in every single way, but each who has helped shape the person I am today. Mom, from mother to close friend, who over the years I have traveled around the world with and am grateful for all of the amazing experiences we've shared. Dad, who has always taught me to be at peace, to not worry, and to venture outside normality. To my two dogs – Nugget and Bugsy. Thank you for bringing me unconditional love and licks every day.

Lastly, I would like to thank my boyfriend Corey Whitt who has unwaveringly supported me each and every day. He has been my soundboard for much of my graduate school experience and has always been my number one fan. Corey has supported my goal of striving to invest in the next generation of scientists that hopefully will comprise of all walks of life and colors. And he has also shared his family with me, who I love just as much as my own, and I am incredibly thankful for. Jo, Jason, Karlye, and Miles – thank you for being supportive of my work.

To everyone mentioned herein: thank you so incredibly much. Words cannot express how grateful I am.

Chapter 1 is a modified version of the publication "Dynamic Ligand Exchange as a Mechanistic Probe in Pd-Catalyzed Enantioselective C–H Functionalization Reactions Using Monoprotected Amino Acid Ligands." Hill, D. E.; Bay, K. L.; Yang, Y.-F.; Plata, R. E.; Takise, R.; Houk, K. N.; Yu, J.-Q.; Blackmond, D. G. *J. Am. Chem. Soc.* **2017**, *139*, 18500–18503. This is a collaboration with Prof. Jin-Quan Yu and Prof. Donna Blackmond from The Scripps Research Institute (TSRI). David Hill led the kinetic experiments with the assistance of Dr. Erik Plata and Ryo Takise. Dr. Yun-Fang Yang and I performed extensive calculations using DFT and carried out the analysis for this work.

Chapter 2 is a modified version of the manuscript "Probing Catalyst Speciation in Palladium-MPAAM-Catalyzed Enantioselective C(sp_3)–H Arylation of Cyclopropanecarboxylic Acids: Catalyst Improvement via Destabilization of Off-Cycle Species" which is undergoing submission. This work was based off of the synthetic methodology developed by Zhe Zhuang from the group of Prof. Jin-Quan Yu. Dr. Wei Hao and David Hill from the group of Prof. Donna Blackmond performed the kinetic experiments and modeling. Daniel King and I performed the DFT calculations in this chapter. Dr. Caleb Harris and Ilia Guzei from the group of Prof. John Berry obtained the crystal structures of the palladacycles of interest.

Chapter 3 is a modified version of the publication "Multiple Roles of Silver Salts in Palladium-Catalyzed C–H Activations." Bay, K. L.; Yang, Y.-F.; Houk, K. N. *J. Organomet.*

Chem. **2018**, *864*, 19–25. This is an invited contribution to a special issue “Modern Computational Organometallic Chemistry”. After our group’s discovery of a heterodimeric Pd–Ag CMD transition state model, there has been debate over whether the Pd or Ag species is responsible for C–H functionalization. The various roles of Ag(I) salts in Pd-catalyzed C–H activation are highlighted in this mini-review

Chapter 4 is a modified version of the publication “Rational Development of Remote C–H Functionalization of Biphenyl: Experimental and Computational Studies.” Fan, Z.[‖]; Bay, K. L.[‖]; Chen, X.; Zhuang, Z.; Park, H. S.; Yeung, K.-S.; Houk, K. N.; Yu, J.-Q. *Angew. Chem. Int. Ed.* **2020**, *59*, 4770–4777. [Hot paper] [‖]Authors contributed equally. This is a collaboration with the Yu group from TSRI. Dr. Zhoulong Fan developed the methodology while Zhe Zhuang, Han Seul Park, and Kap-Sun Yeung assisted with expanding the substrate scope. Dr. Xiangyang Chen and I performed all DFT calculations described in this chapter.

Chapter 5 is a modified version of the publication “Differentiation and Functionalization of Remote C–H Bonds in Adjacent Positions.” Shi, H.; Lu, Y.; Weng, J.; Bay, K. L.; Chen, X.; Tanaka, K.; Verma, P.; Houk, K. N.; Yu, J.-Q. *Nature Chemistry* **2020**, *12*, 399–404. This is a collaboration with the Yu group from TSRI. Dr. Hang Shi and Dr. Yi Lu developed the remote site-selective arylation of benzoazines. Dr. Hang Shi, Dr. Yi Lu, Dr. Jiang Weng, and Dr. Keita Tanaka prepared the Pd templates and reaction substrates. Pritha Verma calculated the initial Fukui indices of quinoline and isoquinoline. Dr. Xiangyang Chen and I performed all DFT calculations to determine the mechanistic pathway of this reaction.

Chapter 6 is modified version of the manuscript “Cyclization by C(sp_3)–H Functionalization with a Transient Directing Group,” which is undergoing submission. This is a collaboration with the group of Jin-Quan Yu from TSRI and the group of Prof. Erik Sorensen from Princeton University. Phillip Provencher performed all of the experiments to develop the methodology. I performed the DFT calculations for the mechanistic pathway in this chapter.

Chapter 7 is a modified version of the publication “Computational Exploration of a Pd(II)-Catalyzed γ-C–H Arylation Where Stereoselectivity Arises from Attractive Aryl–Aryl Interactions.” Bay, K. L.; Yang, Y.-F.; Houk, K. N. *J. Org. Chem.* **2018**, *83*, 14786–14790. I performed the DFT calculations and Dr. Yun-Fang Yang provided valuable discussion for this project.

I am grateful for the support of the Saul and Sylvia Winstein Dissertation Award for the completion of this dissertation.

Vita

Education

University of California, Los Angeles
Ph.D. Candidate 09/2018
University of La Verne
B.S. Chemistry 06/2016
Cum Laude, with Honors citation

Teaching

Graduate Teaching Assistantships: Chemistry and Biochemistry Department, UCLA (Fall 2016 – present)

- Courses taught: CHEM14B (1 quarter), CHEM14C (2 quarters), CHEM14D (1 quarter)

Academic Tutor: Academic Success Center, University of La Verne (Fall 2013-Spring 2016)

- Subjects tutored: chemistry, writing

Undergraduate Teaching Assistantships: Department of Chemistry, University of La Verne (Fall 2013-Spring 2016)

- Course taught: General Chemistry Laboratory I and II (2 semesters), Organic Chemistry Laboratory I and II (4 semesters)

Publications

1. Hill, D. E.; **Bay, K. L.**; Yang, Y.-F.; Plata, R. E.; Takise, R.; Houk, K. N.; Yu, J.-Q.; Blackmond, D. G. "Dynamic Ligand Exchange as a Mechanistic Probe in Pd-Catalyzed Enantioselective C–H Functionalization Reactions Using Monoprotected Amino Acid Ligands," *J. Am. Chem. Soc.* **2017**, *139*, 18500–18503.
2. **Bay, K. L.**; Yang, Y.-F.; Houk, K. N. "Multiple roles of silver salts in palladium-catalyzed C–H activations," *J. Organomet. Chem.* **2018**, *864*, 19–25.
3. **Bay, K. L.**; Yang, Y.-F.; Houk, K. N. "The Stereoselectivity of a Pd(II)-Catalyzed γ-C–H Arylation of Picolinamides with BINOL Phosphate Ligands Arises from Attractive Aryl–Aryl Interactions," *J. Org. Chem.* **2018**, *83*, 14786–14790.
4. Lee, G. L.‖; **Bay, K. L.**‖; Houk, K. N. "Evaluation of DFT Methods and Implicit Solvent Models for Anion-Binding Host-Guest Systems," *Helv. Chim. Acta* **2019**, *102*, e1900032. ‖Authors contributed equally.
5. Mu, X.; Axtell, J. C.; Bernier, N. A.; Kirlikovali, K. O.; Jung, D.; Umanzor, A.; Qian, K.; Chen, X.; **Bay, K. L.**; Kirollos, M.; Rheingold, A. L.; Houk, K. N.; Spokoyny, A. M. "Sterically Unprotected Nucleophilic Boron Reagents," *Chem* **2019**, *5* 2461–2469.
6. Fan, Z.‖; **Bay, K. L.**‖; Chen, X.; Zhuang, Z.; Park, H. S.; Houk, K. N.; Yu, J.-Q. "Rational Development of Remote C–H Functionalization of Biphenyl: Experimental and Computational Studies," *Angew. Chem. Int. Ed.* **2020**, *59*, 4770–4777. [Hot paper] Authors contributed equally.
7. Shi, H.; Lu, Y.; Weng, J.; **Bay, K. L.**; Chen, X.; Tanaka, K.; Verma, P.; Houk, K. N.; Yu, J.-Q. "Differentiation and Functionalization of Adjacent, Remote C–H Bonds," *Nature Chemistry* **2020**, 1*2*, 399–404.

8. Kiel, G. R.; **Bay, K. L.**; Samkian, A. E.; Schuster, N. J.; Lin, J. B.; Handford, R. C.; Nuckolls, C.; Houk, K. N.; Tilley, T. D. “Expanded Helicenes as Synthons for Chiral Macrocyclic Nanocarbons,” *J. Am. Chem. Soc.* **2020**, Just accepted.
9. Ding, , W.-Y.; Yu, P.; An, Q.-J.; **Bay, K. L.**; Xiang, S.-H.; Li, S.; Chen, Y.; Houk, K. N.; Tan, B. "DFT-guided phosphoric acid-catalyzed atroposelective arene functionalization of nitrosonaphthalene," *Chem* **2020**, Just accepted.
10. Provencher, P.; **Bay, K. L.**; Houk, K. N.; Yu, J.-Q. Sorensen, E. “[3+2] Cyclization by Double C(sp_3)–H Functionalization with a Transient Directing Group,” In review.
11. Hao, W.; **Bay, K. L.**; King, D. S.; Plata, R. E.; Harris, C. F.; Hill, D. E.; Berry, J. F.; Yu, J.-Q.; Houk, K. N.; Blackmond, D. G. “Catalyst Speciation in Enantioselective C(sp_3)-H Functionalization Reactions With Monoprotected Aminoethyl Amine and Thioether Ligands,” In preparation.

Select Presentations

- Fan, Z.; **Bay, K. L**.; Chen, X.; Zhuang, Z.; Park, H. S.; Houk, K. N.; Yu, J.-Q. “Experimental and Computational Studies on Ligand-Enabled Nitrile-Directed Remote C–H Functionalizations of 2-Cyanobiphenyls.” Zhejiang University, Hangzhou, China, Aug. 24, 2019. (invited, oral)
- **Bay, K. L.**; Houk, K. N. “Differentiation and Functionalization of Remote, Adjacent C–H Bonds.” IBS, ITbM, NSF-CCHF Joint Summer Workshop at Korea Advanced Institute of Science and Technology (KAIST), Daejeon, South Korea, July 11, 2019. (oral)
- **Bay, K. L.**; Houk, K. N. “Computational Exploration of Pd-Catalyzed C–H Activation Reactions,” Seoul National University, Seoul, South Korea, July 10, 2019. (oral)
- **Bay, K. L.**; Houk, K. N. “Computational Exploration of Pd-Catalyzed C–H Activation Reactions,” Nagoya University, Nagoya, Japan, July 2, 2019. (oral)
- Lee, G. L.; **Bay, K. L.**; Houk, K. N. “Evaluations of DFT Methods and Implicit Solvation Models for Anion-Binding Host-Guest Systems,” SoCal Theoretical Chemistry Conference, University of Southern California (USC), Los Angeles, CA, May 18, 2019. (poster)
- **Bay, K. L.**; Houk, K. N. “The Stereoselectivity of a Pd(II)-Catalyzed γ-C–H Arylation of Picolinamides with BINOL Phosphate Ligands Arises from Attractive Aryl–Aryl Interactions,” University of La Verne, La Verne, CA, Nov. 5, 2018. (oral, invited)
- Hao, W.; **Bay, K. L.**; King, D. S.; Plata, R. E.; Harris, C. F.; Hill, D. E.; Berry, J. F.; Yu, J.-Q.; Houk, K. N.; Blackmond, D. G. “Catalyst Speciation in Enantioselective C(sp_3)-H Functionalization Reactions With Monoprotected Aminoethyl Amine and Thioether Ligands,” Emory University, Atlanta, GA, Sept. 20, 2018. (oral)
- **Bay, K. L.**; Yang, Y.-F.; Houk, K. N. “Origins of Reactivities and Enantioselectivities of Pd(II)-Catalyzed α-C–H Arylation of Thioamides,” ACS National Meeting, Boston, MA, Aug. 22, 2018. (oral)
- **Bay, K. L**.; Yang, Y.-F.; Houk, K. N. “Origins of Enantioselectivities of Pd(II)-Catalyzed α-C–H Arylation of Thioamides,” Stereoselectivity Gordon Research Conference, Newport, RI, July 24, 2018. (poster)
- **Bay, K. L.**; Yang, Y.-F.; Houk, K. N. “Origins of Reactivities and Enantioselectivities of Pd(II)-Catalyzed α-C–H Arylation of Thioamides,” Emory University, Atlanta, GA, Jan. 10, 2018. (oral)

Chapter 1. Dynamic Ligand Exchange as a Mechanistic Probe in Pd-Catalyzed Enantioselective C–H Functionalization Reactions Using Monoprotected Amino Acid Ligands

1.1 Abstract

A new tool for probing enantioselective reaction mechanisms is introduced. Monitoring the temporal change in product enantiomeric excess after addition of the opposite enantiomer of the ligand during reaction provides a means of probing dynamic ligand exchange in enantioselective C–H iodination catalyzed by Pd with monoprotected amino acid ligands (MPAA). This work has general potential for providing insights about the dynamics of catalyst and ligand molecularity and exchange.

1.2 Introduction

Pd-catalyzed C–H functionalizations employing mono-protected amino acid (MPAA) ligands have emerged as a powerful class of reactions that provide striking ligand-accelerated catalysis, and, in cases of prochiral substrates, highly enantioselective transformations.[1] Both experimental[2] and computational[3] mechanistic studies have contributed to our understanding of these reaction systems, invoking weak coordination of substrates and ligands to Pd. It has been shown that MPAA-ligated Pd catalysts exhibit significant rate accelerations over non-ligated Pd.[1] Most recently, a novel role for Pd(IV) in enantioselective iodination was uncovered in the highly selective desymmetrization of diarylmethylamines via iodination catalyzed by Pd(MPAA) (Scheme 1.1).[2c,4]

Scheme 1.1. Iodination of Diarylmethylamines.

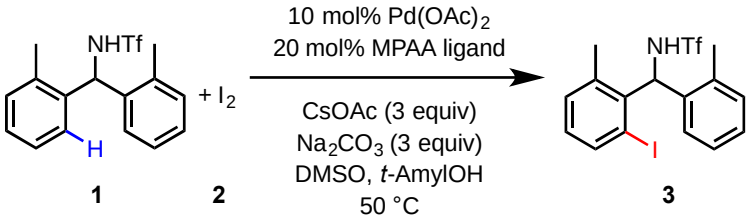

In the present study, we show how temporal monitoring of product enantioselectivity may be employed as a probe of dynamic ligand exchange in reactions where the opposite hand of the MPAA ligand is introduced as the reaction proceeds. Understanding the capability of the chiral ligand to undergo exchange with different Pd species along the catalytic cycle provides a new tool that uses the reaction itself to probe and report on enantioselective reaction mechanisms.

1.3 Results and Discussion

Our initial studies followed the optimized system developed by Yu and coworkers,[4c] employing benzoyl-protected leucine Bz-Leu-OH as the MPAA ligand. We found that this ligand reacts to produce palladacycle **4** upon mixing with $Pd(OAc)_2$.[2c] Species **4** is an inert precatalyst that is rapidly iodinated to produce **5** upon exposure to the reaction conditions of Scheme 1. Complex **6** was synthesized as an analogous catalyst so that the reaction could be followed by ^{19}F NMR spectroscopy. All three Pd species produce competent catalysts and give similar kinetic profiles in the reaction of Scheme 1.1. Interestingly, however, we found that none of the species **4**-**6** interacts with substrate **1** in the absence of I_2.[2c] This observation led to ^{19}F-NMR spectroscopic studies as well as electrochemical investigations that implicate a Pd(IV) species **7**, formed from oxidative addition of I_2 to **6**, in the catalytic cycle prior to addition of the diarylmethylamine substrate.

Scheme 1.2. Palladacycles of Interest for C–H Iodination.

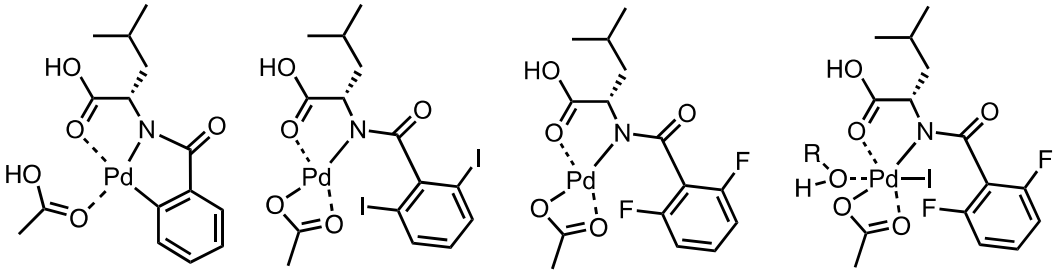

Figure 1.1 shows that nearly identical rates are observed for Pd:ligand ratios from 1:1.25 to 1:4 in the reaction of Scheme 1.1. In addition, the reaction exhibits first order kinetics in $[Pd]_{2c}$ and no nonlinear effect in ligand enantiomeric excess (Figure 1.2). Together these observations suggest that the active catalyst is a monomeric Pd(MPAA) species and that neither higher order Pd species nor Pd species with multiple ligands exist either on or off the catalytic cycle.[5]

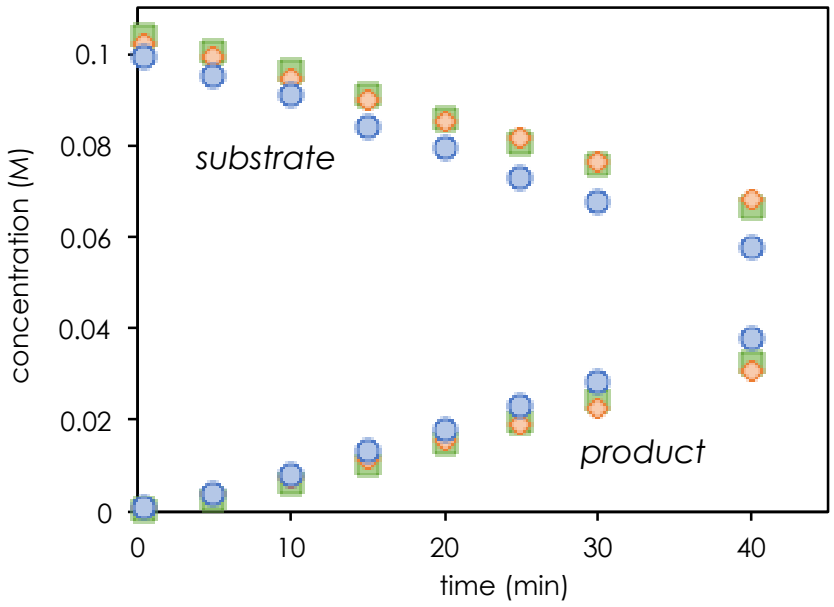

Figure 1.1. Temporal product formation and substrate consumption. Carried out using 10 mol% $Pd(OAc)_2$ Bz-Leu-OH ligand at Pd:L ratios of 1:1.25 (green squares), 1:2 (orange diamonds) 1:4 (blue circles). $[1]_0$= 0.1 M; $[2]_0$=0.3 M; 3 equiv. CsOAc, 3 equiv. Na_2CO_3 in DMSO/t-Amyl-OH at 50_0C.

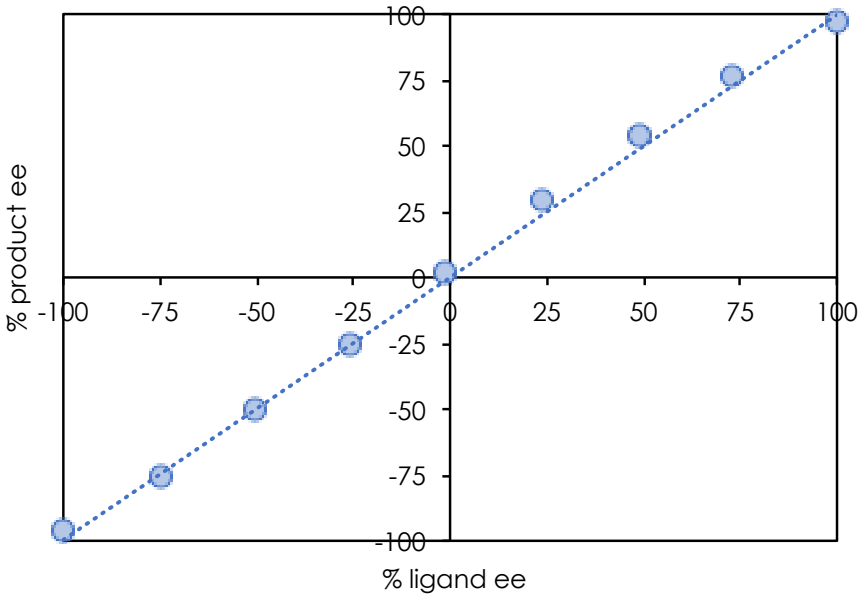

Figure 1.2. Product %*ee* vs. ligand %*ee*. Carried out using 10 mol% $Pd(OAc)_2$ and 20 mol% Bz-Leu-OH ligand. $[1]_0$= 0.1 M; $[2]_0$=0.3 M; 3 equiv. CsOAc, 3 equiv. Na_2CO_3 in DMSO/t-Amyl-OH at 50ºC.

We aimed to study the dynamic behavior of the chiral ligands in this reaction network by spectroscopic characterization as well as using the reaction itself as a probe. To accomplish the latter, we devised a ligand addition protocol in which we injected the ligand of the opposite chirality into a running reaction after ca. 10% conversion. Because the results in Figs. 1.1 and 1.2 confirm that monomeric Pd(MPAA) catalysts operate independently from one another in the cycle, we may monitor any temporal change in enantiomeric excess to evaluate whether and how rapidly the ligands exchange (eq. 1), where $K_{eq} = k_{on}/k_{off} = 1$.

$$Pd(MPAA)_D + (MPAA)_L \underset{k_{off}}{\overset{k_{on}}{\rightleftharpoons}} Pd(MPAA)_L + (MPAA)_D \quad (1)$$

Ligand exchange reactions were initiated using $Pd(OAc)_2$ and the D-Bz-Leu-OH ligand in a 1:1 ratio, which is immediately converted to catalyst D-**5**.[2c] The reaction of Scheme 1.1 was then allowed to proceed for 20 minutes, or to ca. 10% conversion (ca. 1 turnover), before addition of 1, 2, or 4 equivalents of ligand of the opposite chirality, L-Bz-Leu-OH. An aliquot

taken from the reaction mixture established product ee and conversion just prior to addition of the opposite ligand. Both *e.e.* and conversion were monitored for a further 40 minutes, or ca. 4 further turnovers.

Figure 1.3 shows the results of these experiments plotted as incremental product *e.e.* vs. % conversion. "Incremental *e.e*." is defined as the enantiomeric excess of product molecules formed in an interval between two conversion points, which provides a measure of the instantaneous behavior of the catalyst by removing the cumulative effect on *e.e.* of product already present in the reaction mixture from earlier reaction times. The dashed horizontal lines in Figure 1.3 show the expected product *e.e*. for a fully equilibrated Pd/ligand mixture in the three cases, 60% *e.e*. for D:L=1:4 (red), 33% for D:L=1:2 (blue) and racemic for D:L=1:1 (green). These data show that immediately upon introduction of the opposite hand of the ligand, product ee in the reaction of Scheme 1.1 begins to reflect its presence, and the system appears to be fully equilibrated within two further turnovers of the catalytic cycle.

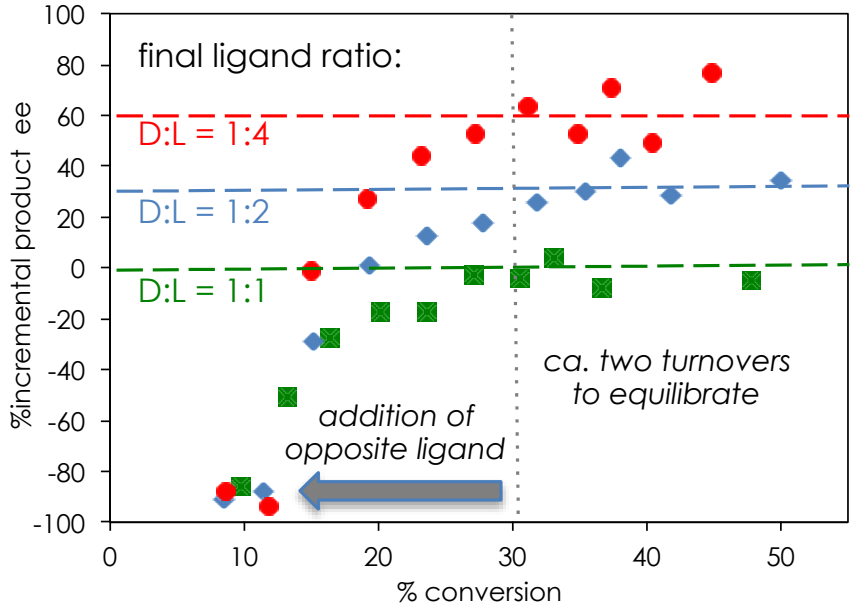

Figure 1.3. Incremental product %ee vs. conversion for the reaction. Carried out using 10 mol% $Pd(OAc)_2$. Reactions initiated with 1 equiv. D-Bz-Leu-OH ligand, with L-Bz-Leu-OH added at ca. 10% conversion to give the ligand enantiomeric ratios shown in the graph. $[1]_0$= 0.1 M;

$[2]_0$=0.3 M. 3 equiv. CsOAc, 3 equiv. Na_2CO_3 in DMSO/t-Amyl-OH at 50_oC. Horizontal lines show product ee values expected from fully equilibrated mixtures of ligands.

Based on the reaction kinetics in Figure 1.1 coupled with simulations of the reaction of eq 1, we may estimate the value of k_{on} and k_{off} to be ca. 0.1 $M^{-1}s^{-1}$.[6] This indicates a relatively rapid exchange mechanism between Pd and ligand on the time scale of the catalytic reaction. The reaction's instantaneous selectivity thus provides an excellent reporter of this ligand exchange.

Figure 1.4 showing ^{19}F NMR of Pd(MPAA) catalysts with the 2,6-difluorobenzoyl protecting group reveals a shift in the Pd-bound ligand as increasing amounts of iodine are added to the system. In accordance with our previous studies, this suggests that the catalytic species shifts from **6** in the absence of iodine to predominantly **7** under catalytic concentrations of I_2. The two peaks corresponding to diastereotopic F atoms are shifted closer in **7**, suggesting more rapid exchange or less hindered rotation in **7** compared to **6**.

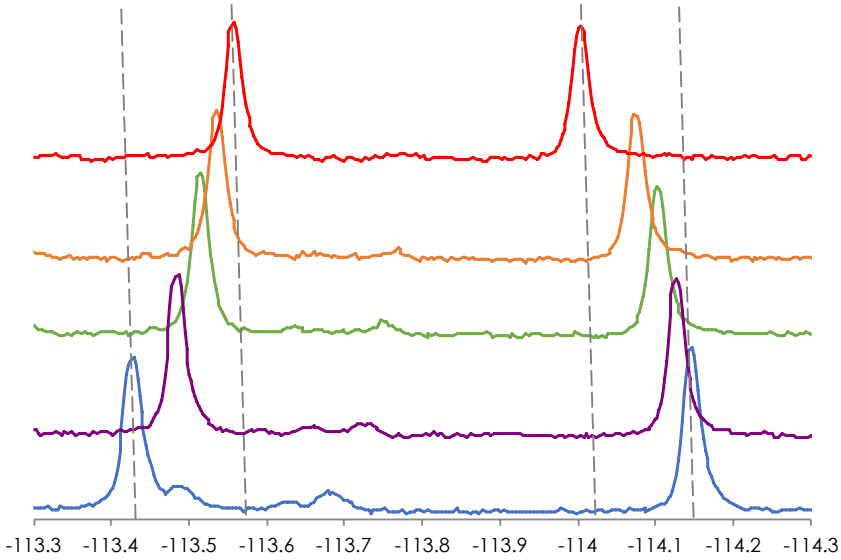

Figure 1.4. ^{19}F NMR spectra of $Pd(OAc)_2$ and the 2,6-difluoro Bz-Leu-OH ligand. Shown at Pd:L = 2:1 and 30 equiv. CsOAc with increasing amounts of I_2. blue: no I_2; purple: 0.05 M I_2; green: 0.10 M I_2; orange: 0.16 M I_2; red: 0.33 M I_2. Spectra acquired after heating to 50 $_oC$ in d_6-DMSO/t-Amyl-OH.

A key question to address is the nature of the species in the active catalytic cycle that are implicated in this ligand exchange. Dissociation of ligand from Pd(II) species **5** or **6** could occur at the close of each turnover in the cycle. Ligand exchange might occur via dissociation of ligand from a Pd(IV) species, either **7** or the subsequent species formed from binding to substrate **1**, both of which were implicated as resting states in the cycle from the observation of saturation kinetics in [**1**].[2c] We employed ^{19}F NMR spectra to monitor exchange between species **5** and **6** and between species **7** and its diiodo counterpart **8**, as shown in Scheme 1.2.

Scheme 1.3. Proposed MPAA Ligand Exchange from Either Pd(II) or Pd(IV) Species.

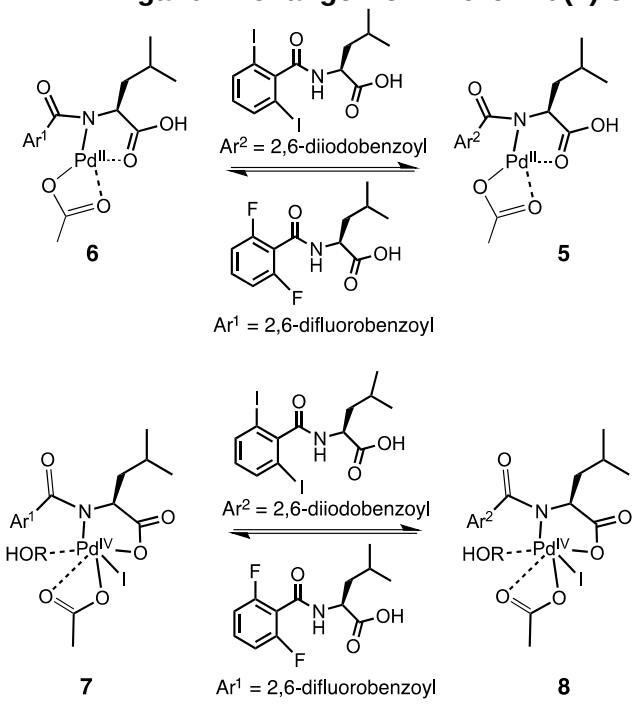

Figure 1.5 plots the time evolution of the PdL species **5** and **7** as the difluorobenzoyl ligand exchanges with the diiodobenzoyl ligand in the processes shown in Scheme 1.2. The results are in good agreement with the estimated chiral ligand exchange rates from the reaction results in Figure 1.3. Further, the difference in the time courses support the suggestion from the NMR shifts in Figure 1.5 that ligand exchange is more rapid between species **7** and **8** than between **5** and **6**.

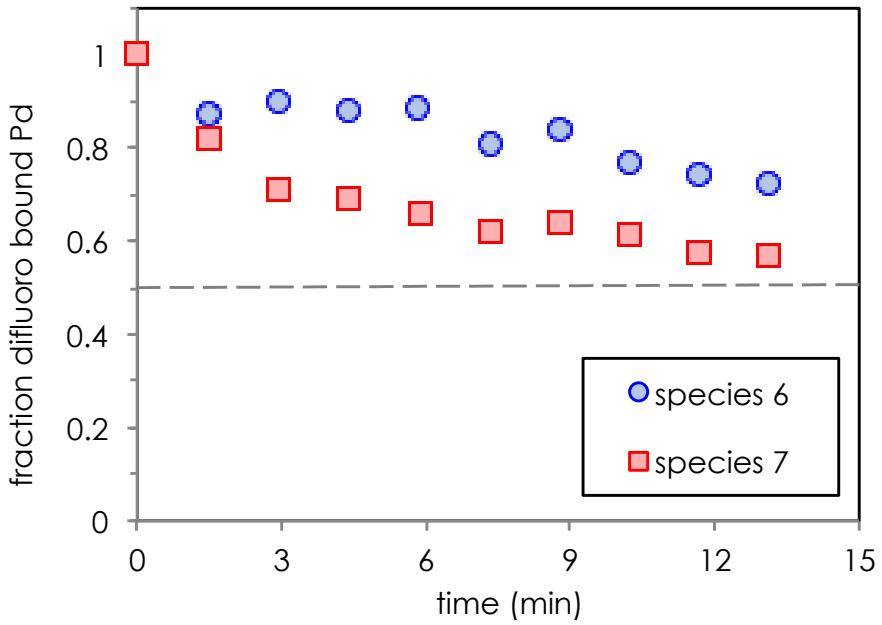

Figure 1.5. Plotted time evolution of PdL during ligand exchange. Fraction of PdL species with MPAA system containing the substituted benzoyl protecting group (Ar_1 = 2,6 difluorobenzoyl) over time after exchange with the substituted benzoyl protecting group (Ar_2 = 2,6 diiodobenzoyl) as monitored by ^{19}F NMR spectroscopy. Initial Pd:L (with Ar_1) = 1:1; 1 equiv. ligand (with Ar_2) added at t=0. 30 equiv. CsOAc in d_6-DMSO/t-Amyl-OH at 50 ^{o}C.

The observation of rapid exchange of ligands on and off the Pd center in the catalyst both during the working catalyst cycle as well as at rest is all the more striking given the high enantiomeric excess values achievable in this reaction. This result reiterates the power of ligand-accelerated catalysis in this system, since high ee indicates that the reaction appears to be completely shut down in the "ligand off" state. It also suggests that probing the dynamics of exchange between enantiomeric ligands by temporal monitoring of product enantiomeric excess may be used as a tool for future catalyst design and mechanistic evaluation. Systems exhibiting facile ligand exchange coupled with high enantiomeric excess are good candidates for successful ligand-accelerated asymmetric catalysis. Understanding which species on the

catalytic cycle are capable of undergoing ligand exchange may add support to a proposed reaction mechanism and may aid in future catalyst design.

Calculations provide support for the mechanistic details of ligand exchange proposed from the experimental data. All the calculations were carried out with the Gaussian 09 package.[7] Geometry optimizations were performed with B3LYP. [8,9,10,11] The LANL2DZ +f (1.472) basis set with ECP was used for Pd and I, and the 6-31G(d) basis set was used for other atoms.[12,13,14,15,16,17] Frequency analysis was conducted at the same level of theory to verify the stationary points to be minima or saddle points. The single-point energies were computed with M06 /SDD -6-311+G(d,p) basis sets.[18,19,20] The relative energies with ZPE corrections and free energies (at 298.15K) are in kcal/mol. Conformational searches were performed for each intermediate and transition state structure. Computed structures are illustrated using CYLView.[21]

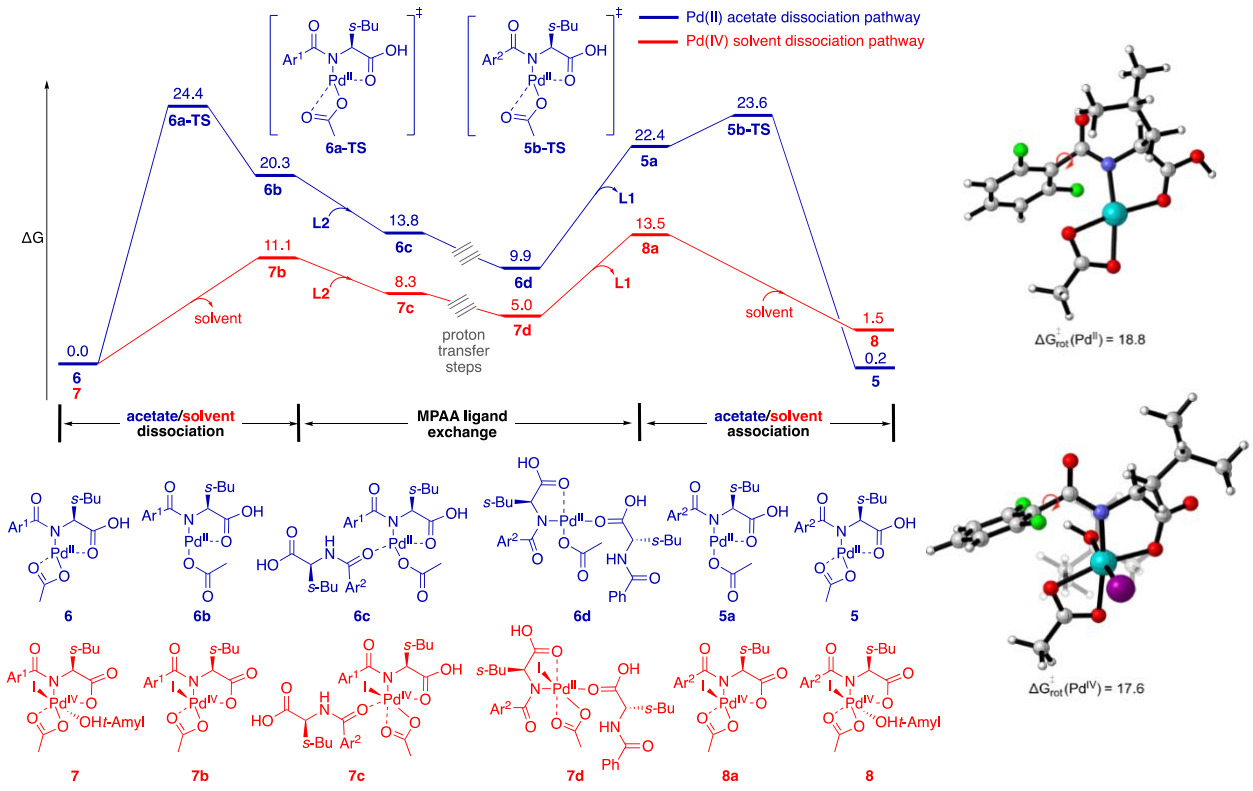

Figure 1.6. Free energy profile for dissociative MPAA ligand exchange. The Pd(II) acetate dissociation pathway is shown in blue, and the Pd(IV) solvent dissociation pathway is shown in

red. M06/SDD(Pd,I)-6-311++G(d,p) energies are reported as ΔG in kcal/mol; Transition states and energy barriers of rotation of the aryl group on the benzoyl protecting group for complex 5 and 6. Activation free energies are given in kcal/mol.

Figure 1.6 investigates the reaction coordinate for exchange between difluoro and diiodo ligands for Pd(II) and Pd(IV). Protonation/deprotonation steps are not calculated due to uncertainties in the mechanism, which could proceed through number of different possible routes including both inter- and intramolecular bases. Assuming that protonation/deprotonation steps are not rate-determining, the results reveal that the Pd(IV) pathway (species **7** to species **8**) is more favorable than the Pd(II) (species **6** to species **5**). Figure 1.6b reveals that the energy barrier for rotation of the aryl group of the difluoro ligand for the Pd(II) species **6** is 1.2 kcal/mol higher than that for the Pd(IV) species **7**. Both computational results are in accord with the experimental NMR data of Figures 1.4 and 1.5.

Scheme 1.4. Pd(IV) Acetate Dissociation Pathway.

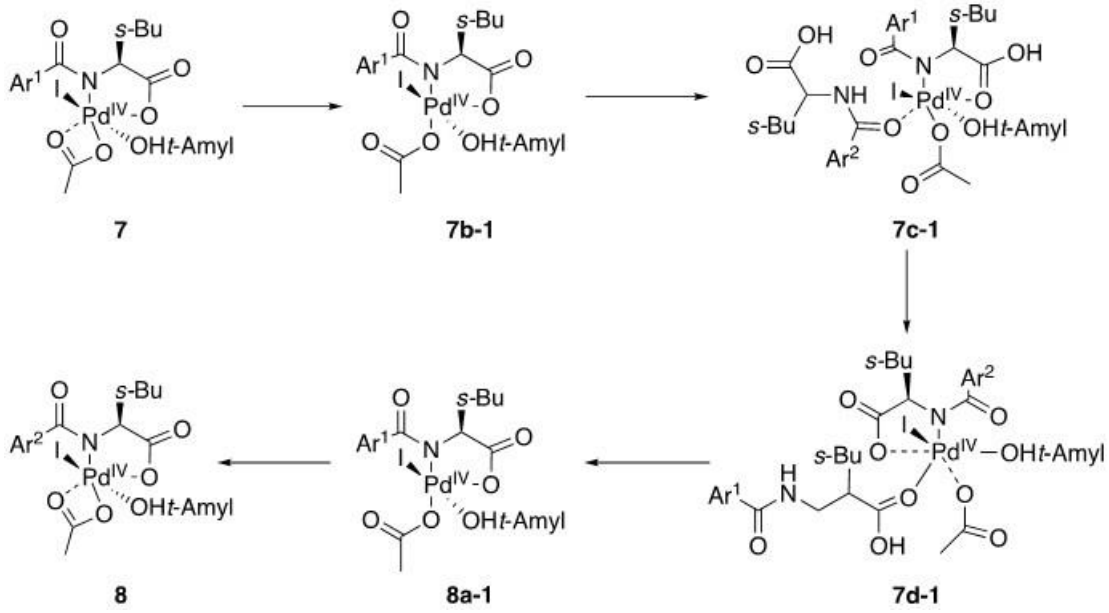

To ensure that the Pd(IV) solvent dissociation pathway was the most energetically favorable, we compared it to the Pd(IV) acetate dissociation pathway, shown in Scheme 1.4. The free energy profile of the Pd(IV) acetate dissociative pathway is shown in Figure 1.7. The

acetate ligand of the Pd(Iv) species **7** dissociates to form a 16 e- Pd complex (**7b-1**). Note that a transition state structure was unable to found, rendering this step barrierless in the pathway. Association of **L2** increased the free energy of **7c-1** to 30.9 kcal mol^{-1} due to the increase of sterics when the second MPAA ligand fills the octahedral coordination site on the Pd-complex. Like the Pd(II) acetate dissociation pathway, the details of the proton transfer steps were not calculated. After dissociation of **L1**, the empty coordination site increases the free energy of **8a-1** to 20.7 kcal mol^{-1}. Species 8 is then formed after association of the acetate ligand.

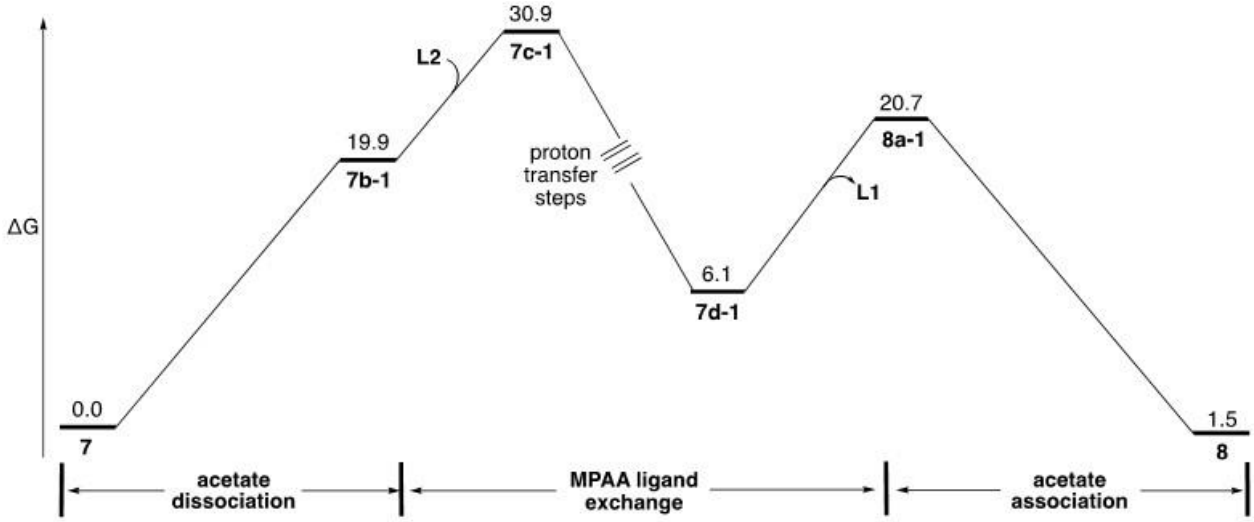

Figure 1.7. Free energy profile for Pd(IV) acetate dissociation pathway.

In comparison to the Pd(IV) solvent dissociation pathway shown in red from Figure 1.6, the Pd(IV) acetate dissociation pathway was unfavorable. Since the *t*-Amyl alcohol solvent molecule coordinated to Pd is more labile than the acetate ligand, we investigated a similar Pd(IV) dissociation pathway but rather the solvent molecule dissociates to open up a coordination site on the Pd-octahedral complex **7b**. This is energetically much more feasible at 11.1 kcal mol^{-1} than that of **7b-1** from the acetate dissociation pathway. Overall, this solvent dissociation pathway was lower in energy than the acetate dissociation pathway and was chosen as the representative pathway to compare to the Pd(II) acetate dissociation pathway.

1.4 Conclusions

In conclusion, we present a protocol for probing dynamic ligand exchange in asymmetric catalytic reactions applied to the Pd(MPAA)-catalyzed iodination of diarylmethylamines. Monitoring the temporal product enantiomeric excess after addition of the opposite enantiomer of the MPAA ligand allows assessment of the dynamics of ligand exchange in the system. While this system exhibits Pd:ligand = 1:1 and the lack of a nonlinear effect, it may be imagined that valuable information concerning the dynamics of ligands might also be obtained in systems exhibiting more complex catalyst speciation. Combining such experiments with spectroscopic characterization and an understanding of the ligand and metal molecularity provides a detailed protocol for comprehensive mechanistic understanding of the catalytic system. Further studies probing the generality of this protocol in other asymmetric catalytic systems of import are underway.

1.5 References

[1] Engle. K. E.; Mei, T. S.; Wasa, M.; Yu, J.-Q.; *Acc. Chem. Res.* **2012**, *45*, 788-802; b) Engle, K. M. *Pure Appl. Chem.* **2016**, *88,* 119-138.

[2] a) Engle, K. M.; Wang, D.-H.; Yu, J.-Q. *J. Am. Chem. Soc.* **2010***, 132*, 14137; b) Baxter, R. D.; Sale, D.; Engle, K. M.; Yu, J.-Q.; Blackmond, D. G. *J. Am. Chem. Soc*. **2012**, *134*, 4600; c) Plata, R. E.; Hill, D.E.; Haines, B. E.; Musaev, D. G.; Chu, L.; Hickey, D. P.; Sigman, M. S.; Yu, J.-Q.; Blackmond, D. G. *J. Am. Chem. Soc.* **2017**, *139*, 9238.

[3] a) Cheng, G. J.; Yang, Y. F.; Liu, P.; Chen, P.; Sun, T. Y.; Li, G.; Zhang, X. H.; Houk, K. N.; Yu, J. Q.; Wu, Y. D. *J. Am. Chem. Soc.* **2014**, *136,* 894-897b) Haines, B. E.; Musaev, D. G. *ACS Catal.* **2015**, *5,* 830-840; c) Musaev, D. G.; Figg, T. M.; Kaledin, A. L. *Chem. Soc. Rev.* **2014**, *43,* 5009-5031.

[4] a) Chu, L.; Wang, Y.-C.; Moore, C. E.; Rheingold, A. L.; Yu, J.-Q. *J. Am. Chem. Soc.* **2013**, *135*, 16344-16347; b) Chu. L.; Xiao, K.-J.; Yu, J.-Q.; *Science*, **2014**, *346*, 451-455.

[5] Dimeric Pd(II)/MPAA complexes which react stoichiometrically with dimethylbenzylamine substrate have been reported: Gair, J. J.; Haines, B. E.; Filatov, A. S.; Musaev, D. G.; Lewis, J. C. *Chem. Science*. **2017**, *8*, 5746.

[6] Hoops, S.; Sahle, S.; Gauges, R.; Lee, C.; Pahle, J.; Simus, N.; Singhal, M.; Xu, L.; Mendes, P.; Kummer, U. *Bioinformatic*s **2006,** *22*, 3067.

[7] M. J. Frisch, G. W. Trucks, H. B. Schlegel, G. E. Scuseria, M. A. Robb, J. R. Cheeseman, G. Scalmani, V. Barone, B. Mennucci, G. A. Petersson, H. Nakatsuji, M. Caricato, X. Li, H. P. Hratchian, A. F. Izmaylov, J. Bloino, G. Zheng, J. L. Sonnenberg, M. Hada, M. Ehara, K. Toyota, R. Fukuda, J. Hasegawa, M. Ishida, T. Nakajima, Y. Honda, O. Kitao, H. Nakai, T. Vreven, J. A. Montgomery Jr., J. E. Peralta, F. Ogliaro, M. Bearpark, J. J. Heyd, E. Brothers, K. N. Kudin, V. N. Staroverov, T. Keith, R. Kobayashi, J. Normand, K. Raghavachari, A. Rendell, J. C. Burant, S. S. Iyengar, J. Tomasi, M. Cossi, N. Rega, J. M. Millam, M. Klene, J. E. Knox, J. B. Cross, V. Bakken, C. Adamo, J. Jaramillo, R. Gomperts, R. E. Stratmann, O. Yazyev, A. J. Austin, R. Cammi, C. Pomelli, J. W. Ochterski, R. L. Martin, K. Morokuma, V. G. Zakrzewski, G. A. Voth, P. Salvador, J. J. Dannenberg, S. Dapprich, A. D. Daniels, O. Farkas, J. B. Foresman, J. V. Ortiz, J. Cioslowski, D. J. Fox, Gaussian 09, rev. D.01 (Gaussian, Inc., 2010).

[8] Becke, A. D. *J. Chem. Phys.* **1993**, 98, 5648–5652.

[9] Lee, C.; Yang, W.; Parr, R. G. *Phys. Rev. B*, **1988**, 37, 785–789.

[10] Becke, A. D. *J. Chem. Phys.*, **1993**, 98, 1372–1377.

[11] Stephens, P. J.; Devlin, F. J.; Chabalowski, C. F.; Frisch, M. J. *J. Phys. Chem.*, **1994**, 98, 11623–11627.

[12] Hay, P. J.; Wadt, W. R. *J. Chem. Phys.,* **1985**, 82, 299–310.

[13] Roy, L. E.; Hay, P. J.; Martin, R. L. *J. Chem. Theory Comput.*, **2008**, 4, 1029–1031.

[14] Ehlers, A. W.; Böhme, M.; Dapprich, S.; Gobbi, A.; Höllwarth, A.; Jonas, V.; Köhler, K. F.; Stegmann, R.; Veldkamp, A.; Frenking, G. *Chem. Phys. Lett.*, **1993**, 208, 111–114.

[15] Ditchfield, R.; Hehre, W. J.; Pople, J. A. *J. Chem. Phys.*, **1971**, 54, 724–728.

[16] Hehre, W. J.; Ditchfield, R.; Pople, J. A. *J. Chem. Phys.*, **1971**, 54, 2257–2261.

[17] Hariharan, P. C.; Pople, J. A. *Theor. Chim. Acta*, **1973**, 28, 213–222.

[18] Zhao, Y.; Truhlar, D. G. *Theor. Chem. Acc.*, **2008**, 120, 215–241.

[19] Dolg, M.; U. Wedig, U.; Stoll, H.; Preuss, H. *J. Chem. Phys.*, **1987**, 86, 866–872.

[20] Andrae, D.; Häußermann, U.; Dolg, M.; Stoll, H.; Preuß, H. *Theor. Chem. Acc.*, **1990**, 77, 123–141.

[21] Legault, C. Y. CYLView, 1.0b (Université de Sherbrooke, 2009); www.cylview.org.

Chapter 2. Probing Catalyst Speciation in Palladium-MPAAM-Catalyzed Enantioselective C(sp_3)–H Arylation of Cyclopropanecarboxylic Acids: Catalyst Improvement via Destabilization of Off-Cycle Species

2.1 Abstract

Chiral monoprotected aminoethyl amine (MPAAM) ligands were recently reported to facilitate enantioselective Pd-catalyzed arylation of strong cyclopropane C(sp_3)–H bonds. Herein, we describe detailed experimental and theoretical investigations into the influence of MPAAM ligands, **L1** and **L3**, as well as monoprotected aminoethyl thioether (MPAThio) ligand, **L2**, on reaction kinetics, product enantioselectivity, and turnover number. An unusual *negative* nonlinear effect in ligand enantiopurity and negative dependence of ligand concentration on reaction rate is observed for **L1** and **L2**, but not for **L3**. NMR titrations, kinetic modeling, crystal structures, and DFT calculations implicate concentration-dependent formation of stable, off-cycle, homoleptic Pd(**L**)$_2$ species occurs in the presence of **L1** or **L2**. However, in the **L3** system, only the catalytically active, mono-substituted [Pd(**L**)(OAc)] species is observed, regardless of ligand concentration, demonstrating the subtle influence of ligand structure on reaction kinetics and mechanism.

2.2 Introduction

Applications of chiral, small molecule ligand architectures in new catalyst design have led to significant advances in the field of site-specific and enantioselective C–H bond functionalization.[1] Amongst the vast library of ligands currently available, those utilizing the privileged AcNH motif have witnessed particularly exceptional successes.[2,3,4,5] Examples of such ligands are shown in Scheme 2.1 and include: MonoProtected Aminoethyl AMine (MPAAM) and it's sulfur derived analog MonoProtected Aminoethyl Thioether (MPAThio),[2] MonoProtected Amino Acids (MPAA),[3] Mono-N-Protected Aminomethyl Oxazoline (MPAO),[4] and Acetyl-Protected Aminoethyl Quinolines (APAQ).[5] This suite of ligands has enabled the

functionalization of a wide variety of difficult C–H bonds including the functionalization of strong cyclopropane C(sp^3)–H bonds.[2] While catalysts that employ these families of ligands have been efficacious in obtaining desired reactivity, little is understood about the coordination mode of the ligands, catalyst speciation in solution, or the overall reaction mechanisms. The versatility and wide applicability of these systems justifies an in-depth study of Pd complexes with these ligands, the role of the AcNH functionality, and the effect of ligand variation on reaction kinetics and enantioselectivity.

Scheme 2.1. Privileged Ligands in C–H Functionalization. (Oxa = oxazole; Q = quinoline)

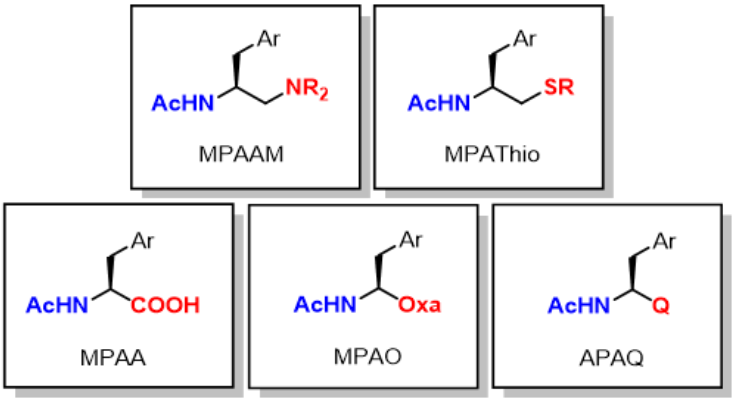

While the vast majority of directing group mediated C–H bond activations typically invoke strong coordination of a metal center with a heteroatom of the directing group, it is important to highlight the AcNH functionality as an exception to this trend. As summarized in Scheme 2.2, the terminal amide moiety has been hypothesized to act bifunctionally, both as a chelate and by being directly involved in a six-membered, C–H cleavage transition state.[2,3,4,5,6] Current computational models suggest an unusual deprotonation of the amide that acts to aid in chelation.[6] In this case, the amide is assigned as an X-type ligand, though little experimental evidence for this coordination mode has been reported.[7] Rather, conventional coordination chemistry often considers the amide functionality as an L-type ligand (Scheme 2.2b).[8] The discrepancies in current literature and an exiguous supply of well-characterized examples not

only warrant further investigation into how these ligands facilitate enantioselective C–H functionalization, but underline the necessity of such studies for improved catalyst design.

Scheme 2.2. Concerted Metallation Deprotonation by a Terminal Amide Moiety. (a) A proposed 6-member C–H cleavage transition state and (b) possible coordination modes of both protonated and deprotonated AcNH directing groups.

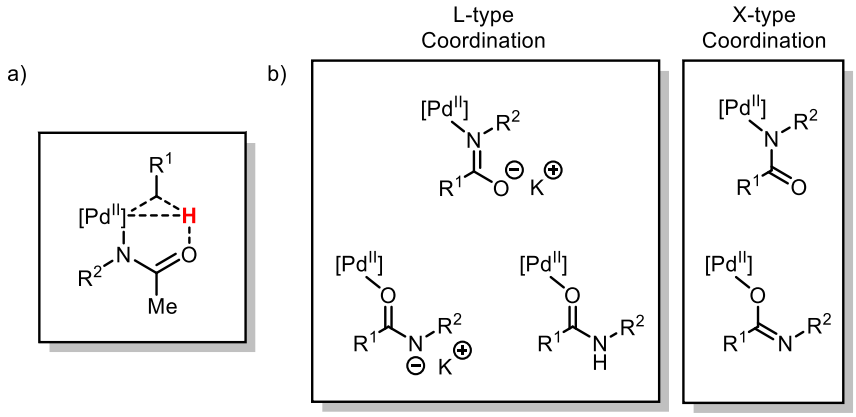

Herein, we report the first structural characterization of mononuclear Pd_{II} complexes bearing the AcNH functionalized MPAAM (**L1**) and MPAThio (**L2**) ligands shown in Scheme 2.3. Furthermore, we describe detailed experimental, computational, and kinetic analyses that examine the nature of the active catalyst and the origins of enantioselectivity. In both ligand systems, **L1** and **L2**, a previously unrecognized and highly unusual *negative* nonlinear effect on enantioselectivity was observed, implicating the formation of stable, off-cycle, homoleptic $Pd(\mathbf{L})_2$ species.[9] Additional NMR experimentation, DFT calculations, and crystallographic data not only provide support that accumulation of this species is the direct result of increased ligand-to-metal loadings, they further induce ramifications on reaction rate, turnover number (TON), and product

Scheme 2.3. Ligands L1–L3.

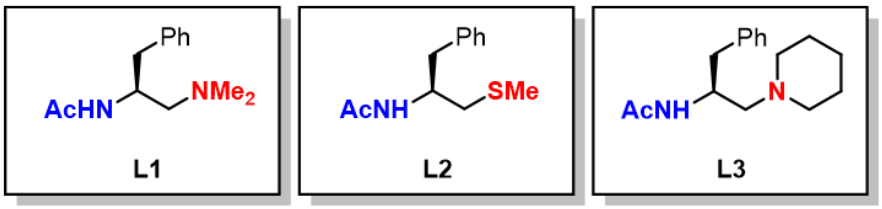

enantiomeric excess (*ee*). These combined findings have led to the development of a new ligand in the MPAAM family, **L3**, which exhibits superior catalytic performance due to the instability of the deleterious Pd(**L3**)$_2$ species, providing insight into improving the future design of enantioselective C–H functionalization catalysts.

2.3 Results and Discussion

2.3.1. Background

Utilizing the reaction conditions described in Scheme 2.4 as a benchmark, Yu and coworkers recently assessed the efficacy of twenty-four ligands in the MPAAM family for their capacity to promote the exceptionally difficult, enantioselective functionalization of cyclopropane C(sp3)–H bonds.[2] Collectively, only ligands featuring an unsubstituted terminal AcNH moiety proved competent in generating the desired product, **3**, further emphasizing the importance of the functionality.

Scheme 2.4. Enantioselective Pd-Catalyzed C(*sp*$_3$)–H Arylation of Cyclopropanecarboxylic Acid.

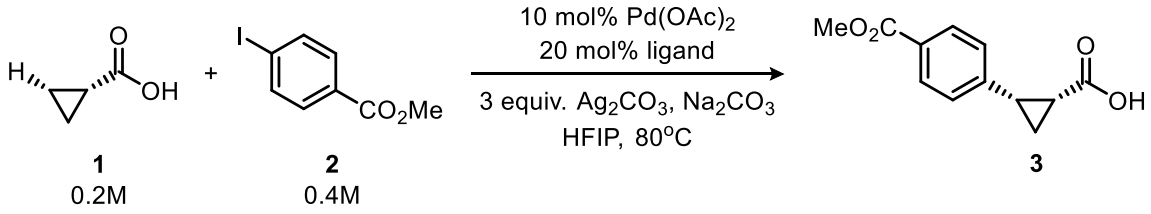

The N,N-dimethyl substituted **L1** was determined to be the most effective under the reported conditions (82% yield; 94% *ee*), however subtle differences in the steric environment of the tertiary amine (-NR$_2$) resulted in significant changes to the overall performances. This precarious nature of these ligands prompted the investigation into catalyst speciation and mechanistic elucidation described in this work.

2.3.2. Evaluation of L1 and L2 Systems.

Under the conditions outlined in Scheme 2.4, results from kinetic studies[9] involving **L1**, and the thioether analog, **L2**, are shown in Figures 2.1 and 2.2. Figure 2.1 provides a qualitative

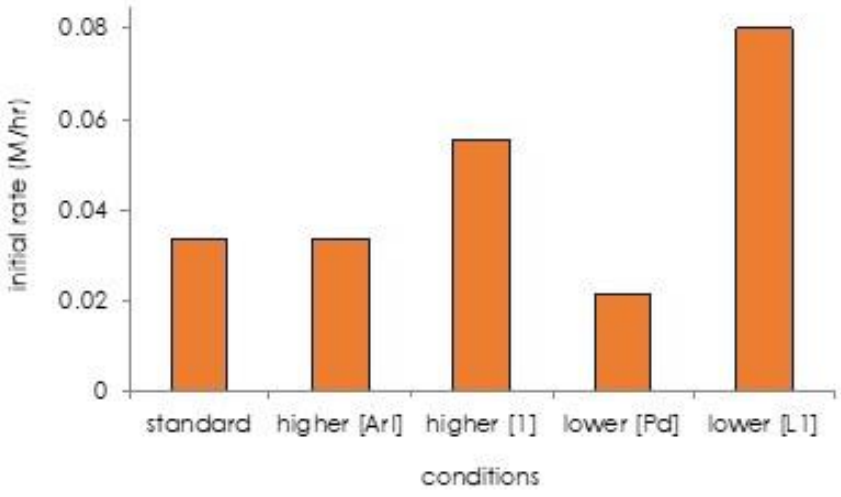

Figure 2.1. Kinetic studies of the reaction from Scheme 2.4.

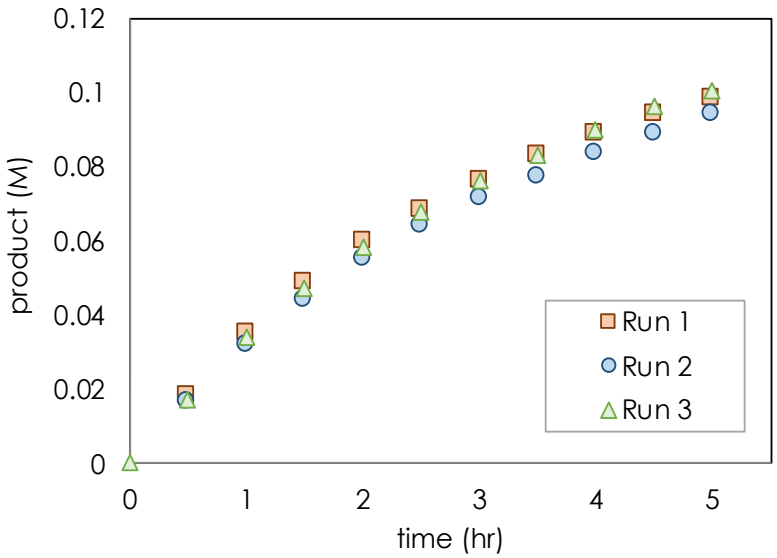

Figure 2.2. Reaction reproducibility. Comparison of three separate experiments under the standard conditions shown in Scheme 2.4 using L1, confirming the reproducibility of the kinetic measurements.

comparison of relative rates, while Figure 2.2 confirms the reproducibility of the measurements. Similar results were observed across both ligand systems, exhibiting first order dependence on [Pd], a positive order in concentration of the carboxylic acid substrate, **1**, and zero order in

concentration of the aryl iodide, **2**. The enantiomeric excess values of the desired product, **3**, ranged between 70 - 80% *ee*.[10,11]

Interestingly, decreasing the L:Pd ratio below the standard 2:1 outlined in Scheme 1 resulted in a significant increase in reaction rate. The unusual negative rate dependence on ligand concentration implies complex Pd-ligand speciation, leading us to consider the possibility of (Pd**L**)$_n$ or Pd(**L**)$_n$ species (where $n > 1$).[9]

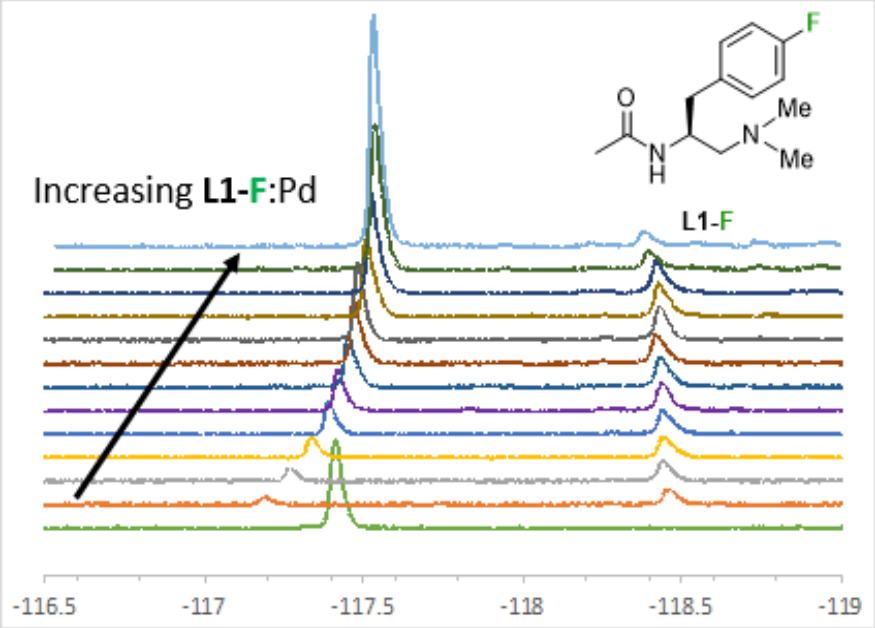

Figure 2.3. ^{19}F-NMR spectra as amount of L1-F increases. ^{19}F-NMR spectra of interactions between Pd(OAc)$_2$ and the fluorinated version of L1 at 55 ^{o}C. [Pd] = 0.06 M. Free L1-F is shown as the lowest spectrum in green. Pd:L ratios 1:0.5, 1:0.67, 1:0.83, 1:1, 1:1.17, 1:1.33, 1:1.5, 1:2, 1:3, 1:4.

We sought evidence for the formation of such higher-order complexes through ligand binding titrations. The interaction of free **L1** and Pd(OAc)$_2$ was initially evaluated by ^{1}H NMR spectroscopy, however, rapid line broadening and the overlapping of signals convoluted the interpretation of the data. Instead, interaction between Pd(OAc)$_2$ and **L1** was probed by ^{19}F NMR spectroscopy using a fluorine-labeled derivative of the ligand, **L1-F**. As shown in Figure 2.3, the spectra show two peaks present in the reaction mixtures. At substoichiometric L:Pd

ratios, the signal for free ligand at -117.4 ppm is shifted to -117.2 ppm but gradually moves back towards that of the free ligand as the concentration of **L1-F** increases. The second peak at -118.4 ppm also appears at a low L:Pd ratio yet experiences less of a change in chemical shift with respect to increased ligand concentrations. These spectra support the suggestion that catalyst speciation is complex in the Pd-**L1** system.

2.3.3. Synthesis of PdL_2 Species.

Since addition of free **L1** to $Pd(OAc)_2$ results in a dynamic system with more than one species present in solution, we developed a targeted synthetic approach that has allowed us to characterize several important Pd species, including those that may be disfavored under the

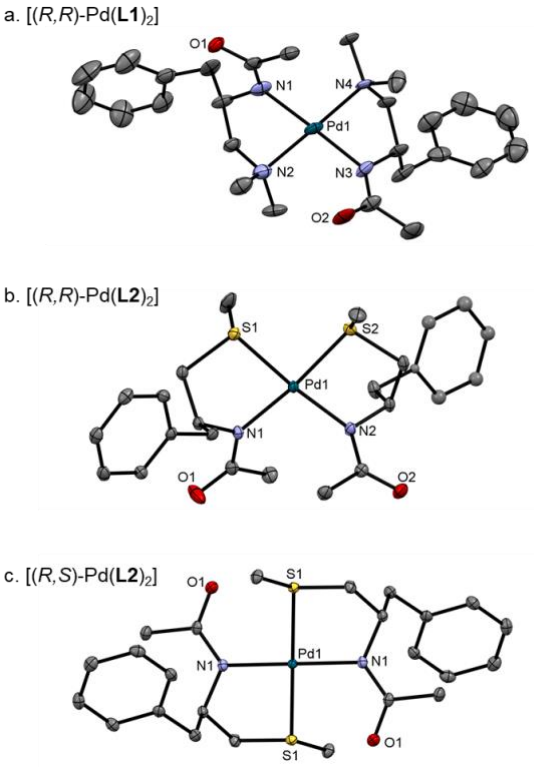

Figure 2.4. Crystal structures of palladaycles. (a) (R,R)-$Pd(L1)_2$, (b) (R,R)-$Pd(L2)_2$, and (c) (R,S)-$Pd(L2)_2$. Thermal ellipsoids are drawn at the 50% probability level with hydrogen atoms and outer sphere LiCl atoms omitted for clarity. For (b), one of the phenyl rings was disordered and stable refinement required isotropic modeling of the thermal parameters.

reaction conditions described in Scheme 2.4. As outlined in Scheme 2.5, the ligands were first deprotonated with either potassium or lithium bis(trimetylsilyl)amide and subsequently transferred to a solution of $Pd(OAc)_2$ or $Pd(MeCN)_2Cl_2$ in a THF/Et_2O mixture. In each case, the corresponding Pd(**L**)$_2$ complex precipitated as a light yellow solid. Single crystals suitable for X-ray diffraction were prepared by solvent diffusion of pentane into concentrated dichloromethane solutions of Pd(**L**)$_2$. These complexes represent the first structural characterizations of Pd complexes with either MPAAM or MPAThio family ligands. In these materials, the deprotonated amide coordinates to Pd through the N-atom as an X-type ligand, while the tertiary amine in **L1,** and thioether in **L2,** acts as an L-type donor, forming a 5-membered palladocycle. his synthetic method appears to be quite general. In addition to the homoleptic Pd(**L**$_R$)$_2$ compounds, [(*R,R*)-Pd(**L1**)$_2$] and [(*R,R*)-Pd(**L2**)$_2$], we have also been able to prepare the heterochiral [(*R,S*)-Pd(**L2**)$_2$] shown in Figure 2.4. The latter complex was prepared by sequentially treating $Pd(OAc)_2$ with one equivalent of K(**L2**$_R$) followed by one equivalent of K(**L2**$_S$). All three of these structures were used as starting points for DFT calculations to explore the relative stabilities of Pd(**L**)$_2$ complexes.

Scheme 2.5. Synthetic route to PdL$_2$ species.

$$2\ HL \xrightarrow[PdX_2]{2\ eq.\ KHMDS/LiHMDS} PdL_2$$

(X = OAc, Cl)

2.3.4. Density Functional Theory of L1 and L2 Species.

The DFT calculated structures for ligand systems **L1** and **L2** are shown in Figures 2.5 and 2.6, respectively. The most stable species for ligand **L1** is the homoleptic *trans*-[(*R,R*)-Pd(**L1**)$_2$], as characterized crystallographically, which lies 1.3 kcal/mol lower than it's *cis*- isomer and 2.6 kcal/mol below the mono-ligated [(*R*)-Pd(**L1**)(OAc)] (Figure 8). This assignment is in good agreement with the crystal structure shown in Figure 2.4a. The next lowest energy configuration, heterochiral *cis*-[(*R,S*)-Pd(**L1**)$_2$], lies 4.8 kcal/mol above *trans*-[(*R,R*)-Pd(**L1**)$_2$].

Dimeric (Pd**L**)$_2$ complexes are significantly (> 20 kcal/mol) less stable than the monomeric Pd(**L**)$_2$ complexes. Thus, the homoleptic *trans*-[(*R,R*)-Pd(**L1**)$_2$] and the mono-ligated species likely comprise most of the [Pd] population for the **L1** system. The mono-ligated [(*R*)-Pd(**L1**)(OAc)] species retains an acetate ligand and presumably represents the active entry into the catalytic cycle.

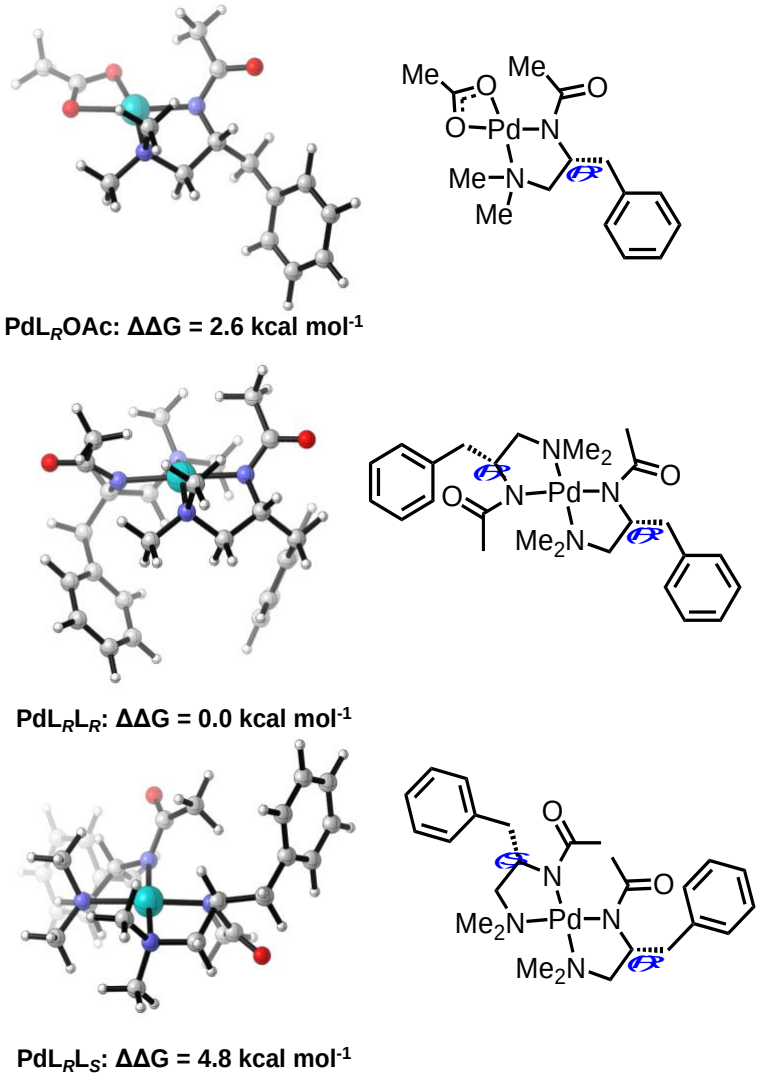

Figure 2.5. Relative stabilities of lowest energy conformers of species formed from Pd(OAc)$_2$ and L1. [Pd(L$_R$)(OAc)] (top), [Pd(L$_R$)(L$_R$)] (middle), and [Pd(L$_R$)(L$_S$)] (bottom). SMD (Generic, eps=16.7)/M06/6-311+G(d,p)//B3LYP/6-31G(d).

Figure 2.6 shows that calculations with ligand **L2** also implicate a homoleptic species, *cis*-[(*S,S*)-Pd(**L2**)$_2$], as the most stable, lower in energy by 4.3 kcal/mol compared to the heterochiral species, *cis*-[(*S,R*)-Pd(**L2**)$_2$]. As with **L1**, the population of [Pd] species for **L2** is likely a mixture of monosubstituted [(*S*)-Pd(**L2**)(OAc)] and homochiral *cis*-[(*S,S*)-Pd(**L2**)$_2$]. In contrast to **L1**, both bis-ligated **L2** complexes prefer the *cis* conformation. The crystal structure of the homochiral *cis*-[(*R,R*)-Pd(**L2**)$_2$] complex shown in Figure 7b supports these calculations.

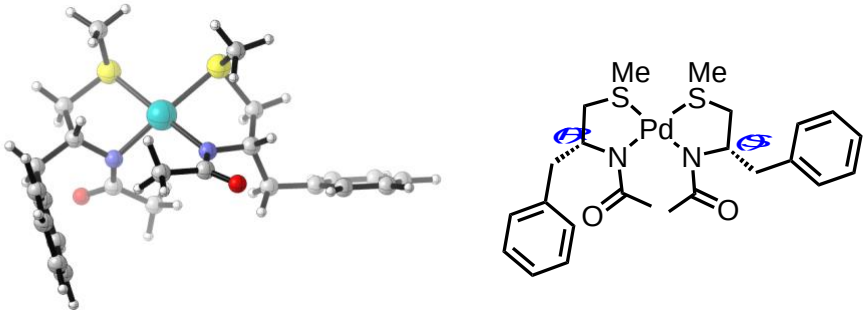

PdL$_R$L$_S$: ΔΔG = 4.3 kcal mol^{-1}

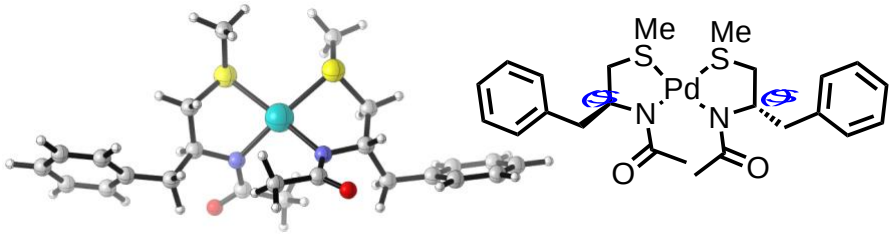

PdL$_S$L$_S$: ΔΔG = 0.0 kcal mol^{-1}

Figure 2.6. Relative stabilities of lowest energy conformers of species formed from Pd(OAc)$_2$ and L2. PdL$_R$L$_S$ (top), PdL$_S$L$_S$ (middle). SMD (Generic,eps=16.7)/M06/6-311+G(d,p)// B3LYP/6-31G(d).

2.3.5. Nonlinear ee effects and L3.

In the field of asymmetric catalysis, Kagan's pioneering work has demonstrated that observation of a nonlinear relationship between ligand enantiopurity and product *ee* is a valuable tool for probing reaction mechanisms.[12] The most common rationalization for this nonlinear effect has been attributed to the formation of higher order M(**L**)$_n$ species (where $n >$

1), although explanations invoking phase behavior have also been proposed in cases where incomplete dissolution of the catalyst and/or ligand occurs. Such species have been observed in [Pd] systems with achiral ligands, however the observation of multi-ligated [Pd] species in chiral systems is extremely rare. Recently, we developed a protocol to probe for the presence of such higher order species in solution by investigating the influence of ligand enantiopurity on both product *ee* and reaction kinetics.[5b]

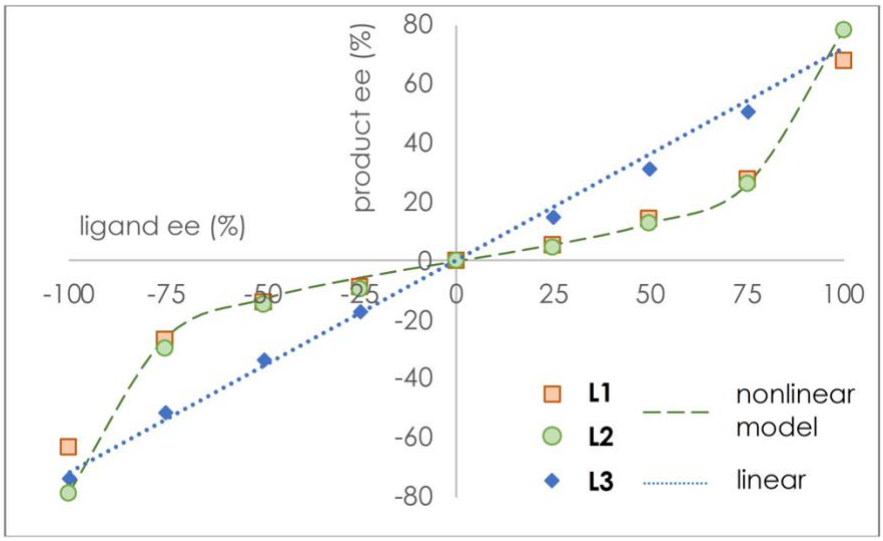

Figure 2.7. Product enantiomeric excess vs. ligand enantiopurity. Carried out using ligands **L1**, **L2**, and **L3** with $[Pd]_0$ = 0.02 M and Pd:L = 1:4. Symbols represent experimental data; dotted line shows linear behavior; dashed line shows the model prediction of the negative nonlinear effect.

The Pd-[**L1**] system displays unusual rate behavior as a function of ligand enantiopurity, as shown in Figure 2.7. Under identical reaction conditions, the use of a racemic **L1** mixture proceeds at 1.5 times the rate of that of the enantiopure ligand. This nonlinear behavior is in marked contrast to our previous studies, which employed both MPAA[3c] and APAQ[5b] ligands, where no nonlinearity is observed. Furthermore, a plot of ligand vs. product *ee*, Figure 2.8, displays a strong nonlinear effect for both the [Pd]-**L1** and [Pd]-**L2** systems. In commonly reported cases of nonlinear effects in asymmetric catalysis, racemic and scalemic catalysts

exhibit lower reaction rates. To the best of our knowledge, this is the first time such an observation has been reported in asymmetric Pd catalysis.[13] We attribute both of these results to the favorable formation of off-cycle $Pd(L)_2$ species.

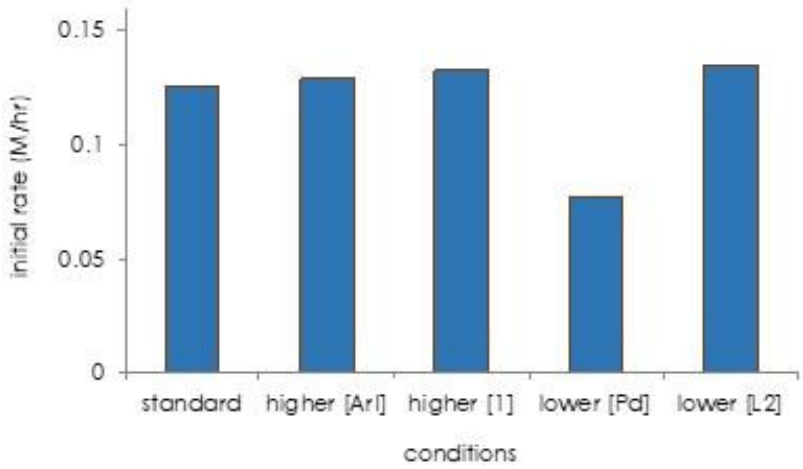

Figure 2.8. Kinetic study of the reaction under standard conditions.

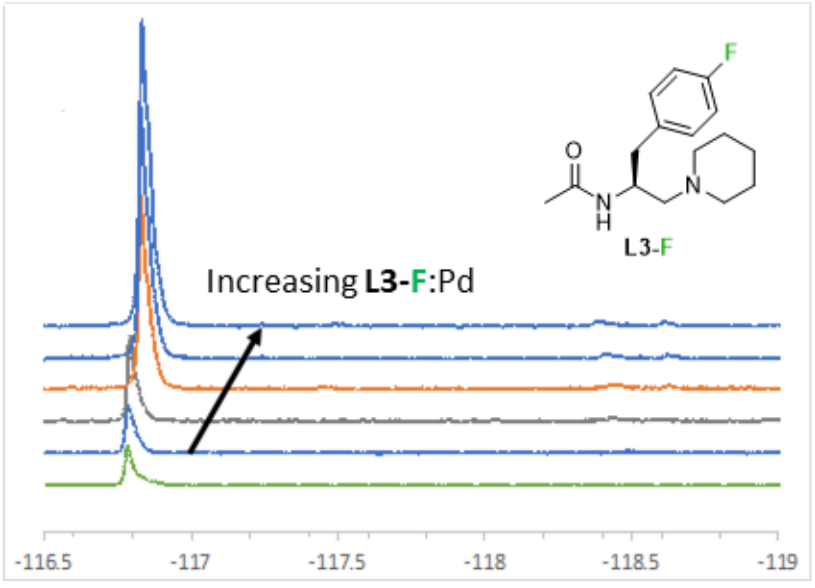

Figure 2.9. ^{19}F-NMR spectra as amount of L3-F increases. ^{19}F-NMR spectra of interactions between $Pd(OAc)_2$ and the fluorinated version of **L3** at 55 ^{o}C. [Pd] = 0.06 M. Free **L3-F** is shown as the lowest spectrum in green. Pd:L ratios 1:1, 1:2, 1:3, 1:4, 1:5.

Since mono-ligated [Pd(L)(OAc)] species likely represent the active entry into the catalytic cycle, we proposed steric modification of the MPAAM family's tertiary -NR_2 group as a methodical approach to circumvent formation of the deleterious $Pd(L)_2$ species. To test the hypothesis, we utilized our protocol[5b] to evaluate a series of ligands and found that **L3** exhibited a linear behavior in its plot of ligand vs product *ee*.

The [Pd]-**L1** system also displays unusual rate behavior as a function of ligand enantiopurity, as shown in Figure 2.7. Under identical reaction conditions, the use of a racemic **L1** mixture proceeds at 1.5 times the rate of that of the enantiopure ligand. In contrast, **L3**, which does not exhibit a nonlinear effect of ligand *ee* on product *ee*, racemic and enantiopure ligands essentially proceed at the same rates.

Kinetic studies[9] involving **L3** were performed in accordance with the standard L:Pd ratio of 2:1 used for the **L1** and **L2** systems shown in Figure 2.1. The results outlined in Figure 2.8 indicate that the [Pd]-**L3** system exhibits a first order dependence on [Pd], and a zero order dependence on **L3** as well as both substrates, **1** and **2**. In comparison to **L1** (k_H/k_D = 1.6), a larger KIE value was observed for **L3** with k_H/k_D = 3.3. Under the benchmark reaction conditions described in Scheme 2.4, the rate of the reaction with **L3** was nearly four times faster than with **L1** while affording comparable enantioselectivity, again ranging between 70-80% *ee*.[10]

A fluorinated analog of **L3** was also synthesized and used in ^{19}F NMR-monitored ligand binding titrations. In contrast to the **L1-F** spectra in Figure 2.3, treating $Pd(OAc)_2$ with increasing concentrations of **L3-F** resulted in simpler spectra, exhibiting one single peak with a negligible shift from that of the free ligand across the full range of ligand concentrations (Figure 2.9). These spectra support the suggestion that catalyst speciation is less complex for the Pd-**L3** system as compared to Pd-**L1**.

Calculations carried out on Pd species formed with **L3** indicate that the mono-substituted [Pd(**L3**)(OAc)] species is the most stable, with homochiral and heterochiral bis-ligated species

found to be 6.1 and 6.5 kcal/mol higher in energy, respectively (Figure 2.10). In this case it is likely that all [Pd] exists as the active mono-ligated [Pd(**L3**)(OAc)] species, in accordance with both the $_{19}$F-NMR studies of Figure 2.9 and the absence of nonlinear effects for **L3** (Figure 2.7)

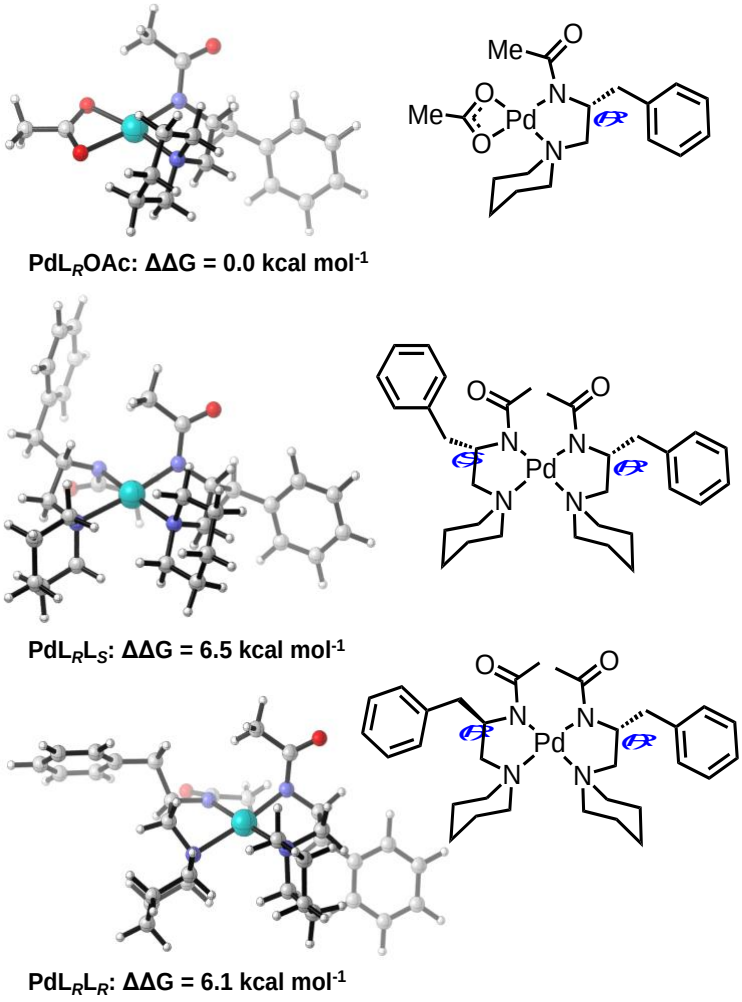

Figure 2.10. Relative stabilities of lowest energy conformers of species formed from Pd(OAc)$_2$ and L3. [(R)-Pd(**L3**)(OAc)] (top), cis-[(R,S)-Pd(**L3**)$_2$] (middle), and cis-[(R,R)-Pd(**L3**)$_2$] (bottom). SMD(Generic,eps=16.7)/M06/6-311+G(d,p)//B3LYP/6-31G(d).

2.3.6. Reaction Mechanism.

The combined findings of the three ligand systems, **L1**–**L3**, implicate the steps shown in Scheme 2.7 as key for determining rate and enantioselectivity. Reversible substrate binding precedes the C-H abstraction step, which is partially rate determining. The relative populations

of [Pd(**L1**)(OAc)] and [Pd(**L1**)(**1-H**)] differ for **L1** and **L3**; the higher KIE value and lower order in substrate [**1**] for **L3** suggest that the [Pd] complex rests predominantly at [Pd(**L3**)(**1-H**)], while for **L1** the catalyst is divided between [Pd(**L1**)(OAc)] and [Pd(**L1**)(**1**-**H**)]. All subsequent steps in the catalytic cycle, including oxidative addition of the aryl iodide, occur after the rate determining step and are kinetically invisible.

Scheme 2.6. Kinetically Relevant Steps in Cyclopropane C–H Bond Activation.

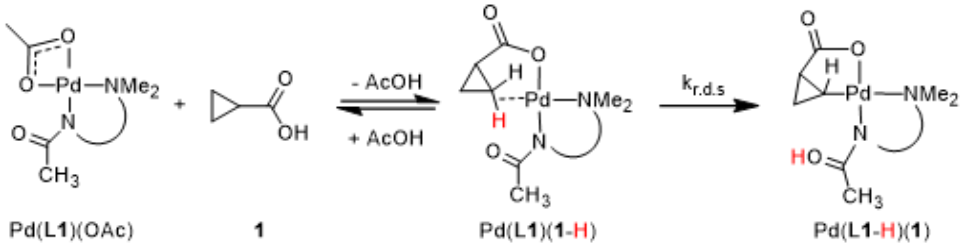

Scheme 2.7. Models for Nonlinear Effects of Ligand Enantiomeric Excess (Active Catalytic Species in Pink).

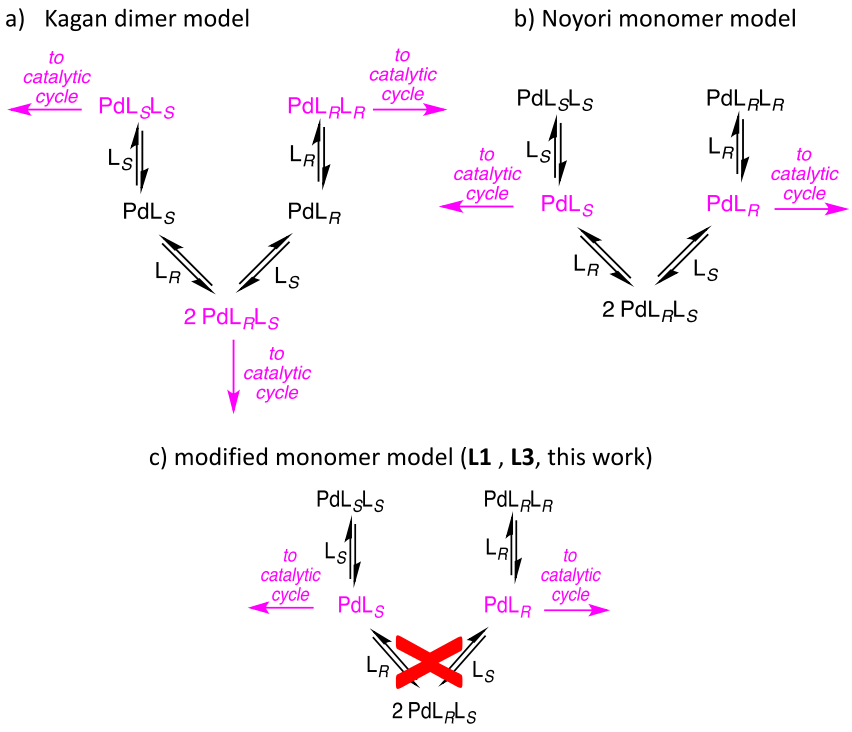

The unusual negative nonlinear effect of ligand *ee* and reaction rate can be discussed in terms of two prominent models in asymmetric catalysis by Kagan and Noyori. The Kagan ML_2 model (Scheme 2.7a) proposes that nonlinear effects will be observed in cases where bis-ligated species dominate the system and serve as the active catalyst. Negative nonlinear effects may be observed when the heterochiral species exhibits higher activity and stability than homochiral species. In this case, the rate of reaction for racemic catalysts is predicted to be higher than that for the enantiopure ligand, which is observed in the **L1** and **L2** system. However, the instability of the calculated heterochiral bis-ligated species makes it unlikely that this model describes ligand systems **L1** and **L2**.

Noyori studied nonlinear effects in the alkylation of aldehydes by dialkylzinc complexes catalyzed by chiral amino alcohols, where monomeric species are active catalysts and dimeric species act as off-cycle spectator species (Scheme 2.7b).[14] A positive nonlinear effect on enantioselectivity is observed when the heterochiral dimeric complex of chiral Zn alkoxides is more stable than the homochiral complexes. In such a case, the rate for enantiopure catalysts will always be higher than that for racemic catalysts, in contrast to our observation.

Our work identifies the features of a further type of a negative nonlinear effect (Scheme 2.7c), related to the Noyori monomer-active case, where equilibria between mono- and bis-ligated species exist only between homochiral species due to the instability of heterochiral bis-ligated species. Because of these equilibria, the relative concentrations of the active PdL_R and PdL_S differ from the total ligand *ee*. At lower ligand concentrations, a higher fraction of the total [Pd] is present as the active mono-ligated species. Indeed, for a given total $L_R + L_S$ ligand concentration, the minor enantiomer of the ligand exhibits a *higher* relative concentration of active mono-substituted [Pd(**L**)(OAc)] than does the major enantiomer, resulting in a nonlinear effect on product *ee*. Given these considerations and the values of K_{eq} derived from our computational models, we were able to successfully predict the magnitude of the nonlinear effect with remarkable accuracy as shown by the dashed line in Figure 2.7.

The formation of off-cycle, homoleptic Pd(**L**)$_2$ species also explains the effect of ligand enantiomeric purity on rate for **L1** and **L3**. When the same absolute concentration of ligand L_{tot} is divided between L_R and L_S, the concentration of the total active PdL species (PdL_R + PdL_S) will be greater than for the case when L_{tot} is comprised of a single enantiomer of the ligand. This consideration predicts that the reaction rate should be higher for a racemic mixture of PdL_R + PdL_S compared with the enantiopure case. Indeed, as shown in Figure 2.7, the racemic mixture is 1.5 times faster than enantiopure ligand, in good agreement with our prediction of a relative rate of 1.7.

We also explored computationally the enantioselectivity in the C–H metalation-deprotonation step using substrate **1** and ligand **L1**. The optimized structures and relative free energies of the most favorable transition states for the two enantiomers are shown in Figure 2.11. In both transition states, the Pd(II) center is coordinated to the tertiary amine of the ligand, the N-atom of the deprotonated amide, and the carboxylate of the substrate **1**. The O- atom of the amide acts as an intramolecular base in a concerted metalation/deprotonation to activate the (sp_3)C–H bond and facilitate the Pd–C bond formation. **TS(*S*)** is more favorable than **TS(*R*)** by 4.5 kcal/mol, which somewhat overestimates the experimental selectivity.

Enantioselectivity arises from the different orientation of the amide group in the *R* and *S* transition states shown in Figure 2.12. There is more severe distortion of the six-membered bis-chelate of **L1** in **TS(*R*)**, where the amide group rotates into the plane of the Pd square planar complex in order to deprotonate the pro-(*R*) proton. This is shown more dramatically in Figure 16, which is an illustration of overlays of the reactant complex in red with **TS(*S*)** in blue (on the left) and with **TS(*R*)** in green (on the right). The amide group in the reactant complex is pre-organized to deprotonate the pro-(*S*) hydrogen, but in TS(*R*), distortions of the amide group and the 6-membered diazapalladacycle are required to achieve the transition state.

These studies lead to the proposed catalytic mechanism shown in Figure 2.13 for **L1**. Reversible substrate binding to form the reactive complex [Pd(**L1**)(OAc)] is followed by rate-

determining C-H activation via the transition state shown in Figure 2.11. Oxidative addition of the aryl iodide is followed by reductive elimination and regeneration of the active mono-ligated catalyst PdL, which is in equilibrium with its homochiral di-ligated species in the case of **L1** and **L2**. The fraction of total Pd diverted to this off-cycle species increases with increasing ligand

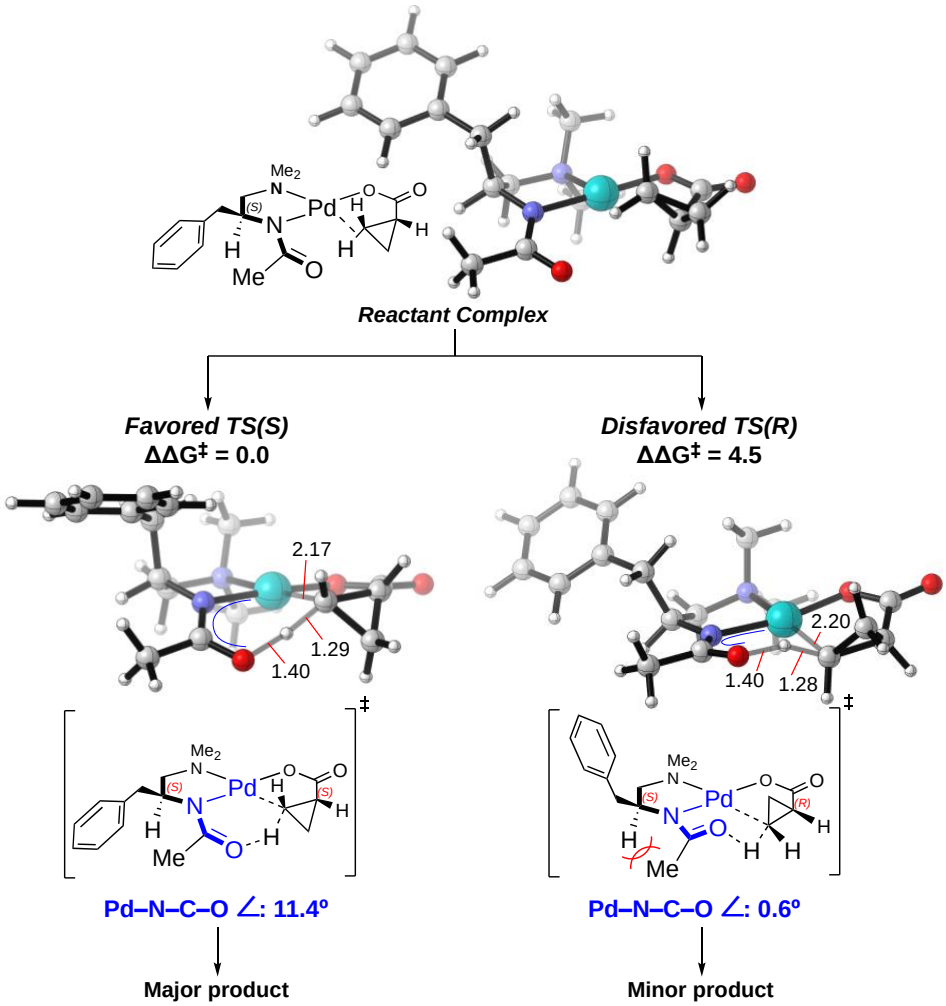

Figure 2.11. CMD TS structures with L1. DFT-optimized structures and relative free energies of the two enantiomeric C–H metalation-deprotonation reactant complex and transition states.

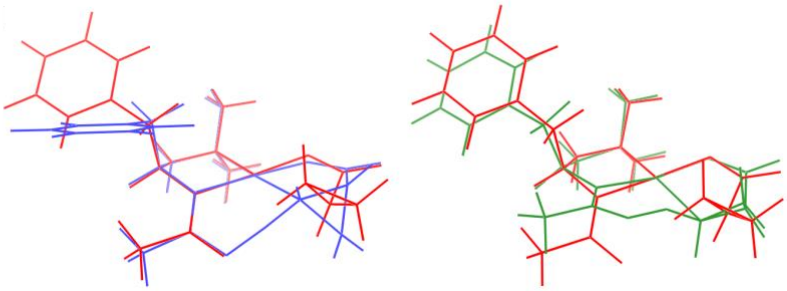

Figure 2.12. Overlay of reactant complex and TS structures. (red = reactant complex; blue = TS(S); green = TS(R))

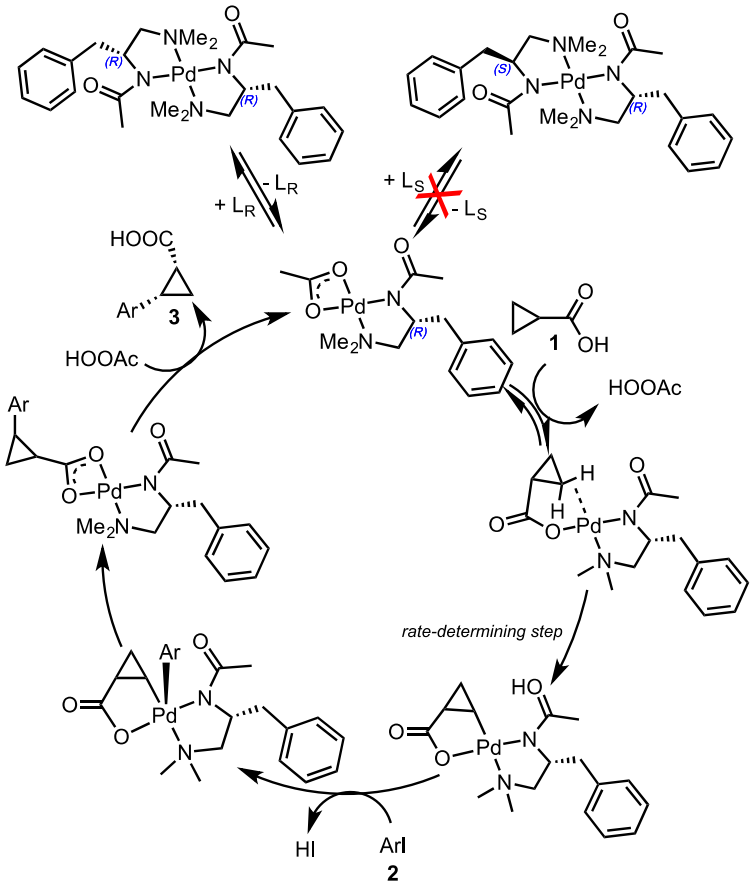

Figure 2.13. Proposed catalytic cycle with ligand L1.

concentration, slowing the rate. **L3**, by contrast, does not exhibit this off-cycle species. The steps within the catalytic cycle pertain to all three ligand systems.

The inverse behavior of rate with ligand concentration for **L1** suggests that higher Pd:L ratios would provide optimal efficiency by effectively allowing a higher fraction of the Pd to be

present as the active monosubstituted species. However, the robustness of the system must also be considered. For **L1**, the reaction begins to exhibit catalyst deactivation at Pd:L ratios less than 1:2, and enantioselectivity is also eroded. In the case of **L3**, **e**xcess free ligand does not adversely influence rate and may also help maintain robustness in the event of catalyst deactivation via ligand dissociation. Indeed, we found that the total turnover number could be tripled for reactions in the presence of eight equivalents of ligand **L3**.[11]

2.4 Conclusions

In summary, experimental observations of an unusual negative nonlinear effect in ligand enantiopurity and negative dependence of ligand concentration on reaction rate for **L1** and **L2** implicate the formation of off-cycle, homoleptic Pd(**L**)$_2$ species under the standard reaction conditions outlined in Scheme 1. The formation of these species in solution was probed by NMR titrations and kinetics modeling, and the structures of several Pd(**L**)$_2$ species were determined by single-crystal X-ray diffraction. DFT calculations and model predictions of reaction rate for the racemic compared to the enantiopure case also support a mechanistic model with the homoleptic Pd(**L**)$_2$ species as an off-cycle spectator. The formation of these species can be prevented by manipulating the steric parameters of the tertiary amine group in the MPAAM family of ligands. For example, the ligand **L3** disfavors the formation of Pd(**L3**)$_2$ complexes. Instead, only the catalytically active, mono-substituted [Pd(**L3**)(OAc)] species is observed, allowing for a higher population of active catalyst to be present in solution. Finally, this work demonstrates the subtle influence of ligand structure on reaction kinetics and mechanism enabling the future design of efficient enantioselective C–H functionalization catalysts.

2.5 References

[1] For selected reviews of enantioselective C−H functionalization, see: (a) Giri, R.; Shi, B.-F.; Engle, K. M.; Maugel, N.; Yu, J.-Q. Transition Metal-Catalyzed C–H Activation Reactions: Diastereoselectivity and Enantioselectivity. *Chem. Soc. Rev*. **2009**, *38*, 3242–3272. (b) Newton,

C. G.; Wang, S.-G.; Oliveira, C. C.; Cramer, N. Catalytic Enantioselective Transformations Involving C–H Bond Cleavage by Transition-Metal Complexes. *Chem. Rev*. **2017**, *117*, 8908–8976. (c) Saint-Denis, T. G.; Zhu, R.-Y.; Chen, G.; Wu, Q.-F.; Yu, J.-Q. Enantioselective C(sp_3)–H Bond Activation by Chiral Transition Metal Catalysts. *Science* **2018**, *359,* eaao4798*.*

[2] Shen, P.-X.; Hu, L.; Shao, Q.; Hong, K.; Yu, J.-Q. Pd(II)-Catalyzed Enantioselective C(sp_3)–H Arylation of Free Carboxylic Acids. *J. Am. Chem. Soc.* **2018***, 140*, 6545–6549.

[3] (a) Shi, B.-F.; Maugel, N.; Zhang, Y.-H.; Yu, J.-Q. Pd(II)-Catalyzed Enantioselective Activation of C(sp_2)–H and C(sp_3)–H Bonds Using Monoprotected Amino Acids as Chiral Ligands. *Angew. Chem. Int. Ed.* **2008**, *47*, 4882–4886. (b) Engle, K. M. The Mechanism of Palladium(II)-Mediated C–H Cleavage with Mono-*N*-Protected Amino Acid (MPAA) Ligands: Origins of Rate Acceleration. *Pure Appl. Chem.* **2016**, *88*, 119–138. (c) Hill, D. E.; Bay, K. L.; Yang, Y.-F.; Plata, R. E.; Takise, R.; Houk, K. N.; Yu, J.-Q.; Blackmond, D. G. A Role for Pd(IV) in Catalytic Enantioselective C-H Functionalization with Monoprotected Amino Acid Ligands Under Mild Conditions. *J. Am. Chem. Soc.* **2017**, *139*, 18500–18503. (d) Bay, K. L.; Yang, Y.-F.; Houk, K. N. Multiple Roles of Silver Salts in Palladium-Catalyzed C–H Activations. *J. Organomet. Chem.* **2018**, *864*, 19–25.

[4] Wu, Q.-F.; Shen, P.-X.; He, J.; Wang, X.-B.; Zhang, F.; Shao, Q.; Zhu, R.-Y.; Mapelli, C.; Qiao, J. X.; Poss, M. A. Yu, J.-Q. Formation of α-Chiral Centers by Asymmetric □-C(sp_3)–H Arylation, Alkenylation, And Alkynylation. *Science* **2016**, *355*, 499–503. b) He, J.; Shao, Q.; Wu, Q.-F.; Yu, J.-Q. Pd(II)-Catalyzed Enantioselective C(sp_3)–H Borylation. *J. Am. Chem. Soc.* **2017**, *139*, 3344–3347

[5] (a) Chen, G.; Gong, W.; Zhuang, Z.; Andrä, M. S.; Chen, Y. Q.; Hong, X.; Yang, Y.-F.; Liu, T.; Houk, K. N.; Yu, J.-Q. Ligand-Accelerated Enantioselective Methylene C(Sp_3)–H Bond Activation. *Science* **2016**, *353*, 1023–1027. (b) Hill, D. E.; Pei, Q.-L.; Zhang, E.-X.; Gage, J. R.; Yu, J.-Q.; Blackmond, D. G. A General Protocol for Addressing Speciation of the Active Catalyst

Applied to Ligand-Accelerated Enantioselective C(sp_3)-H Bond Arylation. *ACS Catal.* **2018**, *8*, 1528–1531.

[6] Rodrigalvarez, J.; Nappi, M.; Azuma, H.; Flodén, N. J.; Burns, M. E.; Gaunt, M. J. Catalytic C(sp_3)–H Bond Activation in Tertiary Alkylamines. *Nat. Chem*. **2020**, *12*, 76–81.

[7] (a) Sugimori, T.; Shibakawa, K.; Masuda, H.; Odani, A.; Yamauchi, O. *Inorg. Chem*. **1993**, *32*, 4951. (b) Haas, K., Ehrenstorfer-Schäfers, E.-M., Polborn, K. and Beck, W. Bis(dipeptide ester–H_+) Complexes of Palladium(II) – Precursors for the Formation of Cyclotetrapeptides. *Eur. J. Inorg. Chem*. **1999**, *3*, 465-469. (c) Hoffmuller, W.; Kramer, R.; Maurus, M.; Polborn, K.; Beck, W. Z. *Naturforsch. B Chem. Sci.* **2000**, *55*, 855. (d) Romero, E. A., Chen, G.; Gembicky, M.; Jazzar, R.; Yu, J.-Q.; Bertrand, G. Understanding the Activity and Enantioselectivity of Acetyl-Protected Aminoethyl Quinoline Ligands in Palladium-Catalyzed β-C(sp_3)–H Bond Arylation Reactions. *J. Am. Chem. Soc.* **2019**, *141*, 16726-16733.

[8] Engle, K. M.; Mei, T.-S.; Wasa, M.; Yu, J.-Q. Weak Coordination as a Powerful Means for Developing Broadly Useful C–H Functionalization Reactions. *Acc. Chem. Res.* **2012**, *45*, 788–802.

[9] (a) Blackmond, D. G. Reaction Progress Kinetic Analysis: A Powerful Methodology for Mechanistic Studies of Complex Catalytic Reactions. *Angew. Chemie Int. Ed*. **2005**, *44*, 4032–4320. (b) Mathew, J. S.; Klussmann, M.; Iwamura, H.; Valera, F.; Futran, A.; Emanuelsson, E. A. C.; Blackmond, D. G. Investigations of Pd-Catalyzed ArX Coupling Reactions Informed by Reaction Progress Kinetic Analysis. *J. Org. Chem.* **2006**, *71*, 4711–4722. (c) Blackmond, D. G. Kinetic Profiling of Catalytic Organic Reactions as a Mechanistic Tool. *J. Am. Chem. Soc.* **2015**, *137*, 10852–10866.

[10] The slightly lower ee values obtained in our studies compared to Ref. 6 may be attributed to the overall lower concentrations employed in our kinetic studies, which were necessary due to

solubility considerations of **1**. Lower ligand concentrations may result in a larger contribution from background reaction.

[11] See Scheme 2.4 for details.

[12] (a) Puchot, C.; Samuel, O.; Dunach, E.; Zhao, S.; Agami, C.; Kagan, H. B. Nonlinear Effects in Asymmetric Synthesis. Examples in Asymmetric Oxidations and Aldolization Reactions. *J. Am. Chem. Soc.* **1986**, *108*, 2353–2357. (b) Guillaneux, D.; Zhao, S.-H.; Samuel, O.; Rainford, D.; Kagan, H. B. Nonlinear Effects in Asymmetric Catalysis. *J. Am. Chem. Soc.* **1994**, *116*, 9430–9439.

[13] For reviews see: (a) Satyanarayana, T.; Abraham, S.; Kagan, H. B. Nonlinear Effects in Asymmetric Catalysis. *Angew. Chem. Int. Ed*. **2009**, *48*, 456–494. (b) Blackmond, D. G. Kinetic Aspects of Nonlinear Effects in Asymmetric Catalysis. *Acc. Chem. Res*. **2000**, *33*, 402–411; (c) Noyori, R.; Kitamura, M. Enantioselective Addition of Organometallic Reagents to Carbonyl Compounds: Chirality Transfer, Multiplication, and Amplification. *Angew. Chem., Int. Ed. Engl*. **1991**, *30*, 49.

[14] Kitamura, M.; Suga, S.; Oka, H.; Noyori, R. Quantitative Analysis of the Chiral Amplification in the Amino Alcohol-Promoted Asymmetric Alkylation of Aldehydes with Dialkylzincs. *J. Am. Chem. Soc*. **1998**, *120*, 9800–9809.

Chapter 3. Multiple Roles of Silver Salts in Palladium-Catalyzed C–H Activations

3.1 Abstract

Many Pd-catalyzed C–H functionalization reactions utilize stoichiometric Ag(I)-salts as additives. Ag additives are typically used either as a terminal oxidant or as a halide scavenger for Pd catalyst regeneration. However, recent experimental and computational studies have shown that Ag(I)-salts may play additional roles in C–H activation processes. Notably, cooperative Pd–Ag bimetallic C–H activations and Ag(I)-mediated Pd-catalyzed C–H arylations can occur. The non-oxidative roles of Ag(I) salts in Pd catalyzed C–H activation are highlighted in this chapter.

3.2 Introduction

C–H activation reactions have become attractive tools for synthesis of complex organic molecules.[1] Palladium remains the most widely used catalyst for C–H activation reactions, yet reaction conditions have become increasingly complex as additives such as acids, bases, and salts are included along with Pd.[2] Pd-catalyzed C–H functionalizations are commonly carried out in the presence of stoichiometric Ag(I) salts. Ag additives are used as a terminal oxidant in oxidative functionalizations, or as a halide scavenger, particularly when iodoarenes are used as coupling partners.[3] Other possible roles have been proposed: (1) Ag(I) salts promote C–C coupling,[4] (2) the formation of a bi- or multimetallic Pd–Ag complex facilitates C–H cleavage at Pd(II),[1] and (3) Ag(I) salts directly promote C–H cleavage to form a Ag-arene intermediate.[2] In this mini-review, we highlight recent papers in which both Pd and Ag have been employed in transition-metal catalysis, and illustrate the significance of Ag^+ in C–H functionalizations.

Pd(II) catalyzes the oxidative dimerization (homocoupling) of benzene, thiophene, and arylpyridine derivatives under mild conditions. Mori *et al.* reported a C–H functionalization reaction in which a homocoupling of 2-formylthiophene **1** to form **2** occurs in the presence of AgF and a Pd(II) catalyst (Fig. 3.1a).[5] Since this seminal work, the utilization of silver salts in this

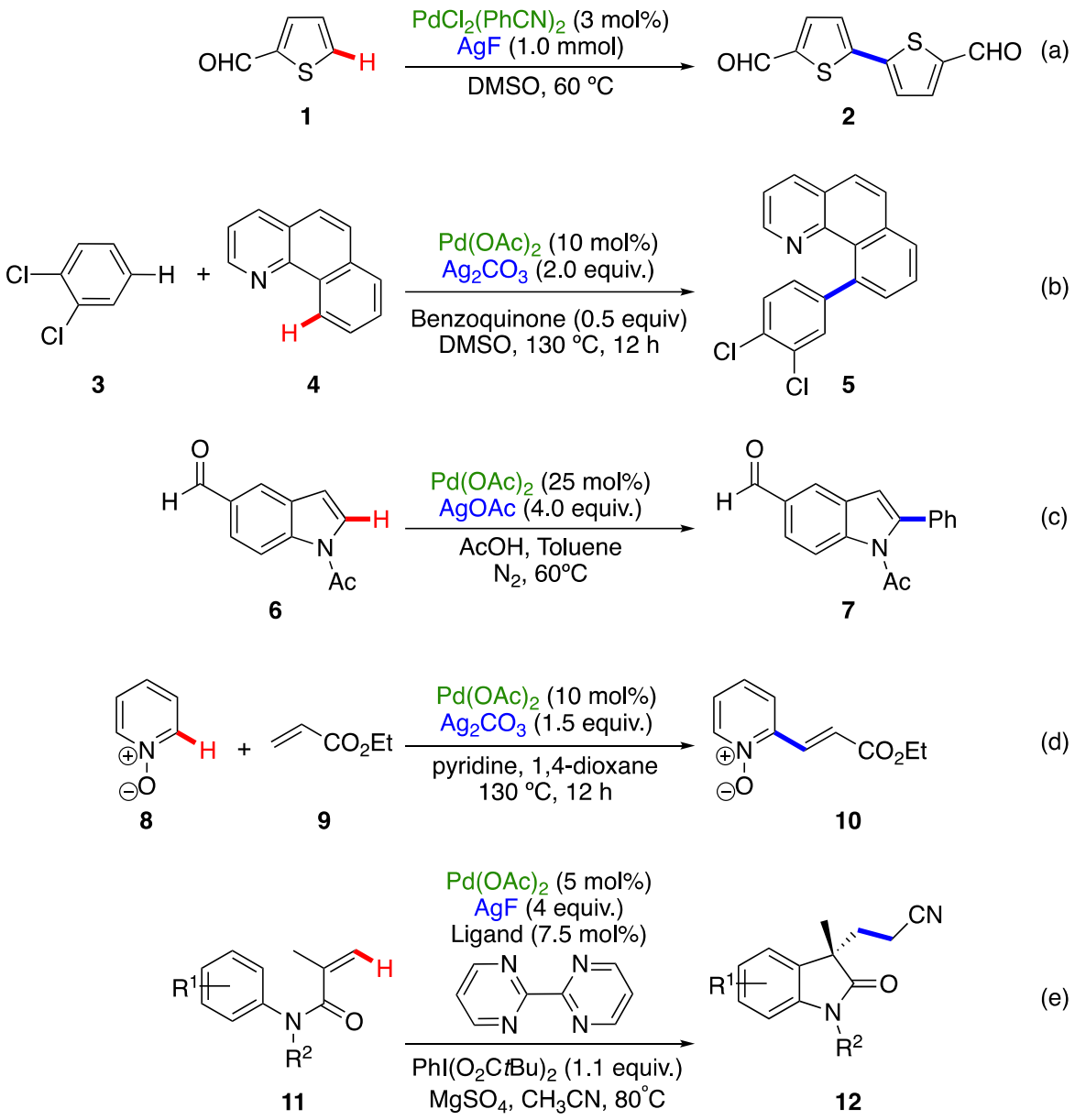

Figure 3.1. Examples of C–H functionalization reactions where Ag(I)-salts are used as an oxidant.

area of chemistry has become common, and has lead to the development of efficient methodology for constructing both C–C and C–X (X = O, N, S) bonds from both aliphatic and aromatic C–H bonds.

Shortly after the published work by Mori *et al.*, Sanford and co-workers showed a novel Pd-catalyzed reaction for highly chemo- and regioselective oxidative cross-coupling of aromatic

compounds **3** and **4** to form product **5** using both Ag(I) salts and benzoquinone as oxidants to regenerate the activated Pd(II) catalyst (Fig. 3.1b).[6] Fagnou and DeBoef independently described that C2 and C3 positions in indoles can be selectively functionalized in Pd-catalyzed cross-coupling reactions depending on whether $Cu(OAc)_2$ or AgOAc is employed as the stoichiometric oxidant (Fig. 3.1c shows the Ag^+ results).[7] Chang and co-workers reported selective alkenylation using pyridine N-oxides **8** and ethyl acrylate **9** to generate (*E*)-**10** with good stereo- and chemoselectivity (Fig. 3.1d).[8] Liu *et al*. reported a Pd-catalyzed oxidative arylalkylation of activated alkenes **11** in the presence of AgF and PhI(OPiv)2 (Fig. 3.1e).[9] Based on these experimental observations, they propose that AgF plays a key role in C–H bond activation step, since 12 does not form in the absence of AgF.

3.3 Pd–Ag Heterodimeric Complexes in C–H Activation Reactions

In a study of heterobimetallic carboxylates, Hor *et al.* isolated a Ag(I)/Pd(II) bimetallic system and determined its structure by single-crystal X-ray crystallographic analysis.[10] This enabled the direct study of the catalytic activity of this heterometallic complex. Furthermore, Strassner and co-workers synthesized a trinuclear Pd–Ag–Pd carbene acetate complex.[11] Through the use of energy-dispersive X-ray spectroscopy, they determined the Pd:Ag ratio to be 2:1. Subsequently, Markov *et al.* reported an acetate-bridged Pd(II)–Ag(I) heterometallic complex **13** (Figure 3.2).[12] They studied its molecular geometry and electronic structure using single-crystal XRD and quantum mechanical density functional theory (DFT) calculations.

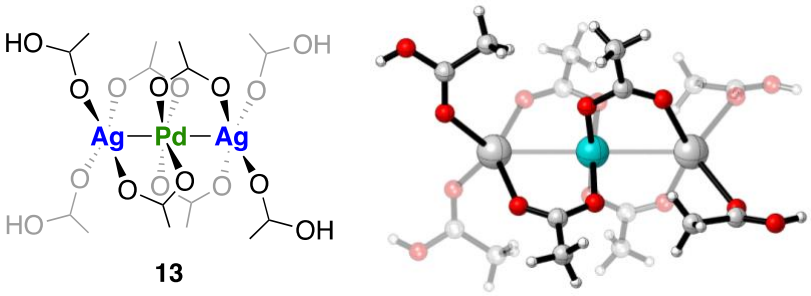

13

Figure 3.2. Fragment of the polymer chain from the crystal structure. $\{Pd_{II}[(\mu\text{-}OOCMe)_2Ag_I(HOOCMe)_2]_2\}_n$

In 2014, a collaboration between our group and the groups of Yun-Dong Wu and Jin-Quan Yu identified a Pd–Ag complex involved in the activation of distal *meta*-C–H bonds of a nitrile-containing template attached to benzyl alcohol, **14** (Fig. 3.3a).[13,14] For the C–H activation step, four possible active catalytic species were studied: monomeric Pd(OAc)2 **16**, dimeric $Pd_2(OAc)_4$ **17**, heterodimeric $PdAg(OAc)_3$ **18**, and trimeric $Pd_3(OAc)_6$ **19** (Fig. 3.3b). The computed structures of Pd, Pd/Pd, and Pd/Ag complexes, predicted energies, and selectivities showed that the use of a rigid nitrile-based directing group favors a cyclophane-type transition state (Fig. 3.4).[14] The U-shape of the directing group and the linear coordination of the nitrile group orient the Pd catalyst away from the *ortho* hydrogen but towards the *meta* hydrogen. The Ag salt is a crucial additive for the Pd(II)-catalyzed olefination of toluene derivatives with the nitrile-containing template. When Ag is replaced with other oxidants, both yield and *meta*-selectivity decrease. We found that silver carboxylate plays a dual role, functioning as both an oxidant and part of the heteronuclear active species in the mechanism involving $PdAg(OAc)_3$. The transition state for the concerted metallation-deprotonation (CMD) C–H activation step involves either a dimeric $Pd_2(OAc)_4$ or a heterodimeric $PdAg(OAc)_3$ complex that drastically lowers the energy of the transition states leading to the *meta* products. This is due to decreased ring strain in the macrocyclic nitrile-coordinated C–H activation transition states in the dimeric mechanisms.

After this discovery of a heterodimeric Pd–Ag transition state model, a more general effort to understand the cooperativity between Pd and Ag in C–H functionalizations was undertaken. For example, Yu and co-workers reported a Pd(II)-catalyzed *ortho*-C–H amination reaction of N-arylbenzamides **24** using additives such as AgOAc and CsF (Fig. 5a).[15] Computations by the Schaefer group suggest that [PdAg(m-$OAc)_3$] is the active catalyst that creates a cooperative interaction between Pd(II) and Ag(I) which stabilizes the C–H activation transition state.[16]

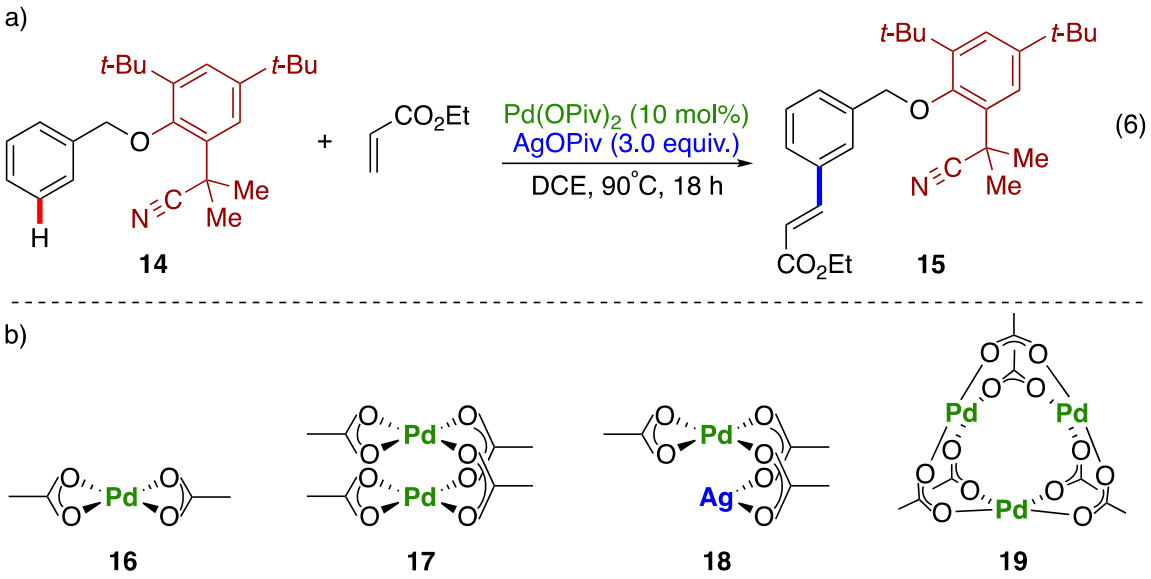

Figure 3.3. Pd-catalyzed *meta*-selective C–H alkenylation of toluene derivatives. (a) Method of interest that contains a nitrile-containing template; (b) Active catalytic species considered in computational study.

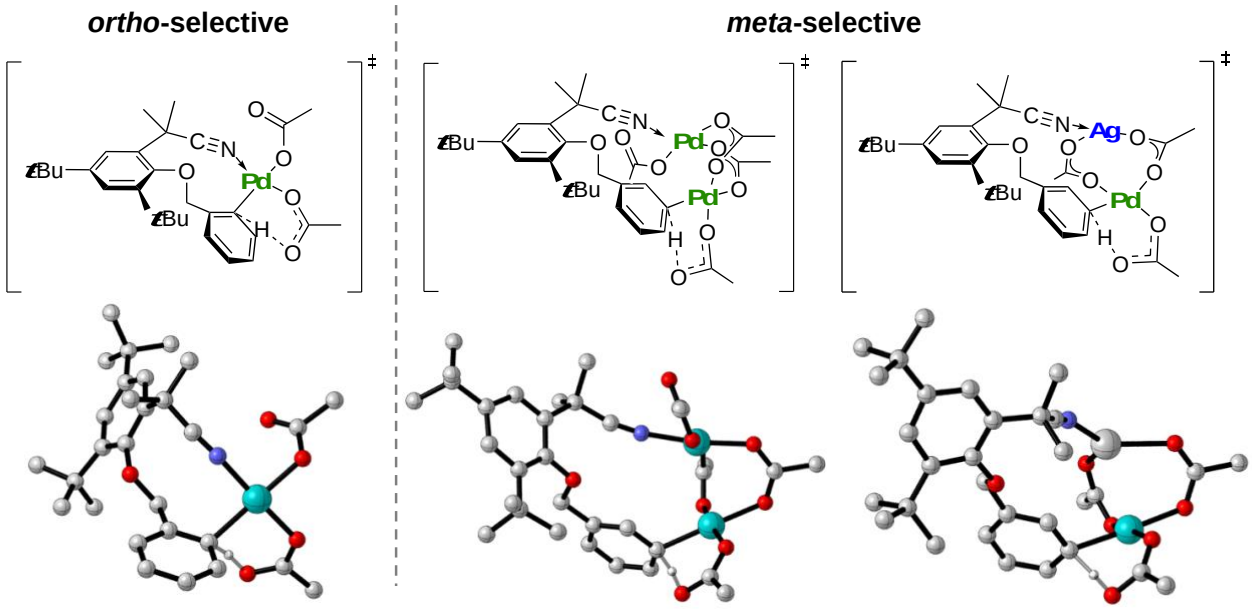

Figure 3.4. Monometallic and bimetallic C–H activation transition states.

Tan *et al.* developed a similar nitrile template containing a silicon atom in the tether, which gives excellent *meta*-selectivity for C–H olefination of benzyl alcohols (Fig. 3.5b).[17] The

larger size of the silicon atom along with elongated Si–C and Si–O bonds allows for greater separation between the directing nitrile and reacting aromatic group.

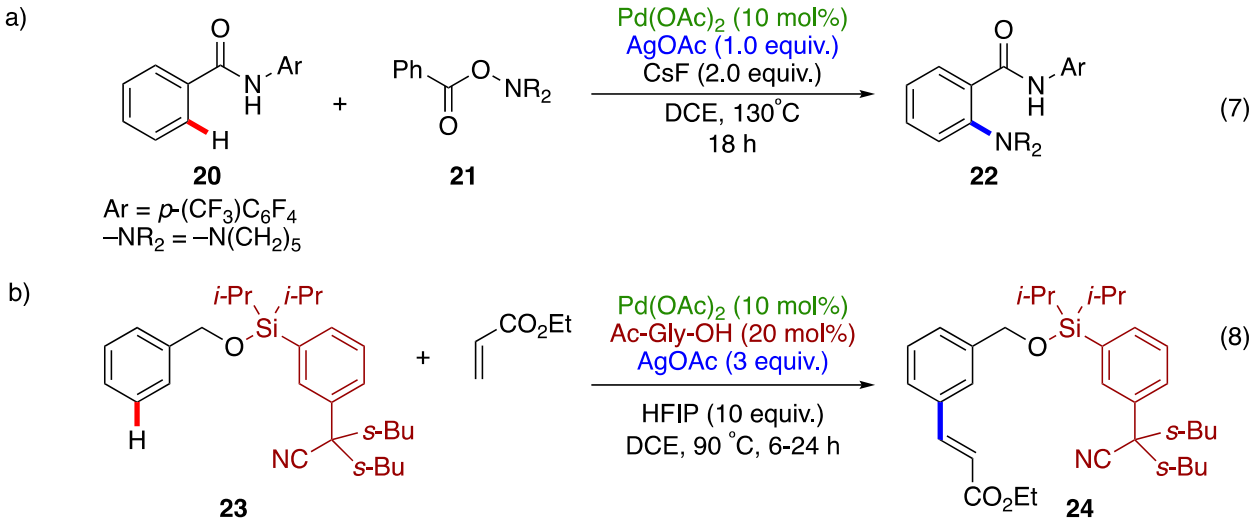

Figure 3.5. C–H Functionalizations with AgOAc. a) Pd(II)-catalyzed *ortho*-C–H amination reaction of *N*-arylbenzamides b) Pd(II)-catalyzed *meta*-C–H activation using a Si-containing tether.

More recently, our group and the Yu group studied a template with a conformationally flexible alkyl chain for *meta*-C–H olefination of benzoic acid derivatives, such as amide **25**, using silver and mono-protected amino acid (MPAA) ligands, such as N-acetyl valine (Fig. 3.6a).[18] Computations showed that MPAA stabilizes the Pd–Ag heterodimer prior to C–H activation and lowers the barrier of coordination to the nitrile group of the template, leading to product **26**. In the absence of the MPAA ligand, the most stable heterodimeric catalyst is **27**, which is 14 kcal mol^{-1} less stable than precatalysts $Pd_3(OAc)_6$ and $Ag_2(OAc)_4$, the reference state for these calculations (Fig. 3.6b). Ligand exchange of the k^2-acetate with *N*-acetyl-glycine gives the more stable heterodimer **28**, which is about 6 kcal mol^{-1} more stable than **27**.

Xu, Jin, and co-workers explored a Pd-catalyzed, remote *meta*-selective C(sp^2)–H activation of distal arene-tethered alcohols consisting of different chain lengths (Fig. 3.7a).[19]

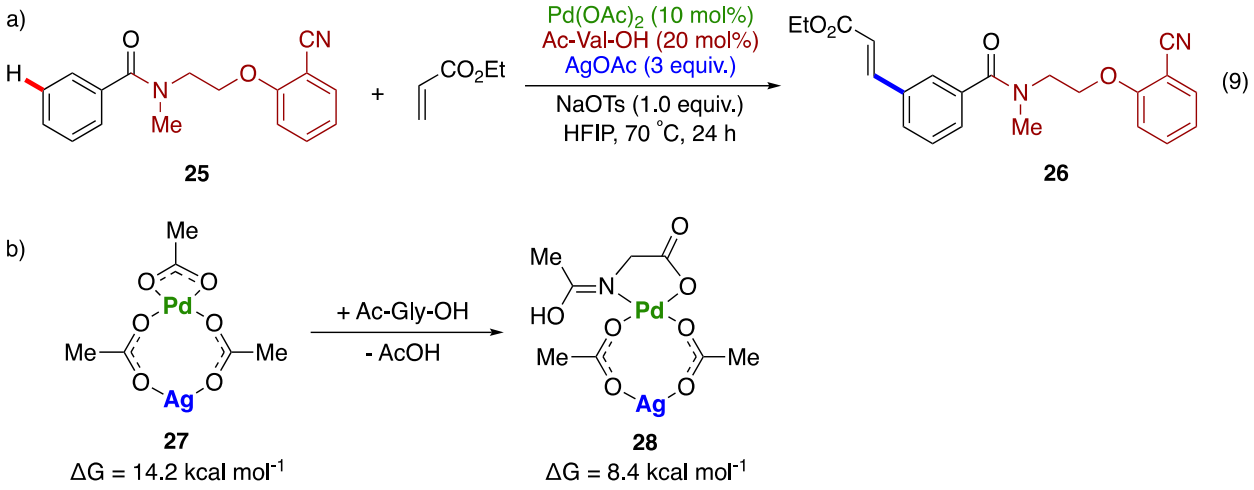

Figure 3.6. Pd-catalyzed *meta*-C–H activation of benzoic acids with an amide template. a) Reaction conditions b) Heterodimer catalyst stabilization by *N*-acetyl–glycine. Energies are relative to $Pd_3(OAc)_6$ and $Ag_2(OAc)_4$.

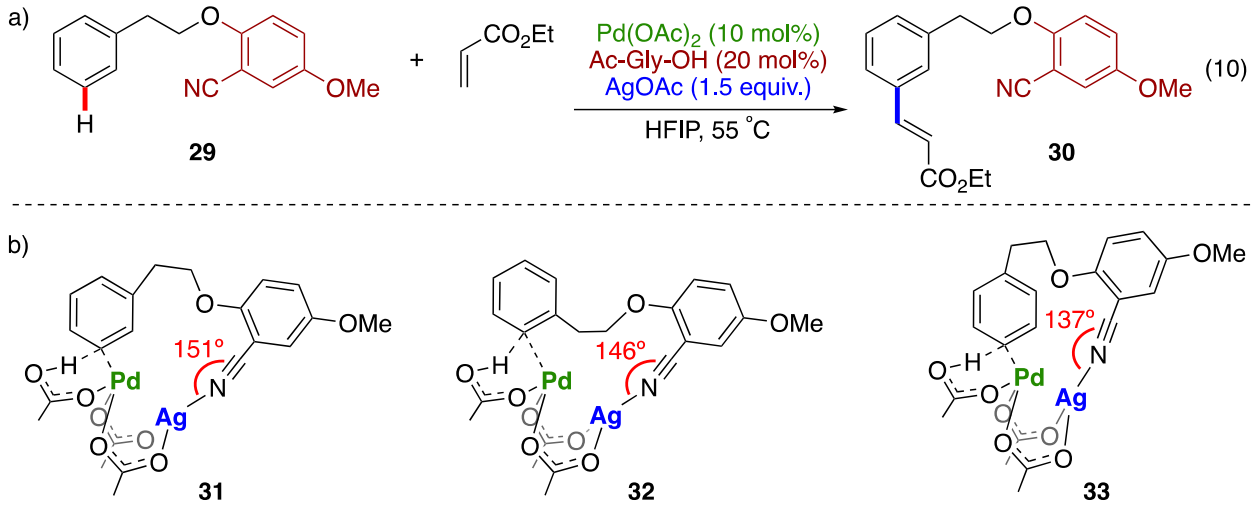

Figure 3.7. Pd-catalyzed *meta*-C–H activation of benzoic acids with an ether template. a) Reaction conditions. b) *Meta*, *ortho*, and *para* heterodimeric C–H activation transition states studied computationally.

They also performed DFT calculations to elucidate the origins of meta-selectivity and the effects of different linker lengths between the directing group and remote C–H bonds. Although the directing template employed in their study is different from that used in Yu's work,[1,17] the reaction likely takes place through a similar Pd–Ag heterodimeric mechanism. Figure 3.7b

shows the most stable TS structures with a short linker. The *meta*-TS **31** is the most stable TS with a C–N–Ag angle of 151º, which is relatively close to the optimal nitrile ligand binding angle of 180º. The *ortho*-TS **32** is less stable due to a less favorable C–N–Ag angle of 146º, which causes steric repulsions between the oxygen atoms of the bridged acetates cis to the Pd–C bond and the benzyl hydrogen atoms. The *para*-TS **33** shows a distorted C–N–Ag angle of 137º, rendering it higher in energy than the *meta*-TS **31**.

3.4 Silver-Mediated, Palladium-Catalyzed C–H Activation

In 2016, Larrosa and co-workers reported that a Ag(I) carboxylate, and not a Pd(II) species, is responsible for C–H activation in a Pd/Ag-mediated C–H arylation system, likely through a CMD mechanism (Figure 3.8).[20] Both stoichiometric and kinetic mechanistic studies were done to show that phosphine ligated Ag(I) carboxylates activate electron-deficient arenes. They showed that the reaction order of Pd, with excess PPh_3 is zero. This implied that a process external to the catalytic cycle is the rate-limiting step of the overall reaction. The proposed mechanism of Ag(I)-mediated C–H activation, rather than a Pd(II)-mediated C–H activation, is consistent with their kinetic studies, and involves an off-cycle process of forming $Ag(O_2CAd)$ from Ag_2CO_3 and $AdCO_2H$. The proposed catalytic cycle is shown in Figure 3.9a.

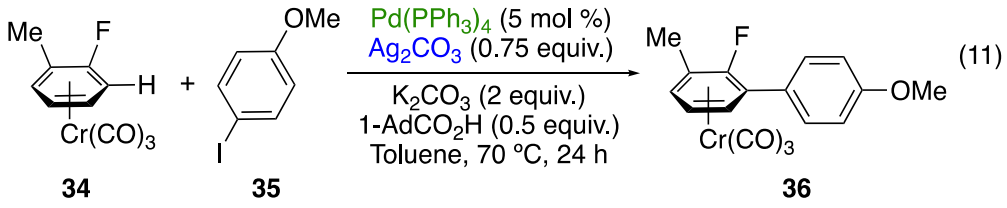

Figure 3.8. Ag(I)-mediated Pd-catalyzed C–H arylation of electron-deficient arenes.

Subsequently, Sanford and co-workers investigated the role of AgOPiv in the stoichiometric activation of C_6F_5H in a well-defined Pd(II) complex and in the Pd(II)-catalyzed oxidative dimerization of 2-alkylthiophenes **37** (Figure 3.9b).[21] Through *in situ* ^{19}F NMR studies, her group was able to detect a $Ag–C_6F_5$ complex and compare it to an authentic sample.

a) Larrosa: Pd/Ag-mediated C–H arylation

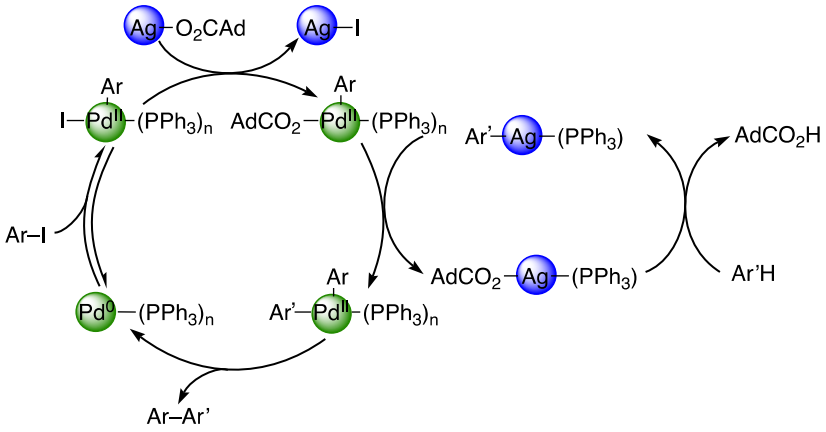

b) Sanford: Pd-catalyzed, Ag-mediated C–H oxidative coupling

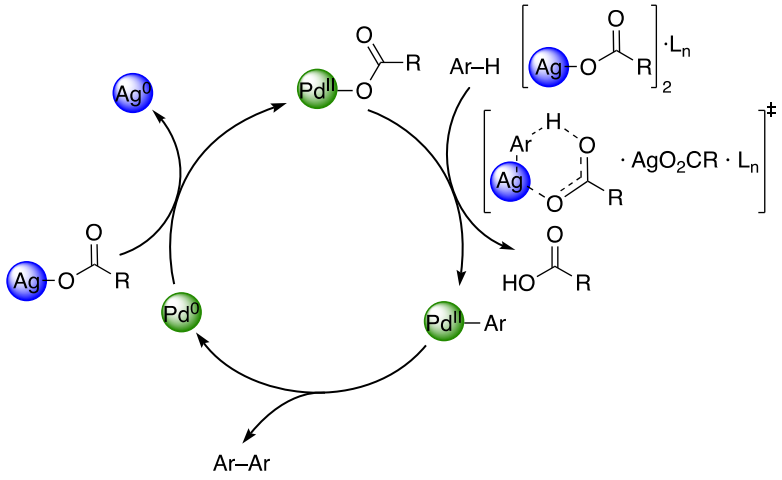

c) Hartwig: Pd-catalyzed allylation by Ag-mediated C–H activation

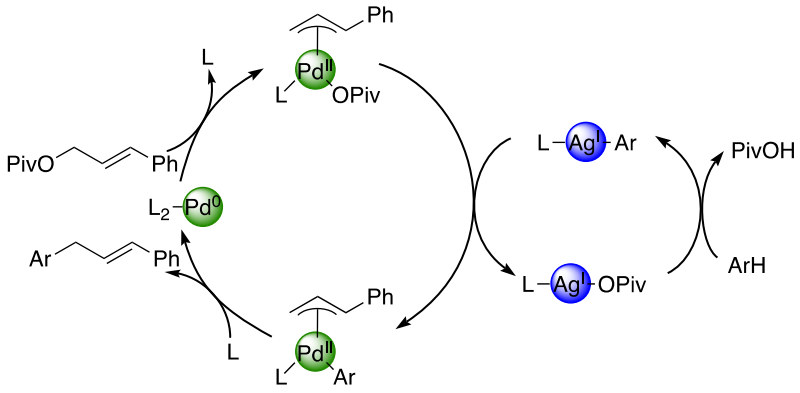

Figure 3.9. Proposed catalytic cycles for Ag(I)-mediated C–H arylation. a) Larrosa[20], b) Sanford[21], and c) Hartwig[22].

Subsequently, H/D exchange between C_6F_5H and D_2O catalyzed by various metal pivalates showed 63% deuterium incorporation in reactions with AgOPiv, as opposed to 9% using CsOPiv. This provided evidence that AgOPiv and C_6F_5H react to generate Ag–C_6F_5, which can then transmetallate Pd to form the resulting product **38** (Figure 3.9a). Sanford and co-workers also showed computationally that a Ag–Ag dimeric TS structure **39** bearing two axial dioxane ligands is lower in energy than the dimer with free axial coordination sites (Figure 3.10b). Based on their DFT calculations, monomeric AgOPiv is unlikely to be the reactive species in this reaction.

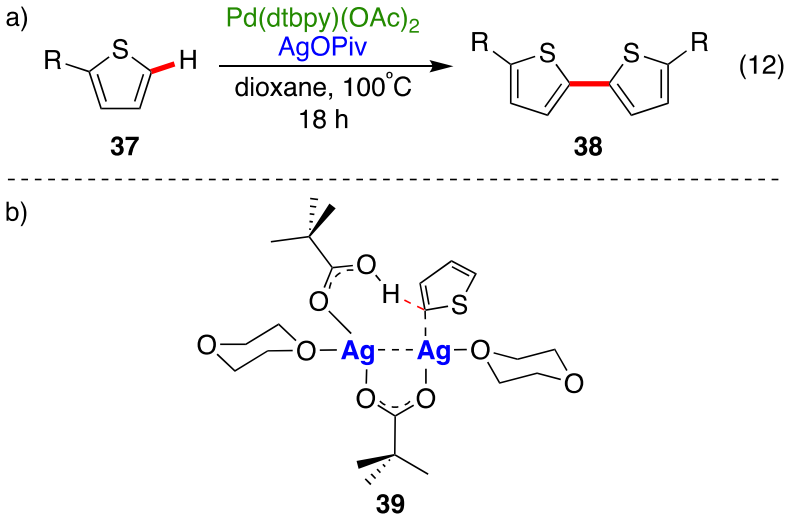

Figure 3.10. Pd-catalyzed oxidative dimerization of 2-alkylthiophenes. a) Reaction of interest. (b) Proposed transition structure for CMD across two Ag centers.

In both studies by Larrosa and Sanford, the silver carboxylate was shown to be capable of cleaving the C–H bonds in arenes. Hartwig and co-workers expanded on the work of Larrosa and Sanford and isolated a phosphine-ligated arylsilver(I) species. They demonstrated its ability to undergo transmetallation of the aryl group to palladium, and its competency as a reaction intermediate in the catalytic process (Figure 3.9c).[22] They report a method of a highly site-selective formation of C(aryl)–C(sp_3) bonds by the Pd-catalyzed and Ag-mediated allylation of aryl C–H bonds **40** with allylic pivalates to make (*E*)-allylarenes **42** (Figure 3.11). A synergistic catalytic process is proposed in which cleavage of an aryl C–H bond occurs through a

phosphine-ligated AgOPiv complex that exists as two rotamers, **43** or **44**. L-AgOPiv reacts with an arene to form an arylsilver intermediate through a pivalate-assisted CMD mechanism. Then, a (π-allyl)palladium pivalate species is formed after aryl transfer, followed by reductive elimination to afford the allylarene product **42** and PdL_2. Hartwig isolated and characterized the Pd and Ag intermediates by X-ray crystallography. This provides convincing support for the proposed catalytic cycle.

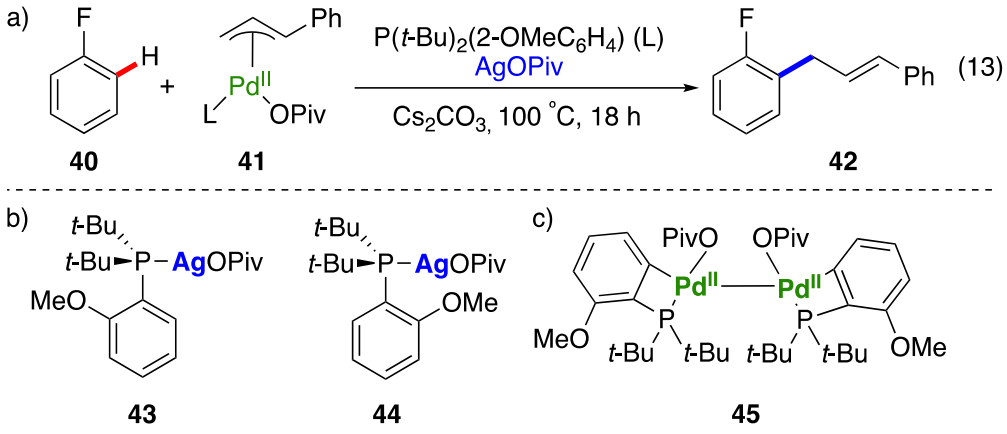

Figure 3.11. Pd-catalyzed direct allylation of arenes with allyllic pivalates. a) Reaction of interest in the presence of AgOPiv, b) Ligated AgOPiv complex, c) Resting state of Pd catalyst during the allylation

3.5 Conclusions

The role of Ag(I)-salts has been described here for various Pd-catalyzed C–H activation processes. A growing number of reports in the area of heterometallic Pd–Ag transition metal catalysis suggest that either a cooperative effect occurs between Pd and Ag throughout the catalytic cycle, or silver carboxylates can cleave the C–H bonds in arenes, and the resulting arylsilver(I) complex can transfer its aryl moiety to a Pd intermediate. More studies are necessary to assess the extent of the contribution of Ag(I) salts in cases other than C–H arylation reactions. An understanding of these reactions will be beneficial to the further development and application of heterometallic C–H activation processes.

3.6 References

[1] For selected examples, see: (a) Zaitsev, V. G.; Shabashov, D.; Daugulis, O. *J. Am. Chem. Soc.* **2005**, *127*, 13154; (b) Yang, S.; Li, B.; Wan, X.; Shi, Z. *J. Am. Chem. Soc.* **2007**, *129*, 6066; (c) Hull, K. L.; Sanford, M. S. *J. Am. Chem. Soc.* **2007**, *129*, 11904; (d) Stuart, D. R.; Villemure, E.; Fagnou, K. *J. Am. Chem. Soc.* **2007**, *120*, 12072; (e) Inamoto, K.; Saito, T.; Katsuno, M.; Sakamoto, T.; Hiroya, K. *Org. Lett.* **2007**, *9*, 2931; (f) Cornella, J.; Lu, P.; Larrosa, I. *Org. Lett.* **2009**, *11*, 5506; (g) He, C.-Y.; Fan, S.; Zhang, X. *J. Am. Chem. Soc.* **2010**, *132*, 12850; (h) René, O.; Fagnou, K. *Org. Lett.* **2010**, *12*, 2116; (i) Ano, Y.; Tobisu, M.; Chatani, N. *J. Am. Chem. Soc.* **2011**, *133*, 12984; (j) Ozaki, K.; Zhang, H.; Ito, H.; Lei, A.; Itami, K. *Chem. Sci.* **2013**, *4*, 3416; (k) Strambeanu, I. I.; White, M.C. *J. Am. Chem. Soc.* **2013**, *135*, 12032; (l) Luo, J.; Preciado, S.; Larrosa, I. *J. Am. Chem. Soc.* **2014**, *136*, 4109.

[2] (a) Torisawa, Y.; Nishi, T.; Minamikawa, J. *J. Bioorg. Med. Chem. Lett.* **2000**, *10*, 2493−2496. (b) Shul'pin, G. B. *J. Mol. Catal. A: Chem.* **2002**, *189*, 39−66. (c) Mee, S. P. H.; Lee, V.; Baldwin, J. E. *Angew. Chem., Int. Ed.* **2004**, *43*, 1132−1136. (d) Fairlamb, I. J. S.; Taylor, R. J. K; Serrano, J. L.; Sanchez, G. *New J. Chem.* **2006**, *30*, 1695−1704.

[3] Arroniz, C.; Denis, J. G.; Ironmonger, A.; Rassias, G.; Larrosa, I. *Chem. Sci.* **2014**, *5*, 3509.

[4] (a) Kraatz, H.-B.; van der Boom, M. K.; Ben-David, Y.; Milstein, D. *Isr. J. Chem*. **2001**, *41*, 163. (b) Lanci, M. P.; Remy, M. S.; Kaminsky, W.; Mayer, J. M.; Sanford, M. S. *J. Am. Chem. Soc.* **2009**, *131*, 15618.

[5] Masui, K.; Ikegami, H.; Mori, A. *J. Am. Chem. Soc.* **2004**, *126*, 5074–5075.

[6] Hull, K. L.; Sanford, M. S. *J. Am. Chem. Soc.* **2007**, *129*, 11904–11905.

[7] (a) Stuart, D. R.; Villemure, E.; Fagnou, K. *J. Am. Chem. Soc.* **2007**, *129*, 12072–12073. (b) DeBoef, B. *Tetrahedron Letters* **2008**, *49*, 4050–4053.

[8] Chang, S. *J. Am. Chem. Soc.* **2008**, *130*, 9254–9256.

[9] Wu, T.; Mu, X.; Liu, G. *Angew. Chem., Int. Ed.* **2011**, *50*, 12578−12581.

[10] Neo, Y. C.; Vittal, J. J.; Hor, T. S. A. *J. Chem. Soc*., *Dalton Trans.* **2002**, 337–342.

[11] Micksch, M.; Herdtweck, E.; Strassner, T.; Anorg. Z. *Allg. Chem.* **2013**, *639*, 1237–1241.

[12] Kozitsyna, N. Y.; Nefedov, S. E.; Klyagina, A. P.; Markov, A. A.; Dobrokhotova, Z. V.; Velikodny, Y. A.; Kochubey, D. I.; Zyubina, T. S.; Gekhman, A. E.; Vargaftik, M. N.; Moiseev, I. I. *Inorg. Chim Acta.* **2011**, *370*, 382.

[13] Leow, D.; Li, G.; Mei, T.-S.; Yu, J.-Q. *Nature* **2012**, *486*, 518.

[14] Yang, Y.-F.; Cheng, G.-J.; Liu, P.; Leow, D.; Sun, T.-Y.; Chen, P.; Zhang, X.; Yu, J.-Q.; Wu, Y.-D.; Houk, K. N. *J. Am. Chem. Soc.* **2014**, *136*, 344–355.

[15] Yoo, E. J.; Ma, S.; Mei, T.-S.; Chan, K. S. L.; Yu, J.-Q. *J. Am. Chem. Soc.* **2011**, *133*, 7652–7655.

[16] (a) Anand, M.; Sunoj, R. B.; Shaefer, H. F.; *J. Am. Chem. Soc.* **2014**, *136*, 5535–5538. (b) Anand, M.; Sunoj, R. B.; Shaefer, H. F. *ACS Catalysis* **2016**, *6*, 696–708.

[17] Lee, S.; Lee, H.; Tan, K. L. *J. Am. Chem. Soc.* **2013**, *135*, 18778–18781.

[18] Fang, L.; Saint-Denis, T. G.; Taylor, B. L. H.; Ahlquist, S.; Hong, K.; Liu, S.; Han, L.; Houk, K. N.; Yu, J.-Q. *J. Am. Chem. Soc.* **2017**, *139*, 10702–10714.

[19] Zhang, L.; Zhao, C.; Liu, Y.; Xu, J.; Xu, X; Zhong, J.; *Angew. Chem. Int. Ed.* **2017**, *56*, 12245–12249.

[20] Whitaker, D.; Bures, J.; Larrosa, I. *J. Am. Chem. Soc.* **2016**, *138*, 8384–8387.

[21] Lotz, M. D.; Camasso, N. M.; Canty, A. J.; Sanford, M. S. *Organometallics* **2017**, *36*, 165–171.

[22] Lee, S. Y.; Hartwig, J. F. *J. Am. Chem. Soc.* **2016**, *138*, 15278–15284.

Chapter 4. Rational Development of Remote C–H Functionalization of Biphenyl: Experimental and Computational Studies

4.1 Abstract

We report simple and efficient nitrile-directed *meta*-C–H olefination, acetoxylation and iodination of biaryls. Compared to our previous approach of installing a complex U-shaped template to achieve a molecular U-turn and assemble the large sized cyclophane transition state for the remote C–H activation, a synthetically useful phenyl nitrile functional group could also direct remote *meta*-C–H activation. This reaction provides a useful method for modifying biaryl compounds because the nitrile can be readily converted to amines, acids, amides or other heterocycles. Notably, the remote *meta*-selectivity of biphenylnitriles could not be expected from previous results with a macrocyclophane nitrile template. DFT computational studies now show that a ligand-containing Pd–Ag heterodimeric transition state (TS) favors the desired remote *meta*-selectivity. Control experiments demonstrate the directing effect of the nitrile and exclude the possibility of non-directed *meta*-C–H activation. Substituted 2-pyridone ligands were found to be key in assisting the cleavage of the *meta*-C–H bond in the concerted metalation-deprotonation (CMD) process.

4.2 Introduction

Remote C–H bond activation/functionalization is essential for ultimately realizing molecular editing of organic structures through site-selective C–H functionalizations.[1] Previously, a number of approaches including electronic and steric effects have been exploited to achieve the site-selectivity of remote C–H activation of aromatic substrates.[2] In 2012, the Yu group has designed a nitrile-containing U-shaped template that directs remote *meta* C–H bonds of benzyl derivatives via a macrocyclophane-like palladated intermediate.[3] The combination of both distance and geometry was recognized as a very effective strategy to obtain the site-selectivity of remote C–H activation. We and others subsequently developed a number of U-shaped nitrile

templates for *meta*- or *para*-selective C–H functionalization of aromatic alcohols, carboxylic acids and amines.[4]

Biphenyl derivatives have wide applications in ligand design as well as in pharmaceuticals.[5] Although a lot of biphenyl scaffolds have been synthesized via Suzuki coupling, however, presence of olefin moiety is not tolerated because of the competition and interference of Heck coupling. Due to the nitrile group is a transformable handle that can conduct a multitude of further transformations into an amine, acid, amide, ketone and heterocycle,[6] the use of readily available biphenyl nitrile substrates to direct remote C–H activation is a very powerful method for biaryl synthesis. In our previous work, we installed a U-template to afford *meta*-selective C–H functionalization of biaryl carboxylic acids (Scheme 4.1a).[3] Computational analysis showed that such design requires a molecular U-turn and a large ring size of the cyclophane transition state.[7] We compared the three possible Pd-containing transition state (TS) species: monomeric $Pd(OAc)_2$, dimeric $Pd_2(OAc)_4$ and heterodimeric $PdAg(OAc)_3$. Interestingly, the Pd–Ag heterodimeric species gave lower activation barriers for CMD C–H activation step.[7b-c] Encouraged by the computational heterodimeric transition state, we envisioned that the installed U-shaped template for the assembly of the large sized cyclophane transition state may not be necessary for *meta*-C–H activation. Instead, the linear nitrile could coordinate to the dimeric transition metal and lead to a similar U-turn to reach the *meta* C–H bond. In this work, we use a 2-cyanobiphenyl substrate to compare the monomeric and dimeric transition states, and show that the Pd–Ag dimeric TS is predicted to give excellent *meta*-selectivity (Scheme 4.1b).

We report 2-pyridone ligand-promoted *meta*-selective C–H olefination, acetoxylation and iodination of the biaryl derivatives via Pd(II)/Pd(0) or Pd(II)/Pd(IV) catalysis (Scheme 4.1c). This approach avoids the design and installation of U-template to accomplish the high *meta*-selectivity. The modified 2-pyridone ligand improves the reactivity and gives moderate to good yields for all three transformations of biaryls. Computational studies reveal that the *meta*-

selectivity resulted from the flexibility of a ligand-containing dimeric transition state structure. The free energy calculations for the *meta*-selective olefination pathway indicate that the CMD C–H activation step is the turnover-limiting step, which is also implied by the large experimentally found KIE values. Compared to the acetate pathway, the involvement of two 2-pyridone ligands gives lower energetic barriers in the all of steps of the mechanism.

Scheme 4.1. Rational development of *meta*-selective C–H functionalizations of biphenyls.

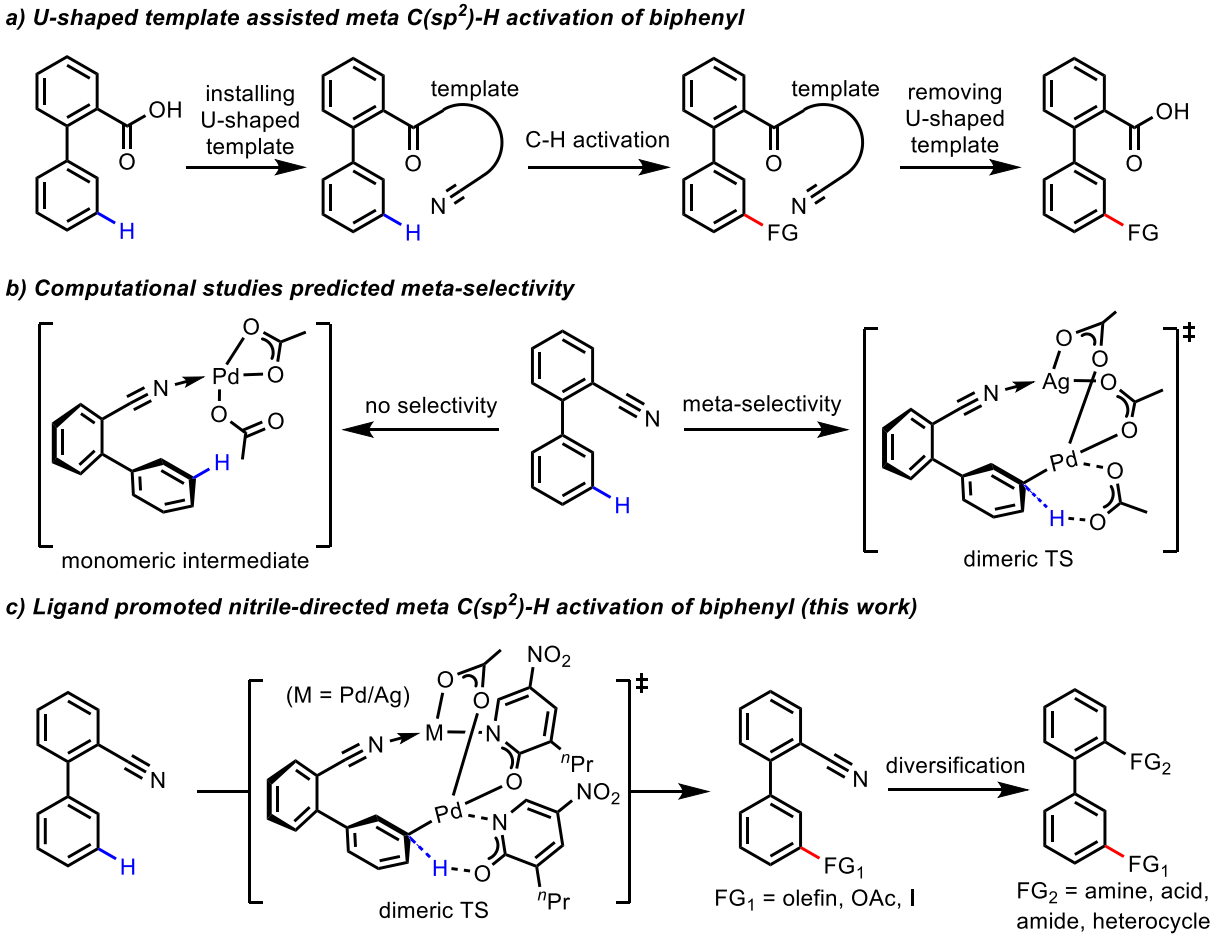

4.3 Results and Discussion

Based on the computed Pd-Ag dimeric model involving simple phenyl nitrile, we began to investigate the feasibility of achieving remote *meta*-selective C–H olefination of 2-cyanobiphenyl (**1a**) with ethyl acrylate (**2a**) as the coupling partner (Table 4.1). We were pleased to find that under the reaction conditions of 10 mol% of Pd(OAc) and 3.5 equivalent of

AgOAc in HFIP at 80 ^{o}C, the olefination product was isolated in 16% yield with the encouraging *meta*-selectivity (*meta*:others = 4:1). To enhance the reactivity and *meta*-selectivity, we added pivalic acid as the ligand; the yield and selectivity showed slight improvement. Then several additional type of pyridine or quinolone ligands (**L2-L4**)[8] developed by our laboratory were evaluated, but no significant acceleration of the reaction was observed. The poor *meta*-selectivity by **L4** is probably due to the strong sulfonic acid destroying the dimetallic bridge. Inspired by the fact that the MPAA ligand improves the *meta*-selectivity for the U-template directed C–H activation, we tested Ac-Gly-OH and other NHAc group containing bidentate ligands (**L6-L7**);[9] unfortunately, the *meta*-selectivity significantly decreased. We suppose that the bidentate ligands may change the angle of dimetallic bridge to activate the *ortho*- or *para*-C–H bond and give a mixture of olefination products. Recently, our group found that the 2-pyridone ligand is very powerful for assisting the C–H bond cleavage in the CMD process.[10] We propose that the aromatic skeleton of 2-pyridone is probably superior for stabilizing the Pd–Ag dimeric bridge and improving the reactivity and selectivity. A suite of commercial available 2-pyridone ligands (**L8-L20**) were investigated. To our delight, the addition of **L18** afforded *meta*-product **3a** in 61% yield and *meta*-selectivity was up to 6:1. To adjust the electronic property of 2-pyridone for further improving the reaction yield, several 3-alkyl-5-nitropyridone ligands (**L21-L27**) were synthesized. The experimental results showed that **L24** gave the best yield (73%) and selectivity (*meta*:others = 6:1).

To exclude the possibility of non-directed C–H olefination of arenes[10b] and to demonstrate the directing function of nitrile, we conducted several control experiments using other 2-substituted biphenyls under the optimal conditions (Scheme 4.2). Replacing nitrile with the electron-withdrawing (NO_2 and CO_2Me) or electron-donating substituents (Me) gave no *meta*-selectivity, albeit with good yield for the olefination products. The results indicate that non-directed C–H olefination easily occurs in the presence of 2-pyridone ligand, but the *meta*-

Table 4.1. Ligand evaluation for *meta*-selective C–H olefination of 2-cyanobiphenyl. [a] Reaction conditions: **1a** (0.1 mmol), **2a** (5.0 equiv), $Pd(OAc)_2$ (10 mol%), ligand (20 mol%), AgOAc (3.5 equiv), HFIP (2.0 mL), 80 °C, air, 60 h. [b] Isolated yields and the *meta*-selectivity was determined by GC-MS analysis (assisted with $_1$H NMR analysis of the crude reaction mixture). HFIP = 1,1,1,3,3,3-Hexafluoro-2-propanol.

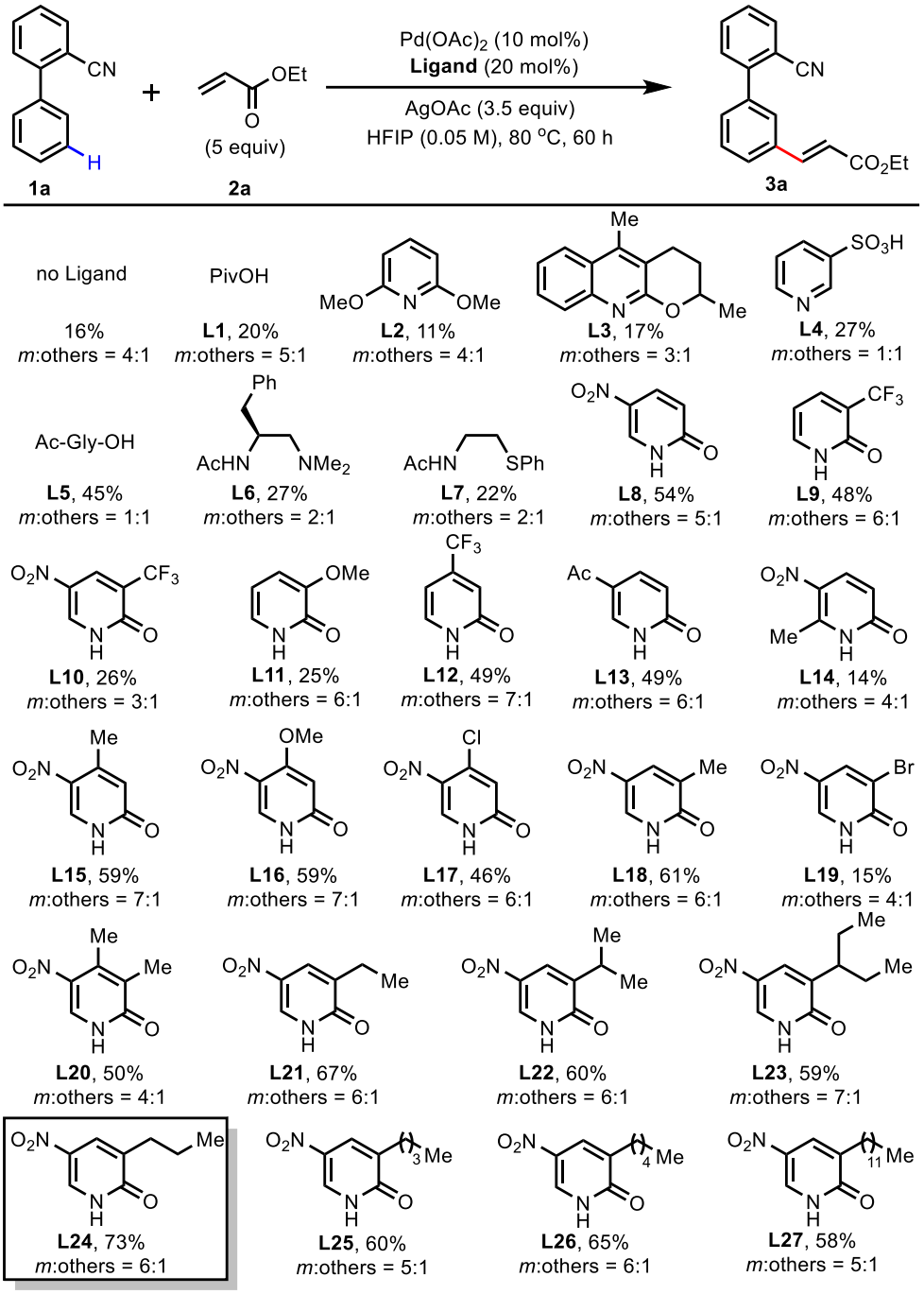

selectivity is hard to control by the electronic biases. Therefore, the directing effect of nitrile is critical for the *meta*-selectivity in the present catalytic cycle.

Scheme 4.2. Control Experiments

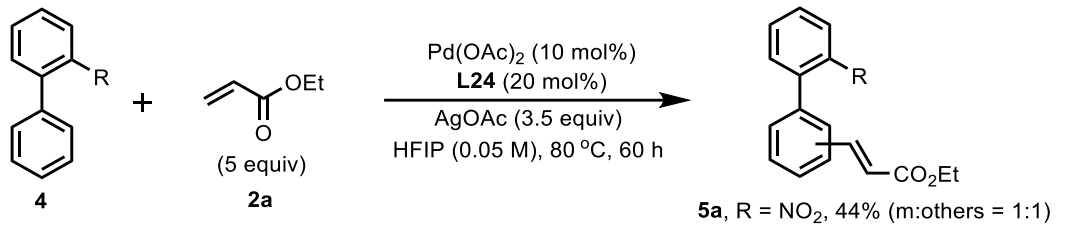

4 **2a**

5a, R = NO_2, 44% (m:others = 1:1)
5b, R = CO_2Me, 14% (m:others = 1:1)
5c, R = Me, 59% mixture

With optimized conditions for *meta*-C–H olefination in hand, we proceeded to investigate the scope of the reaction with biphenyl derivatives (Scheme 4.3). When electron-donating or -withdrawing substituents were attached to the nitrile-containing phenyls, the olefination reaction occurred smoothly and gave the desired products **3b-f** in good yields with high *meta*-selectivity. Because the *ortho*-substitution may contribute to the torsion of biphenyl about the joining single bond to form the favorable activation conformation, high yields and selectivity of **3g**, **3i**, **3q** and **3r** are observed. A broad range of *meta*- and *para*-substituents on the olefination phenyls are tolerated, providing the products in good yields. In the cases of *ortho*- or *para*-chloro-substituted substrates, the electronic biases decrease the yields of the corresponding products **3h** and **3p**, and give lower *meta*-selectivity. In contrast, *meta*-ester substituted biphenyl gave low yield for the desired product **3l** but the selectivity still favored *meta*-position. We surveyed the compatibility of the present *meta*-olefination on the complex natural product derivatives. The reactions were accomplished by treating with biphenyl-containing dihydrocholesterol and menthol derivatives. Despite low yields observed, likely due to steric hindrance, the *meta*-selectivity was good. These biologically active derivatives may provide more possibilities for drug discovery. We also evaluate the C–H olefination reaction on 1 mmol scale to synthesize *meta*-olefination product **3n**, which was purified on a silica gel column to give 71% isolated yield

Table 4.2. Substrate scope for *meta*-C(*sp*$_2$)–H olefination. [a] Reaction conditions: 1 (0.1 mmol), 2a (5.0 equiv), $Pd(OAc)_2$ (10 mol%), L24 (20 mol%), AgOAc (3.5 equiv), HFIP (2.0 mL), 80 °C, air, 60 h. [b] Isolated yields and the *meta*-selectivity was determined by GC-MS analysis (assisted with $_1$H NMR analysis of the crude reaction mixture).

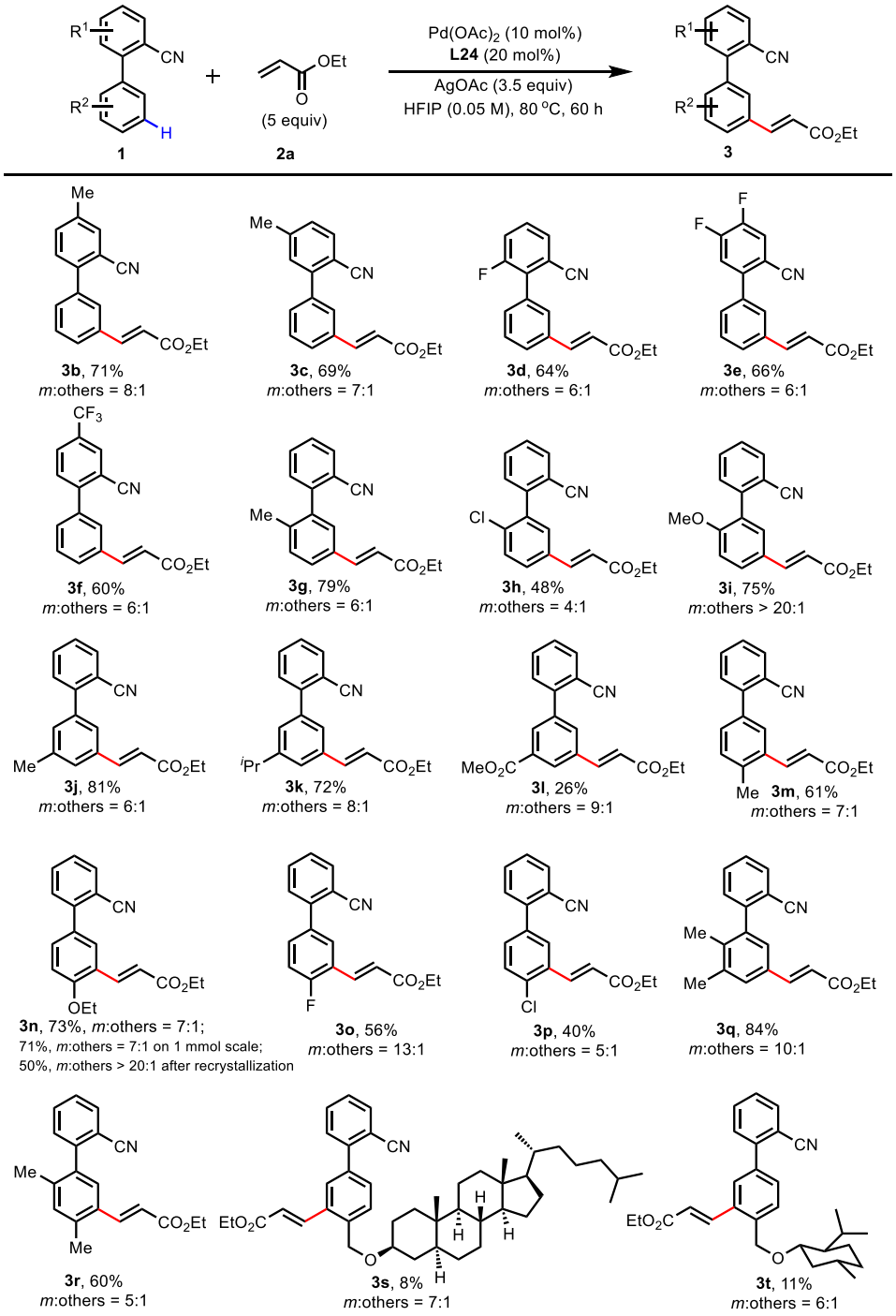

with 7:1 ratio for *meta*:others. The almost pure *meta*-product **3n** was obtained in 50% yield after recrystallization with EA/hexane and *meta*-selectivity is more than 20:1 via H_1 NMR analysis.

We next explored the scope of olefin coupling partners (Scheme 4.4). The acyclic or cyclic α,β-unsaturated esters underwent the olefination and gave the desired products **3u, 3v, 3z** and **3aa** in moderate to good yields with high selectivity. The geometry of the **3z** was determined to be *Z* configuration comparing the $_1$H NMR analysis with the previous literature.[10b] The transformation was also suitable for α,β-unsaturated ketone and amide, albeit providing lower yields (**3w** and **3ab**). Interestingly, the olefins attaching with sulfonate and phosphonate afforded high yields and excellent *meta*-selectivity for the corresponding products **3x-y**.

Table 4.3. Olefin scope for *meta*-C(sp$_2$)–H olefination. [a] Reaction conditions: **1a** (0.1 mmol), **2** (5.0 equiv), $Pd(OAc)_2$ (10 mol%), **L24** (20 mol%), AgOAc (3.5 equiv), HFIP (2.0 mL), 80 °C, air, 60 h. [b] Isolated yields and the *meta*-selectivity was determined by GC-MS analysis (assisted with $_1$H NMR analysis of the crude reaction mixture).

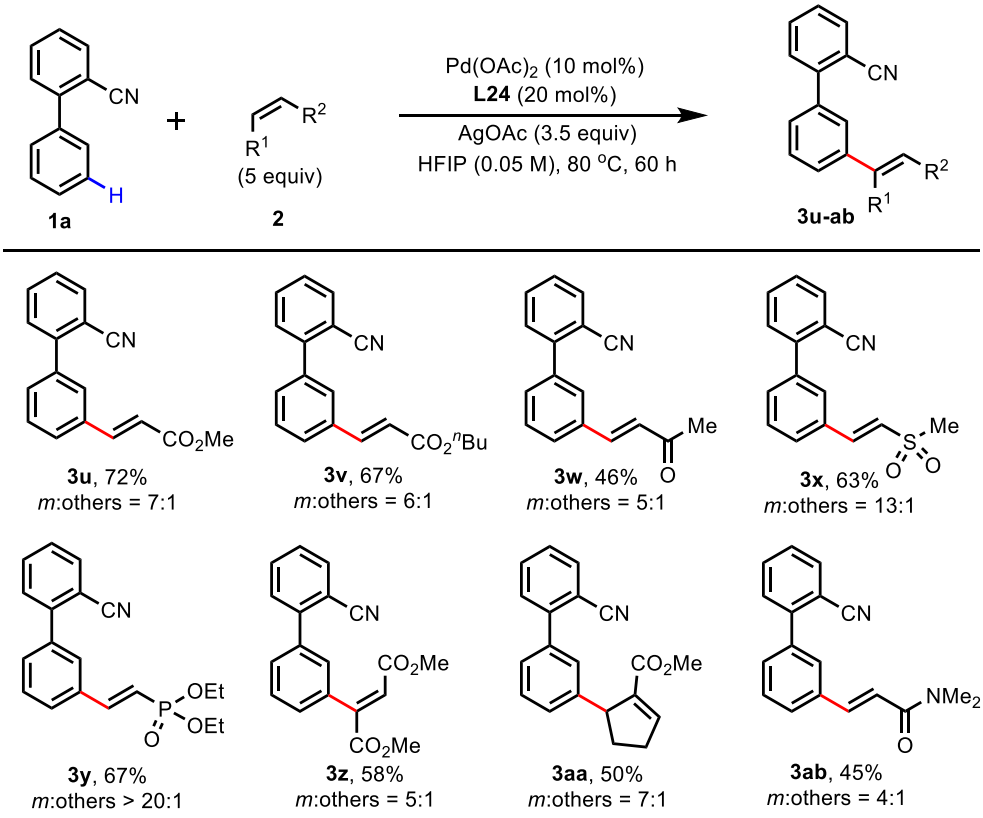

Having established the feasibility of nitrile-directed *meta*-C–H olefination, we turned our attention to the use of the catalytic system to investigate other *meta*-C–H transformations. We first attempted to use Pd(II)/Pd(IV) catalysis to realize the *meta*-acetoxylation reaction under the nitrile-template directed *meta*-C–H oxidation conditions (Scheme 4.5).[4d-e] Fortunately, when the $PhI(OAc)_2/Ac_2O$ oxidation system was employed, the *meta*-oxidation product **6a** was isolated in 51% yield with 9:1 ratio of *meta*:others. The yield of **6a** significantly dropped in the presence of AgOAc as the oxidant, indicating no Pd–Ag dimeric complex was involved in this catalytic cycle. A variety of substitutions on different positions of biphenyl substrates were tested, giving the desired products **6b-g** in moderate yields with good selectivity. We proposed that the Pd–Pd dimeric intermediate having higher activation barriers is less favorable than Pd–Ag species, which led to the lower reactivity of oxidation reaction than olefination. In order to accomplish diverse *meta*-selective transformations, we then studied the *meta*-C–H iodination reaction. As shown in Scheme 4.6, *meta*-C–H iodination reaction has been realized using *N*-iodosuccinimide (NIS) as iodinating reagent via Pd(II)/Pd(IV) catalysis.

Scheme 4.3. Representative examples for *meta*-C(sp_2)–H iodination. [a] Reaction conditions: **1** (0.1 mmol), *N*-Iodosuccinimide (3.0 equiv), $Pd(OAc)_2$ (10 mol%), **L24** (20 mol%), AgOAc (1 equiv), HFIP (2.0 mL), 100 °C, air, 60 h. [b] Isolated yields and the *meta*-selectivity was determined by GC-MS analysis (assisted with $_1$H NMR analysis of the crude reaction mixture).

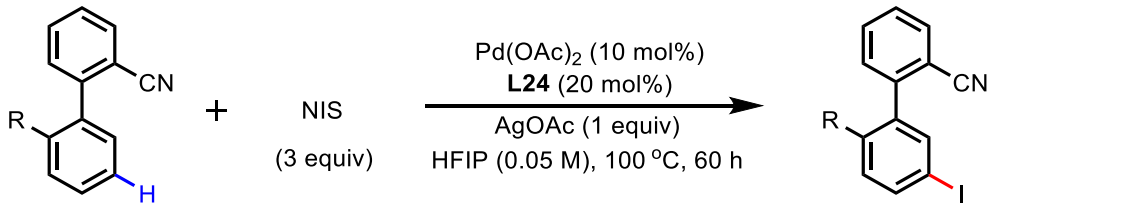

7a, R = H, 40% (*m*:others = 5:1)
7b, R = OMe, 79% (*m*:others > 20:1)

To showcase the broad synthetic utility of biphenyl nitrile, the *meta*-functionalization products were converted to diverse functional groups (Scheme 4.7). The olefination product **3a** was firstly reduced to aliphatic motif **8**, which is more common in nature, and then the further

reduction of **8** afforded a free amine and alcohol-bearing biphenyl **9**. The nitrile could be easily converted to amide **10** and ester **11** under basic or acidic condition, respectively. Remarkably, tetrazole derivative **12,** which owns the 2-biphenyl tertazole privilege skeleton of anti-hypertension Sartan drugs,[11] could also be generated in the presence of azide reagent.

Scheme 4.4. Diversifying transformations of nitrile directing group. a) Pd/C (20%), H_2, EtOH, 40 ^oC, 1 h; b) $LiAlH_4$ (6 equiv), Et_2O, rt, 5 h; c) 30% H_2O_2, K_2CO_3 (20 equiv), DMSO/H_2O, rt, 15 h; d) AcOH, H_2O/H_2SO_4, 120 ^oC, 6 h; after work-up, H_2SO_4 (5 drops), EtOH, 90 ^oC, 3 h; e) $TMSN_3$ (12 equiv), Bu_2SnO (0.3 equiv), toluene, 80 ^oC, 2 days.

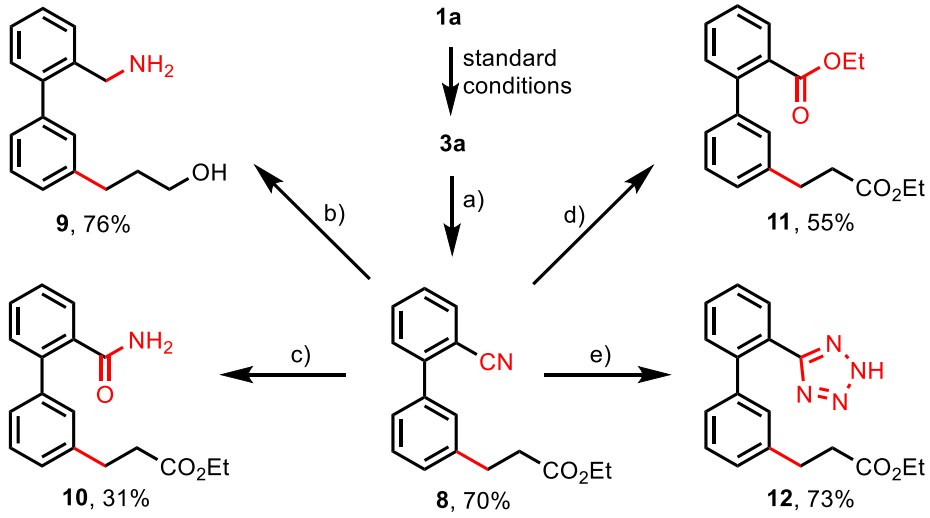

Mechanistic experiments were conducted to support the proposed origins of *meta*-selectivity. We initially performed a H/D exchange experiment of deuterated substrate **[D_5]-1a** in the presence of 5 equivalents of water (Scheme 4.8a), but no protonated product as well as starting material was observed, supporting that the C–H bond cleavage is irreversible. Kinetic isotope effect (KIE) studies were also conducted (Scheme 4.8b). The intermolecular competition experiments provided a P_H/P_D value of 4.6 and parallel KIE was measured and the value of k_H/k_D was 2.6. These results indicate that C–H cleavage is probably the turnover-limiting step.[12]

Scheme 4.5. Preliminary mechanistic studies.

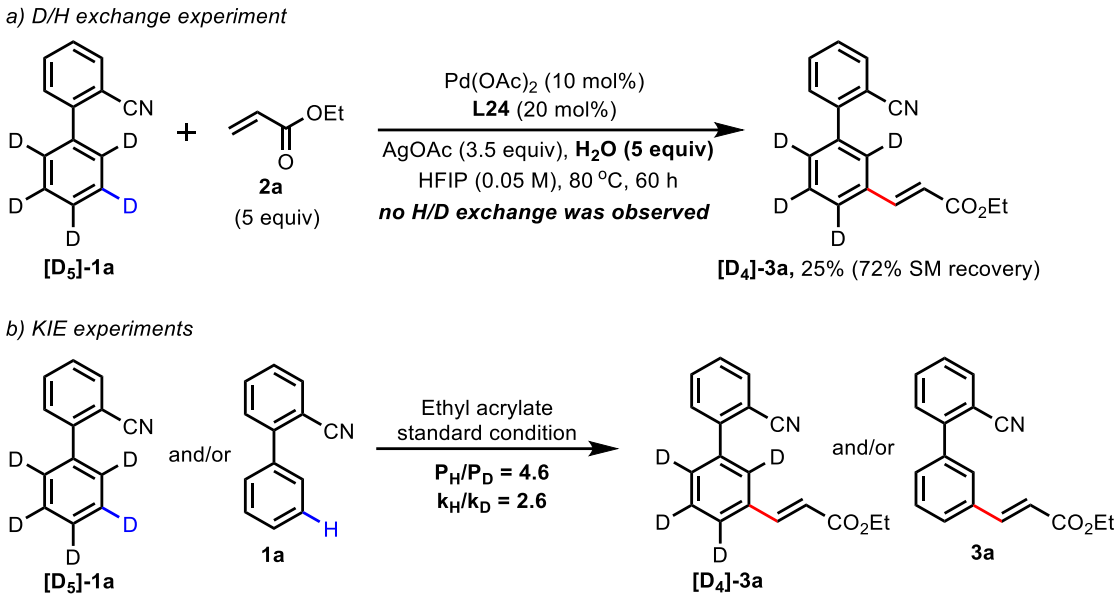

We conducted the computational studies to understand how the *meta*-selectivity occurred, and why the 2-pyridone ligand promoted reactivity. Quantum mechanical calculations were performed with Gaussian 09.[13] Ground state and transition state geometries were optimized in the gas phase using the B3LYP-D3[14] functional with the 6-31G(d)[15] basis set for all nonmetal atoms and the LANL2DZ[16] basis set with effective core potential (ECP) for Pd. Single-point corrections were calculated using Truhlar's M06[17] functional with the 6-311++G(d,p)[18] basis set for all nonmetal atoms and the SDD[19] effective core potential for Pd. Single-point solvation energies were calculated by using SMD solvation model (solvent = generic, eps = 16.7, epsinf = 1.625625) to model HFIP. Vibrational frequencies were computed to determine if the optimized structures are minima or saddle points on the potential energy surface corresponding to minima and transition state geometries, respectively. The reported free energies include zero-point energies and thermal corrections calculated at 298.15 K and 1 atm. Molecular structures were illustrated with CYLview.[20]

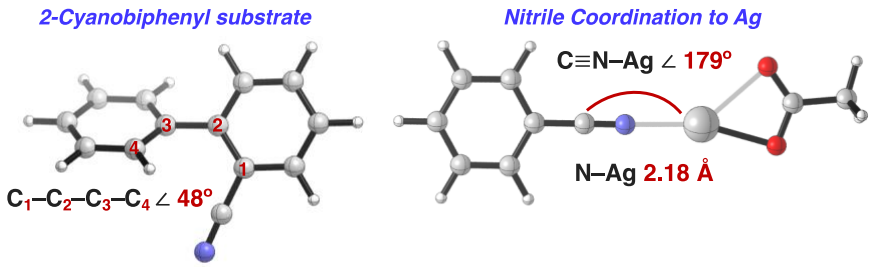

Figure 4.1. Optimized geometries and angles of the substrate and AgOAc model.

First, we investigated the intrinsic optimized geometries of the 2-cyanobiphenyl substrate and a model system of a benzonitrile group coordinated to an Ag center (Figure 4.1). The substrate has a C_1–C_2–C_3–C_4 dihedral angle of 48º. The optimal C≡N–Ag angle of benzonitrile is 179º, showing that linear coordination to the metal center dictates a strong ligand binding.

In order to understand the origin of *meta*-selectivity, we investigated and compared several possible *ortho*-, *meta*- and *para*-selective CMD transition state structures involving a $Pd(OAc)_2$ monomer, a $Pd_2(OAc)_4$ dimer, and a $PdAg(OAc)_3$ heteronuclear dimer using an acetate ligand to assist CMD process (Figure 4.2). To our surprise, each model system was *meta*-selective. The Pd–Ag heterodimeric model gave an energetic barrier 5.7 and 10.0 kcal mol^{-1} lower than the Pd–Pd dimer and Pd monomer models, respectively. Our results are in accord with previous studies of Pd-catalyzed *meta*-selective C–H activation reactions[7b-c] where the longer intrinsic length of a Pd–Ag complex compared to a monomeric Pd complex accommodates a more favorable coordination of the 2-cyanobiphenyl substrate.

We found the 2-pyridone ligand gives an improvement of *meta*-selectivities. To explain the observation, we compared the free energies of 2-pyridone and acetate assisted CMD TS. To construct the 2-pyridone-containing TS, the first question is how many 2-pyridone ligands are coordinated to the metal centers at the CMD TS? In order to reduce computational burden, we use zero, one, two, and three 2-pyridone ligand **L18** instead of **L24** to compare the relative free energies of TSs. Interestingly, the CMD TS was lowest in energy when one **L18** bridged the Pd

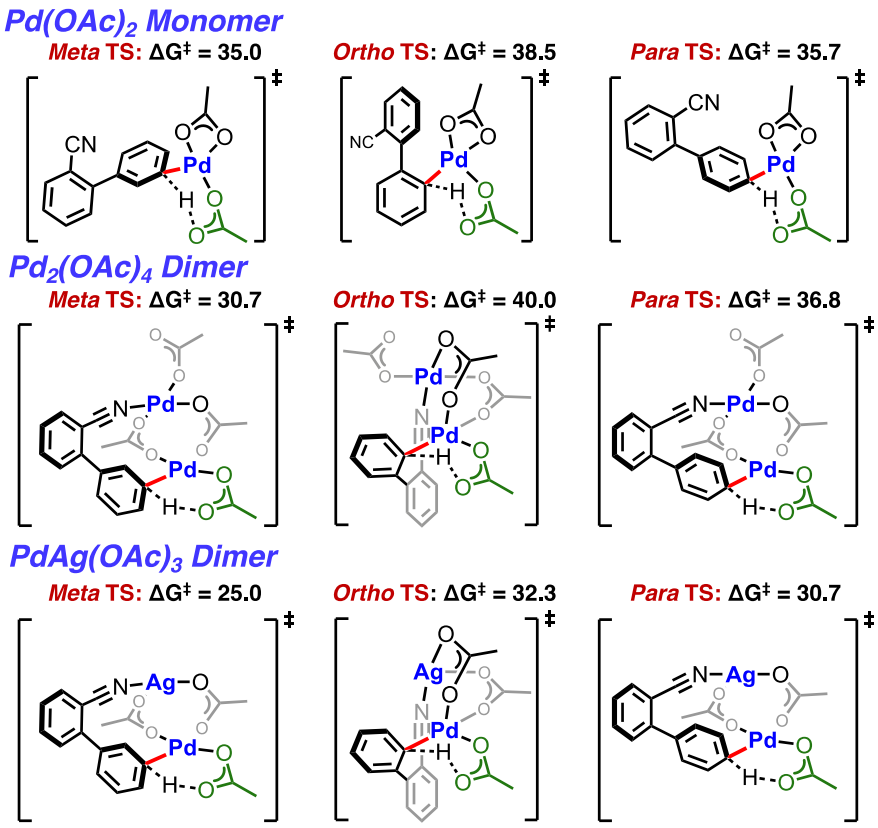

Figure 4.2. Summary of CMD transition structures in the presence of an acetate ligand.

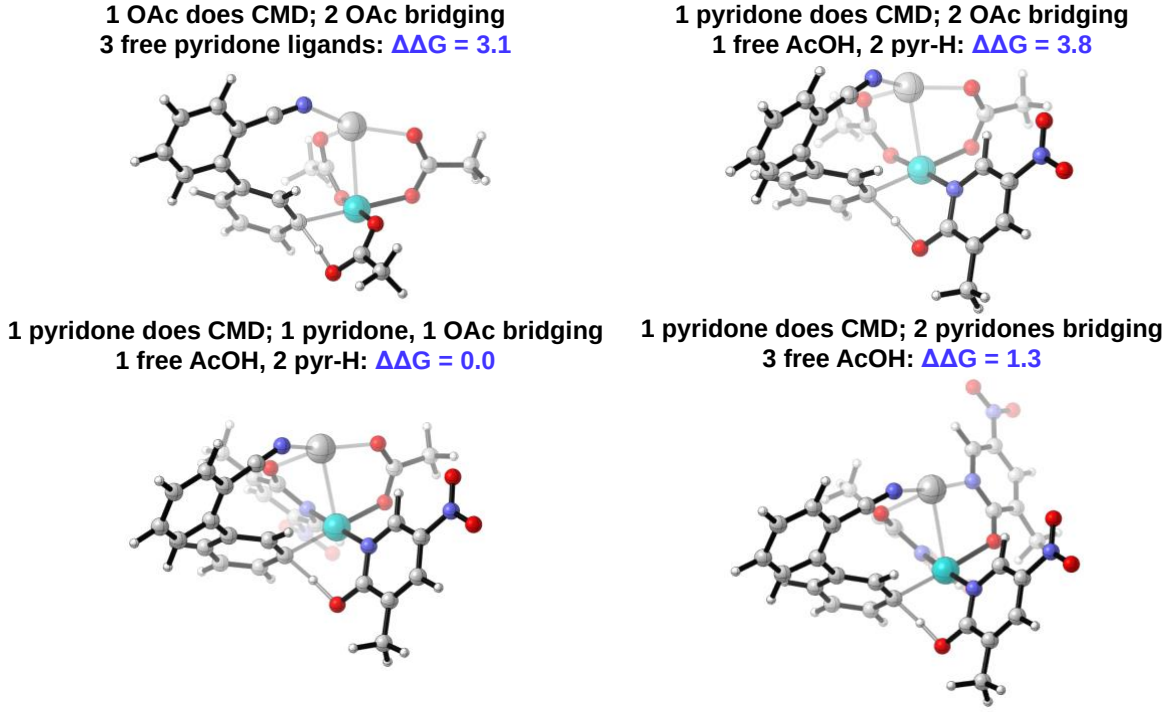

Figure 4.3. Varying the number of L18 at the $PdAg(OAc)_3$ *meta*-selective CMD TS.

and Ag metal centers while another **L18** assist CMD. Using these calculations, we found the optimal $PdAgL_2(OAc)$ TS (Figure 4.3).

The detailed *ortho*-, *meta*- and *para*-selective $PdAgL_2(OAc)$ CMD transition states are shown in Figure 4. In the *ortho*-selective transition state structure, we found that the dihedral angle between carbons 1-4 is about 115º, but the dihedral angle of an optimized 2-cyanobiphenyl by itself is 48º. Also, the C≡N–Ag angle is 104º, which is far from an ideal ligand-to-metal coordination angle of 179º. This causes the Ag–N bond distance to increase to 2.45 Å. The *para*-selective TS in blue shows similar characteristics to the *ortho*-TS where a longer N–Ag bond distance destabilizes the TS structure. But the *meta*-selective CMD TS in green has the lowest energetic barrier of 21.9 kcal mol^{-1}, and its dihedral angle between carbons 1-4 of 48º shows that the substrate has not been as distorted as seen in *ortho*- or *para*-TS structures. Also the N–Ag distance is much shorter, at 2.26 Å, indicating a stronger chelation to Ag, which stabilizes the TS. Also, the shorter C–H bond distance indicates an earlier transition state for *meta*-selectivity, which shows the ease of achieving the most favorable *meta*-TS structure.

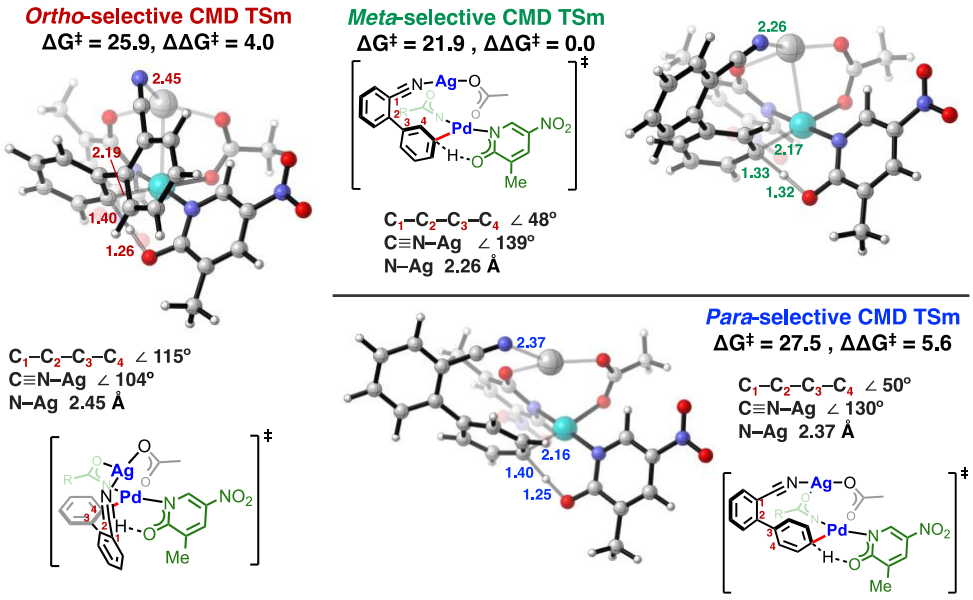

Figure 4.4. $PdAgL_2(OAc)$ CMD transition state structures for *ortho*-, *meta*- and *para*-selectivities.

We also analyzed the distortion energy at the transition state. To do this, we separated both the reactant complex and transition state structures into two parts: the substrate includes the 2-cyanobiphenyl with the proton undergoing CMD while the catalyst contains everything else in the system. We performed single point calculations of the two separated parts, the substrate and the catalyst, for reactant complex 1 and *meta*- selective CMD TS structure. Then we subtracted the energy of the substrate in the CMD TS from the energy of the substrate in the reactant complex to obtain the distortion energy of the substrate, E_{sub} (Figure 4.5). The same can be done to find the distortion energy of the catalyst E_{cat}, where this equals the energy of the catalyst in the CMD TS minus the energy of the catalyst in the reactant complex. To get the total distortion energy E_{total}, we add E_{sub} + E_{cat} together and overall, we found that the total distortion of the *meta*-structure was the smallest in comparison to that of the *ortho*- and *para*-structures.

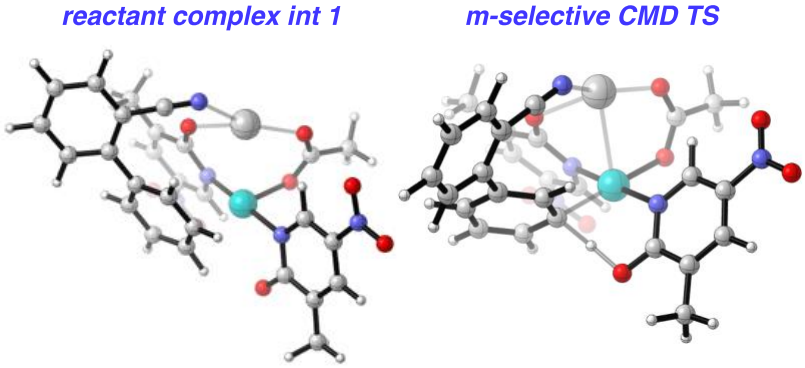

Distortion energy	*Meta* CMD TS	*Ortho* CMD TS	*Para* CMD TS
E_{cat} (kcal/mol)	1.2	3.3	3.6
E_{sub} (kcal/mol)	28.2	36.5	32.4
E_{total} (kcal/mol)	29.5	39.8	36.0

Figure 4.5. Distortion analysis of the CMD TS involving two L18 ligands.

To demonstrate the 2-pyrdione ligand enhanced the reactivity, we used M06 for single point calculations in the free energy profile for the *meta*-pathway in the heterodimeric $PdAg(OAc)_3$ and $PdAgL_2(OAc)$ mechanisms. As shown in Figure 4.6, the $PdAgL_2(OAc)$ mechanism lowers the energy barriers of every step compared to the $PdAg(OAc)_3$ mechanism.

Outside of the catalytic cycle, trimeric $Pd_3(OAc)_6$ dissociates into monomeric $Pd(OAc)_2$ and dimeric $Ag_2(OAc)_4$ dissociates into $Ag(OAc)_2$ Two pyridone ligands can displace two acetate groups to form the heterodimeric activated catalyst. The first key step is the CMD C–H activation in which one pyridone acts as a base to deprotonate the arene (**TS 1**), while a new Pd–C bond is formed, leading to **Int 2**. The second step is alkene insertion (**TS 2**) involving the olefin-coordinated palladacycle **Int 3** to form **Int 4**. The third step is β-hydride elimination (**TS 3**)

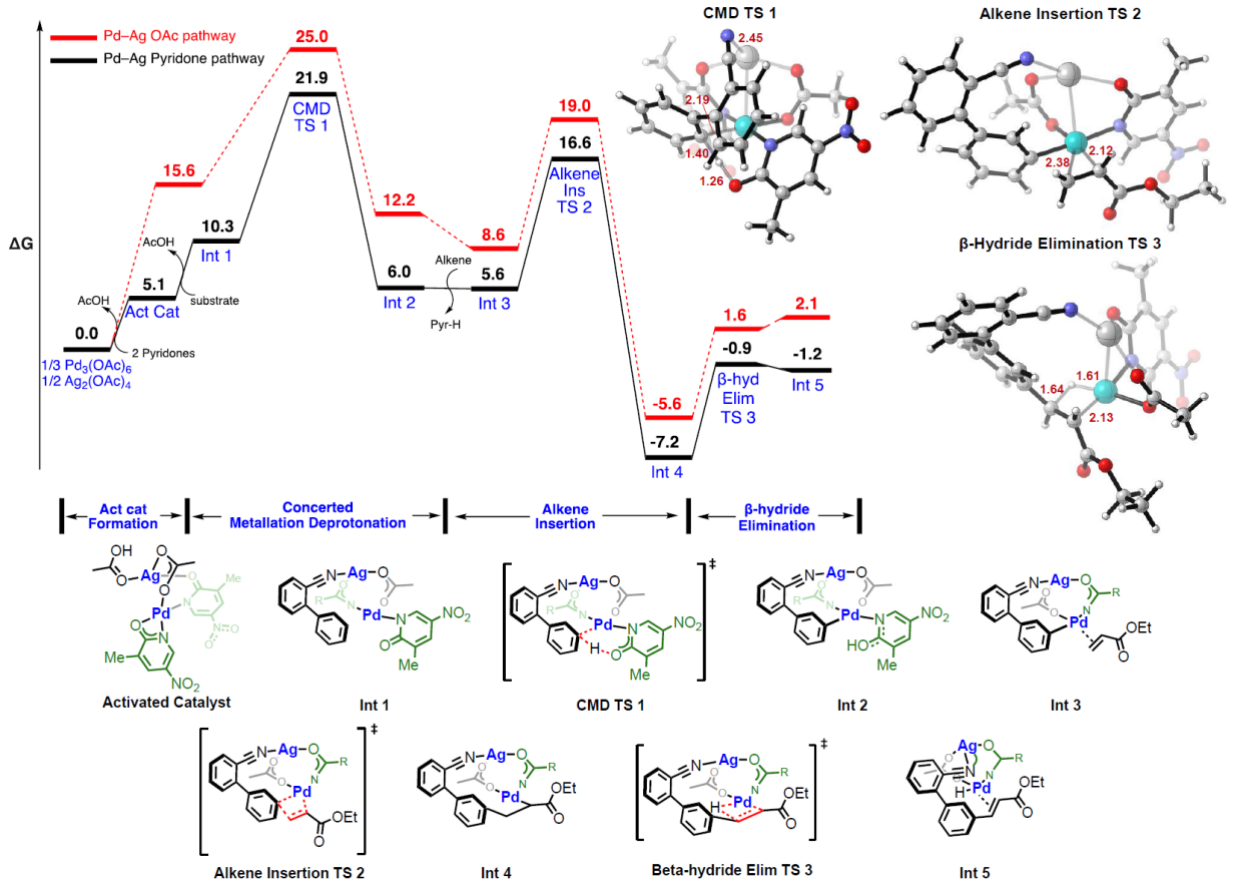

Figure 4.6. Free energy profile for *meta*-selective C–H olefination of 2-cyanobiphenyl. The pathway in red represents the Pd–Ag dimeric system with acetate ligands. The pathway in black represents the Pd–Ag dimeric system with 2-pyridone **L18** ligands. Structures shown above correspond to the pyridone pathway.

where the hydride is transferred to Pd to form the π-complex **Int 5**. In the last few steps of the catalytic cycle, the palladium hydride intermediate **Int 5** undergoes product dissociation, reductive elimination to release the acetic acid, and oxidation of Pd_0 with the Ag_I oxidant to regenerate the Pd_{II} catalyst. There are several possibilities with the different orders of these steps. This process is expected to be highly exergonic and require low activation barriers. The details of these steps were not calculated. The calculation also shows that the C–H activation step suffers highest energy barriers in the whole mechanism, which is consistent with the KIE experimental results.

4.4 Conclusion

We have developed methods for *meta*-C–H olefination, acetoxylation and iodination of 2-cyanobiphenyl derivatives via palladium/2-pyridone catalysis. The 2-pyridone ligand is critical for improving the reactivity and *meta*-selectivity. The reaction could be used to synthesize diversely substituted biaryls due to the versatile transformations of the simple phenyl nitrile. Though the nitrile is spatially and geometrically unfavorable to direct *meta*-C–H activation, DFT calculations proposed a nitrile assisted Pd–Ag dimeric transition state that favors the *meta*-selectivity. Among acetate, NHAc and 2-pyridone as proton acceptor in the CMD process, only 2-pyridone ligand could provide both good yields and highly *meta*-selectivity for these transformations. The computational results also indicated that one molecule of 2-pyridone and one acetate molecule participate in the bimetallic bridge to give the lower energy barriers. The computational dimetallic bridge mechanism opens a new avenue for other remote C–H activation reaction design.

4.5 References

[1] a) R. Breslow, M. A. Winnik, *J. Am. Chem. Soc.* **1969,** *91,* 3083; b) R. Breslow, R. J. Corcoran, B. B. Snider, *J. Am. Chem. Soc.* **1974,** *96*, 6791; c) R. Breslow, *Acc. Chem. Res.* **1980,** *1*3, 170.

[2] For other examples of site-selective C–H activation, see: a) Y.-H. Zhang, B.-F. Shi, J.-Q. Yu, *J. Am. Chem. Soc.* **2009,** *131*, 5072; b) C. Cheng, J. F. Hartwig, *Science* **2014,** *343*, 853; c) R. J. Phipps, M. J. Gaunt, *Science* **2009,** *323*, 1593; d) Y. Yang, R. Li, Y. Zhao, D. Zhao, Z. Shi, *J. Am. Chem. Soc.* **2016,** *138*, 8734; e) Y. Kuninobu, H. Ida, M. Nishi, M. Kanai, *Nat. Chem.* **2015,** *7*, 712; f) H. J. Davis, M. T. Mihai, R. J. Phipps, *J. Am. Chem. Soc.* **2016,** *138*, 12759; g) X.-C. Wang, W. Gong, L.-Z. Fang, R.-Y. Zhu, S. Li, K. M. Engle, J.-Q. Yu, *Nature* **2015,** *519*, 334; h) Z. Dong, J. Wang, G. Dong, *J. Am. Chem. Soc.* **2015,** *137*, 5887; i) O. Saidi, J. Marafie, A. E. Ledger, P. M. Liu, M. F. Mahon, G. Kociok-Köhn, M. K. Whittlesey, C. G. Frost, *J. Am. Chem. Soc.* **2011,** *133*, 19298; j) N. Hofmann, L. Ackermann, *J. Am. Chem. Soc.* **2013,** *135*, 5877.

[3] D. Leow, G. Li, T.-S. Mei, J.-Q. Yu, *Nature* **2012,** *486*, 518.

[4] For examples of nitrile template-directed *meta* or *para* C–H activation, see: a) H.-X. Dai, G. Li, X.-G. Zhang, A. F. Stepan, J.-Q. Yu, *J. Am. Chem. Soc.* **2013,** *135*, 7567; b) S. Lee, H. Lee, K. L. Tan, *J. Am. Chem. Soc.* **2013,** *135*, 18778; c) L. Wan, N. Dastbaravardeh, G. Li, J.-Q. Yu, *J. Am. Chem. Soc.* **2013,** *135*, 18056; d) R.-Y. Tang, G. Li, J.-Q. Yu, *Nature* **2014,** *507*, 215; e) G. Yang, P. Lindovska, D. Zhu, J. Kim, P. Wang, R.-Y. Tang, M. Movassaghi, J.-Q. Yu, *J. Am. Chem. Soc.* **2014,** *136*, 10807; f) S. Bag, T. Patra, A. Modak, A. Deb, S. Maity, U. Dutta, A. Dey, R. Kancherla, A. Maji, A. Hazra, M. Bera, D. Maiti, *J. Am. Chem. Soc.* **2015,** *137*, 11888; g) S. Li, L. Cai, H. Ji, L. Yang, G. Li, *Nat. Commun.* **2016,** *7*, 10443; h) A. Maji, S. Guin, S. Feng, A. Dahiya, V. K. Singh, P. Liu, D. Maiti, *Angew. Chem. Int. Ed.* **2017,** *56*, 14903; *Angew. Chem.* **2017,** *129*, 15099; i) A. Modak, T. Patra, R. Chowdhury, S. Raul, D. Maiti, *Organometallics* **2017,** *36*, 2418; j) L. Zhang, C. Zhao, Y. Liu, J. Xu, X. Xu, Z. Jin, *Angew. Chem. Int. Ed.* **2017,** *56*, 12245; *Angew. Chem.* **2017,** *129*, 12413; k) M. Li, M. Shang, H. Xu, X. Wang, H.-X. Dai, J.-Q. Yu, *Org. Lett.* **2019,** *21*, 540; l) H.-J. Xu, Y.-S. Kang, H. Shi, P. Zhang, Y.-K. Chen, B. Zhang, Z.-Q. Liu, J. Zhao, W.-Y. Sun, J.-Q. Yu, Y. Lu, *J. Am. Chem. Soc.* **2019,** *141*, 76; m) J. Xu, J. Chen, F. Gao, S. Xie, X. Xu, Z. Jin, J.-Q. Yu, *J. Am. Chem. Soc.* **2019,** *141*, 1903.

[5] a) M. E. Welsch, S. A. Snyder, B. R. Stockwell, *Curr. Opin. Chem. Biol.* **2010,** *14*, 347; b) Y.-B. Wang, B. Tan, *Acc. Chem. Res.* **2018,** *51*, 534.

[6] a) C. W. Liskey, X. Liao, J. F. Hartwig, *J. Am. Chem. Soc.* **2010,** *132*, 11389; b) P. Anbarasan, T. Schareina, M. Beller, *Chem. Soc. Rev.* **2011,** *40*, 5049.

[7] a) G.-J. Cheng, Y.-F. Yang, P. Liu, P. Chen, T.-Y. Sun, G. Li, X. Zhang, K. N. Houk, J.-Q. Yu, Y.-D. Wu, *J. Am. Chem. Soc.* **2014,** *136*, 894; b) Y.-F. Yang, G.-J. Cheng, P. Liu, D. Leow, T. Y. Sun, P. Chen, X. Zhang, J.-Q. Yu, Y.-D. Wu, K. N. Houk, *J. Am. Chem. Soc.* **2014,** *136*, 344; c) L. Fang, T. G. Saint-Denis, B. L. H. Taylor, S. Ahlquist, K. Hong, S. Liu, L. Han, K. N. Houk, J.-Q. Yu, *J. Am. Chem. Soc.* **2017,** *139*, 10702; d) Y.-F. Yang, X. Hong, J.-Q. Yu, K. N. Houk, *Acc. Chem. Res.* **2017,** *50*, 2853.

[8] For examples of pyridine or quinolone ligand promoted C–H activation, see: a) J. He, S. Li, Y. Deng, H. Fu, B. N. Laforteza, J. E. Spangler, A. Homs, J.-Q. Yu, *Science* **2014,** *343*, 1216. b) S. Li, G. Chen, C.-G. Feng, W. Gong, J.-Q. Yu, *J. Am. Chem. Soc.* **2014,** *136*, 5267; c) S. Li, R.-Y. Zhu, K.-J. Xiao, J.-Q. Yu, *Angew. Chem. Int. Ed.* **2016,** *55*, 4317; *Angew. Chem.* **2016,** *128*, 4389; d) H. Park, N. Chekshin, P.-X. Shen, J.-Q. Yu, *ACS Catal.* **2018,** *8*, 9292.

[9] a) P.-X. Shen, L. Hu, Q. Shao, K. Hong, J.-Q. Yu, *J. Am. Chem. Soc.* **2018,** *140*, 6545; b) Z. Zhuang, C.-B. Yu, G. Chen, Q.-F. Wu, Y. Hsiao, C. L. Joe, J. X. Qiao, M. A. Poss, J.-Q. Yu, *J. Am. Chem. Soc.* **2018,** *140*, 10363.

[10] For examples of 2-pyridone ligand promoted C–H activation, see: a) P. Wang, M. E. Farmer, X. Huo, P. Jain, P.-X. Shen, M. Ishoey, J. E. Bradner, S. R. Wisniewski, M. D. Eastgate, J.-Q. Yu, *J. Am. Chem. Soc.* **2016,** *138*, 9269; b) P. Wang, P. Verma, G. Xia, J. Shi, J. X. Qiao, S. Tao, P. T. W. Cheng, M. A. Poss, M. E. Farmer, K.-S. Yeung, J.-Q. Yu, *Nature* **2017,** *551*, 489; c) Y.-Q. Chen, Z. Wang, Y. Wu, S. R. Wisniewski, J. X. Qiao, W. R. Ewing, M. D. Eastgate, J.-Q. Yu, *J. Am. Chem. Soc.* **2018,** *140*, 17884; d) R.-Y. Zhu, Z.-Q. Li, H. S. Park, C. H. Senanayake, J.-Q. Yu, *J. Am. Chem. Soc.* **2018,** *140*, 3564.

[11] T. Mavromoustakos, G. Agelis, S. Durdagi, *Expert Opin. Ther. Pat.* **2013,** *23*, 1483.

[12] E. M. Simmons, J. F. Hartwig, *Angew. Chem. Int. Ed.* **2012,** *51*, 3066; *Angew. Chem.* **2012,** *124*, 3120.

[13] M. J. Frisch, G. W. Trucks, H. B. Schlegel, G. E. Scuseria, M. A. Robb, J. R. Cheeseman, G. Scalmani, V. Barone, B. Mennucci, G. A. Petersson, H. Nakatsuji, M. Caricato, X. Li, H. P. Hratchian, A. F. Izmaylov, J. Bloino, G. Zheng, J. L. Sonnenberg, M. Hada, M. Ehara, K. Toyota, R. Fukuda, J. Hasegawa, M. Ishida, T. Nakajima, Y. Honda, O. Kitao, H. Nakai, T. Vreven, J. A. Montgomery, J. E. Peralta, F. Ogliaro, M. Bearpark, J. J. Heyd, E. Brothers, K. N. Kudin, V. N. Staroverov, R. Kobayashi, J. Normand, K. Raghavachari, A. Rendell, J. C. Burant, S. S. Iyengar, J. Tomasi, M. Cossi, N. Rega, J. M. Millam, M. Klene, J. E. Knox, J. B. Cross, V. Bakken, C. Adamo, J. Jaramillo, R. Gomperts, R. E. Stratmann, O. Yazyev, A. J. Austin, R. Cammi, C. Pomelli, J. W. Ochterski, R. L. Martin, K. Morokuma, V. G. Zakrzewski, G. A. Voth, P. Salvador, J. J. Dannenberg, S. Dapprich, A. D. Daniels, Ö. Farkas; J. B. Foresman, J. V. Ortiz, J. Cioslowski, D. J. Fox, Gaussian 09; Gaussian Inc.: Wallingford, CT, **2009**.

[14] a) A. D. Becke, *J. Chem. Phys.* **1993,** *98*, 5648; b) C. Lee, W. Yang, R. G. Parr, *Phys. Rev. B: Condens. Matter Mater. Phys.* **1988,** *37*, 785; c) A. D. Becke, *J. Chem. Phys.* **1993,** *98*, 1372; d) P. J. Stephens, F. J. Devlin, C. F. Chabalowski, M. J. Frisch, *J. Phys. Chem.* **1994,** *98*, 11623.

[15] a) R. Ditchfield, W. J. Hehre, J. A. Pople, *J. Chem. Phys.* **1971,** *54*, 724; b) W. J. Hehre, R. Ditchfield, J. A. Pople, *J. Chem. Phys.* **1972,** *56*, 2257.

[16] a) P. J. Hay, W. R. Wadt, *J. Chem. Phys.* **1985,** *82*, 299; b) L. E. Roy, P. J. Hay, R. L. Martin, *J. Chem. Theory Comput.* **2008,** *4*, 1029.

[17] Y. Zhao, D. G. Truhlar, *Theor. Chem. Acc.* **2008,** *120*, 215.

[18] A. V. Marenich, C. J. Cramer, D. G. Truhlar, *J. Phys. Chem. B* **2009,** *113*, 6378.

[19] a) M. Dolg, U. Wedig, H. Stoll, H. Preuss, *J. Chem. Phys.* **1987,** *86*, 866; b) D. Andrae, U. Häussermann, M. Dolg, H. Stoll, H. Preuss, *Theor. Chim. Acta* **1990,** *77*, 123.

[20] C. Y. Legault, CYLview, 1.0b; Universitéde Sherbrooke, **2009** (http://www.cylview.org).

Chapter 5. Differentiation and Functionalization of Adjacent, Remote C–H Bonds

5.1 Abstract

Site-selective functionalization of C–H bonds will ultimately afford chemists transformative tools for editing and constructing complex molecular architectures. Towards this goal, developing strategies to activate C–H bonds that are distal from a functional group is essential. In this context, distinguishing remote C–H bonds on adjacent carbon atoms is an extraordinary challenge due to the lack of electronic or steric bias between the two positions. Herein, we report the design of a catalytic system leveraging a remote directing template and a transient norbornene mediator to selectively activate a previously inaccessible remote C–H bond that is one bond further away. The generality of this approach has been demonstrated with a range of heterocycles, including a complex anti-leukemia agent, and hydrocinnamic acid substrates.

5.2 Introduction

Functionalizing C–H bonds selectively at various locations of molecules will ultimately afford synthetic chemists transformative tools to modify and construct molecular structures.[1,2,3] C–H bonds that are remote from functional groups (>6 bonds away) are widespread, and distinguishing these C–H bonds bearing little difference in electronic property is a formidable challenge in C–H activation.[4,5,6,7,8,9,10,11,12] For example, benzoazine, especially quinoline, is a ubiquitous motif in natural products, pharmaceuticals, agrochemicals, and functional materials. Multiple C–H bonds on these structures are remote from the chelating nitrogen atom and difficult to distinguish electronically (Figure 5.1a). While the selective functionalization of C–H bonds on the azine ring was achieved by taking advantage of strong electronic and steric bias,[13,14,15,16,17,18,19] directed C–H activation on the benzene moiety is limited to C8 position via chelation assisted process.[20,21] To functionalize the remaining remote C–H bonds, a recoverable and bifunctional template was developed to direct the palladium(II) catalyst selectively to the

remote C5 position through the coordination with the nitrogen of quinoline.[22] This raises a fundamental question of whether such remote directing effect can be exploited to reach other C–H bonds that are one bond further away, thereby significantly expanding our toolkit for functionalizing remote C–H bonds selectively. For example, it would be highly enabling if a directing template can selectively activate the distal C6 or C7 positions of (iso)quinolines which are similarly electron-deficient and unreactive according to the calculated Fukui indices of various heterocycle substrates. While engineering the template to match the distance and geometry is potentially feasible, such alternation of the template will inevitably vary with different classes of substrates. Thus, we began to investigate the possibility of combining the remote

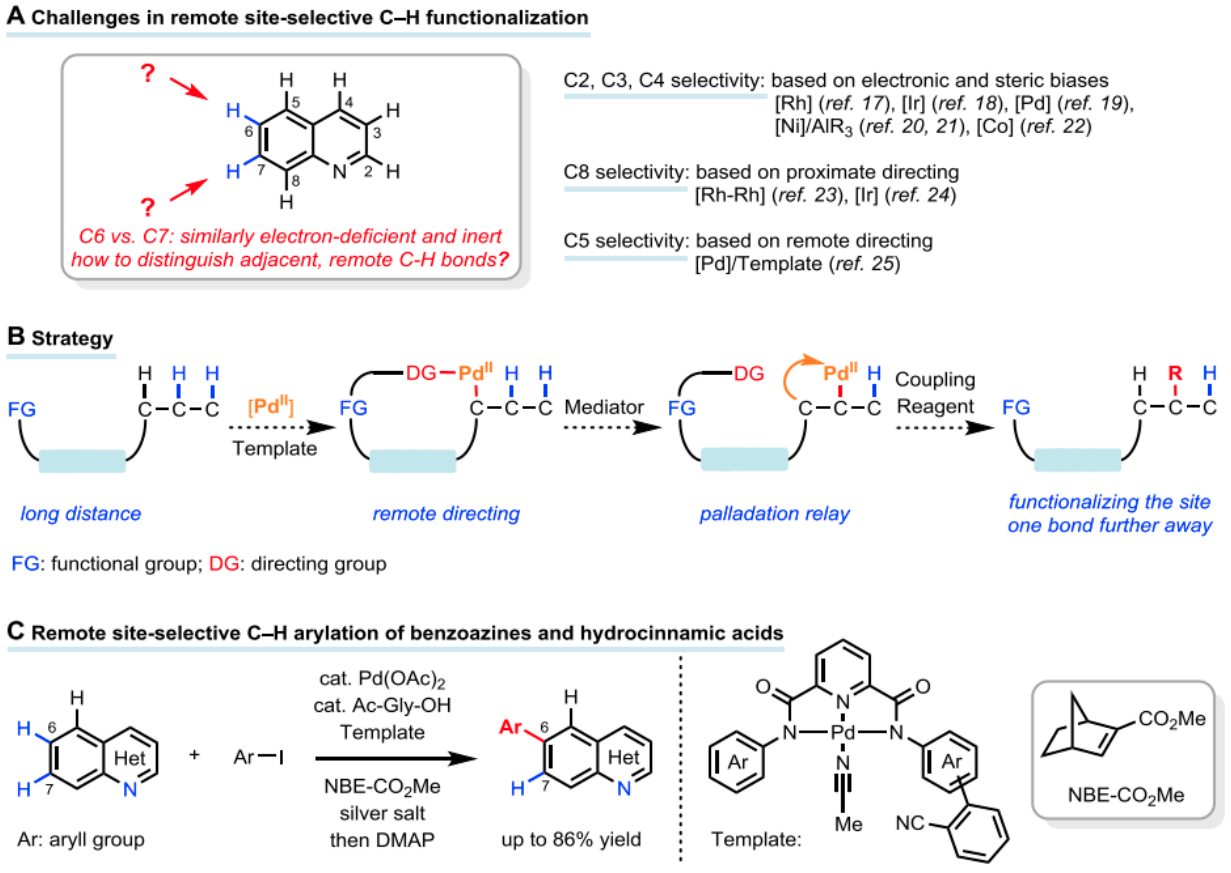

Figure 5.1. Remote site-selective C–H functionalization. a) Challenges in remote site-selective C–H functionalization. b) Strategy using remote directing and one-bond relay. c) Remote site-selective C–H arylation of benzoazines.

directing effect with a one-bond relay strategy using a transient mediator (Figure 5.1b). We envision that the template directs the initial remote palladation at the C5 position, and subsequently, the norbornene[23,24,25,26,27] relays the palladation to the C6 position (Figure 5.1c). This strategy could provide a reliable method to distinguish remote C–H bonds which are adjacent to each other and have similar electronic and steric properties (i.e. C6 position and C7 position of quinoline), as well as to override the electronic bias (i.e. the more reactive C5 position and the less reactive C6 position of quinoline).

To reduce this design into practice, the orchestration of remote directing and the subsequent relaying step faces multiple challenges that must be addressed by carefully engineering molecular structures of the nitrile template, norbornene and ligand. First, the initial C–H palladation directed by the weakly coordinating nitrile template might be prevented by the competitively binding norbornene. On the other hand, the formed macrocyclic C–H palladation intermediate is highly reactive and could undergo the functionalization with aryl iodide prior to the desired norbornene interception and subsequent relay. Second, the norbornene-relayed meta-C–H activation, a highly complex multiple-step sequence, could only proceed with a limited number of previously identified monodentate pyridine and pyridone type of ligands.[23,25,28] In contrast, the weakly coordinating nitrile template often requires a different set of bidentate ligand for remote directing.[9,11,22] Finally, the β-carbon elimination step in the norbornene relay has always relied on the ortho-directing group that is adjacent to the initially formed palladium-carbon bond. However, the remote directing group is further away and cannot provide the necessary steric hindrance.

5.3 Results and Discussion

Owing to the pivotal importance of quinolines and isoquinolines in drug discovery, we selected 3-methyl-isoquinoline as the model substrate to explore the feasibility of remote directing and subsequent relay (Table 5.1). Exploratory studies were conducted using template **T1** that was previously shown to selectively direct C5 C–H palladation of quinolines.[22] Since

Table 5.1. Exploration of reaction conditions that enables remote site-selective arylation of benzoazines.

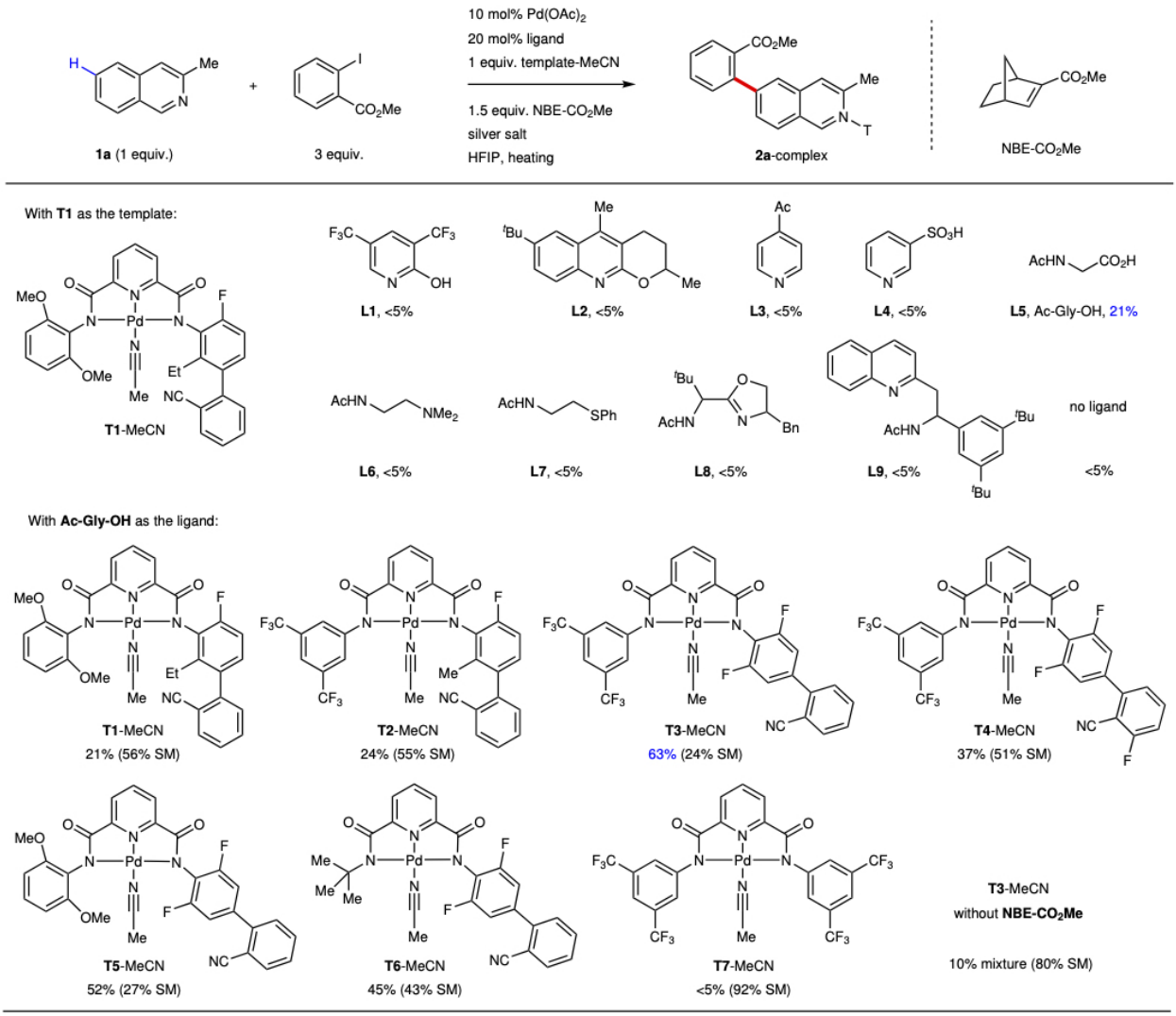

pyridone and pyridine type ligands have been shown to be critical for enabling the Pd-catalyst-relay by norbornene analogues,[23,25,28] we attempted C6 arylation of isoquinoline-**T1** substrate using such monodentate ligands (**L1**, **L2**, **L3**, **L4**). The lack of desired reactivity under these conditions may be attributed to the fact that the weakly coordinating nitrile directing group is prevented from binding to the Pd(II) center in the presence of pyridone and pyridine additives. To ensure the coordination of the nitrile directing group, we decided to evaluate bidentate ligands bearing weakly coordinating group (**L5**, **L6**, **L7**). To our delight, N- acetylglycine (Ac–

Gly–OH, **L5**), one of the mono-N-protected amino acid (MPAA) ligands, turned out to be compatible with the nitrile template, affording the desired C6 arylated isoquinoline-template complex in 21% yield. The recyclable template that bound to the product could be readily removed by in situ treatment with 4-dimethylaminopyridine. Notably, displacement of the carboxylic acid group of MPAA ligand with a strongly coordinating group, N-heterocycle (bidentate ligand **L8**, **L9**), led to loss of reactivity (< 5% yield). These findings demonstrate the importance of matching both the directing template and norbornene with a specific ligand. With this promising lead in hand, we proceeded to evaluate the templates. Firstly, replacing the electron rich left-wing (**T1**) with electron deficient aryl group (**T2**) slightly increased the yield to 24%. Switching the directing phenyl nitrile moiety from meta- to para-position on the right-wing (**T3**) improved the yield markedly (63%). These results are consistent with the notion that site selectivity in remote C–H activation is based on the precise recognition of distance and geometry. Other structural variations of templates reduced the yields (**T4**, **T5**, **T6**). Absence of the nitrile moiety (**T7**) or the norbornene reagent resulted in loss of the desired reactivity.

The established remote site-selective C–H arylation protocol was then extended to other pharmaceutically important benzoazines (Table 5.2). Firstly, we evaluated the isoquinolines and found that a range of derivatives (**2a** to **2d**) were compatible, providing C6 arylation products in moderate yields by using template **T3**. Notably, bromine and chlorine, which serve as useful synthetic handles for subsequent chemical manipulation, were tolerated (**2b**, **2d**). We were delighted to find that this strategy is also applicable to quinoline family by using template **T1** or **T2** depending on substitution pattern: **T1** for quinolines bearing no functional group on C2-position; **T2** for C2-substituted quinolines. The C6 arylation of simple quinoline proceeded smoothly (**2e**), giving 71% isolated yield. A broad range of quinoline derivatives bearing C2, C3,

Table 5.2. Remote site-selective arylation of benzoazines.

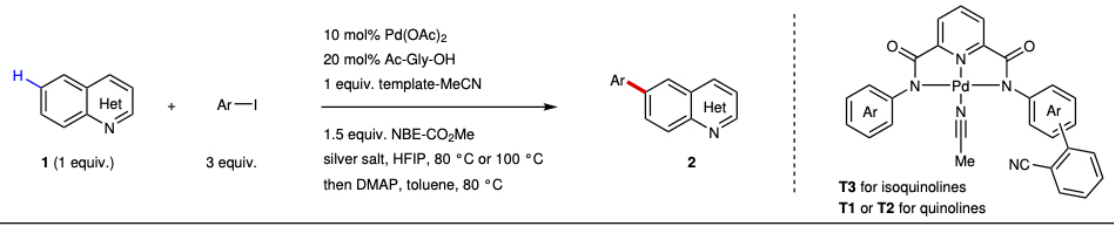

With methyl 2-iodobenzoate as the aryl iodide

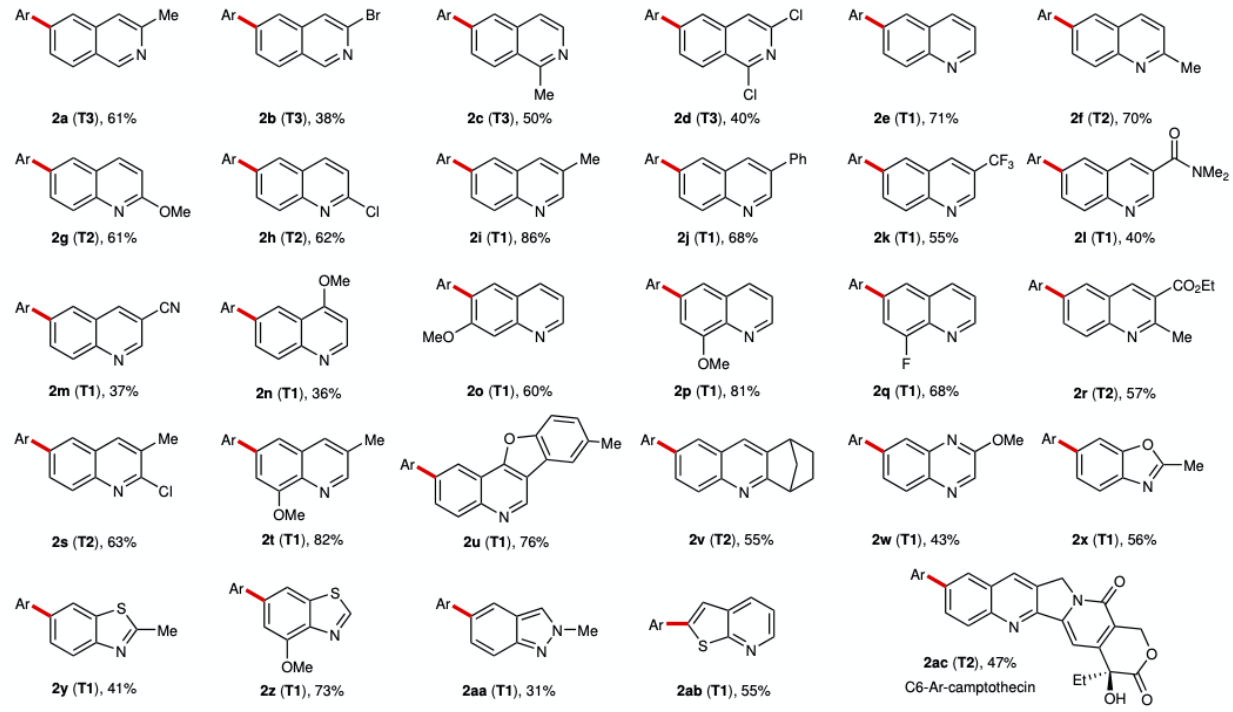

With **T1** as the template

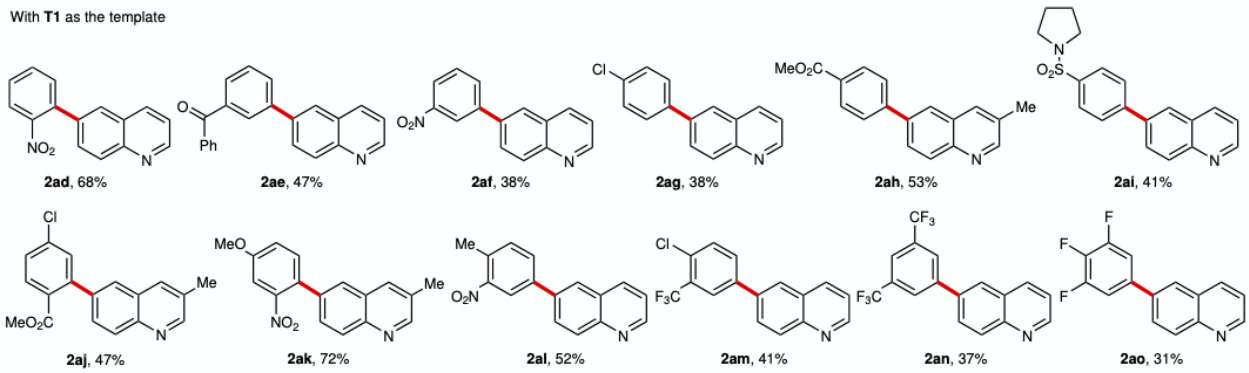

C4, C7, or C8 substituents (**2f**-**2q**) were suitable substrates. Electron-neutral, electron-donating, and electron-withdrawing substituents were all well tolerated, providing yields of up to 86%. Substrates 3-cyano quinoline (**2m**) and 4-methoxy quinoline (**2n**) gave lower yields due to the presence of the coordinative nitrile (competing with the template) and the C4 substitution (hindering the C5 palladation) respectively. Disubstituted quinolines were also compatible, affording the desired products in moderate to good yields (**2r**, **2s**, **2t**). Notably, polycyclic quinolines also afforded the remote arylation products in good yields (**2u**, **2v**). The broad utility of this method is demonstrated with a wide range of benzoazines including quinoxaline (**2w**), benzoxazole (**2x**), benzothiazole (**2y**, **2z**), indazole (**2aa**), and thienopyridine (**2ab**). Late-stage modification of an antileukaemic and antitumour alkaloid, camptothecin (**2ac**), at previously inaccessible site was also successful. In conjunction with our previous methods, we have thus far developed tools to functionalize this highly complex natural product at C5, C6 and C8 with precision demonstrating the unique power of site selective C–H activation.[22,29] Notably, the structural modifications at these positions through semi-synthesis had led to the discovery of drugs, such as topotecan and irinotecan.[30]

We next surveyed the scope of aryl iodides using quinoline as the substrate (Table 5.2). Ortho-, meta- and para-monosubstituted aryl iodides (**2ad** to **2ai**) were all suitable coupling partners, providing desired products in moderate yields. Furthermore, the di and trisubstituted aryl iodides were compatible under the reaction conditions, giving the desired products in moderate to good yields (**2aj** to **2ao**). Electron rich aryl iodides were not effective coupling partners (less than 15% yields), implying that the oxidative addition of aryl iodides to palladacycle is not facile. In comparison, the reactivity of these electron-rich aryl iodides can be restored by attaching an electron-withdrawing group (**2ak**, 72% yield). The regioselectivities observed with various heterocycle substrates and aryl iodide coupling partners are consistently high. In the representative examples (**2a**, **2e**, **2af**), either none (**2e**, **2af**) or less than 5% of the over-arylated product (**2a'**) was detected. Notably, Fukui indices of most heterocycle substrates

show that the electronic density of the remote C6 and C7 sites has little difference, thus further showcasing the unique advantage of our approach using distance and geometry to differentiate remote C–H bonds.

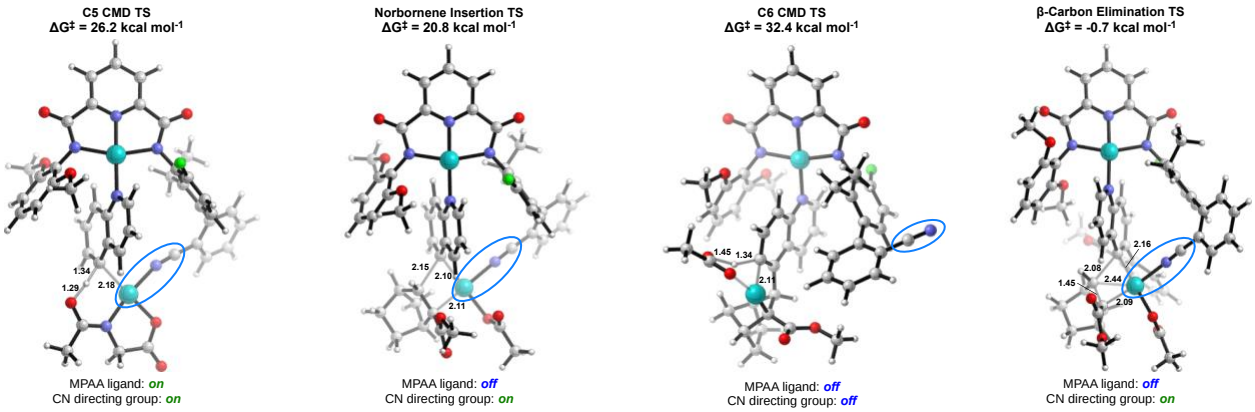

Figure 5.2. DFT-optimized CMD transition state structures. a) CMD transition state for C–H bond at C5 position; b) Transition state for norbornene insertion; c) CMD transition state for C–H bond at C6 position; d) Transition state for β-carbon elimination.

Although the nitrile directed remote C–H palladation[9,11,22] and the norbornene relay from ortho- to meta-positions has been previously shown separately,[22,23,24,25] how these two processes are successfully merged in such a complex catalytic cycle is puzzling based on previous mechanistic understanding. Computational studies provided detailed information about the incredibly complex C–H functionalization mechanism which utilizes a bifunctional template coordinated to two Pd metal centers. Figure 5.2 highlights the transition state structures for C5 CMD (concerted metalation-deprotonation), norbornene insertion, C6 CMD, and β-carbon elimination steps. The nature of the Pd template allows the nitrile group of the side arm to direct the second Pd catalyst to reach the C5 position of quinoline, but surprisingly the nitrile group has to come on and off of the Pd center in order for the catalytic cycle to proceed. The MPAA ligand promotes the first C5 CMD step but then dissociates in order to provide a vacant coordination site for subsequent norbornene insertion. These studies reveal the extraordinary complexity of merging the nitrile template and the norbornene transient mediator for palladation

relay. The ability of both the MPAA ligand and the nitrile group to only associate during certain steps of the catalytic cycle is essential for completing the catalytic cycle, as shown in Figure 5.3.

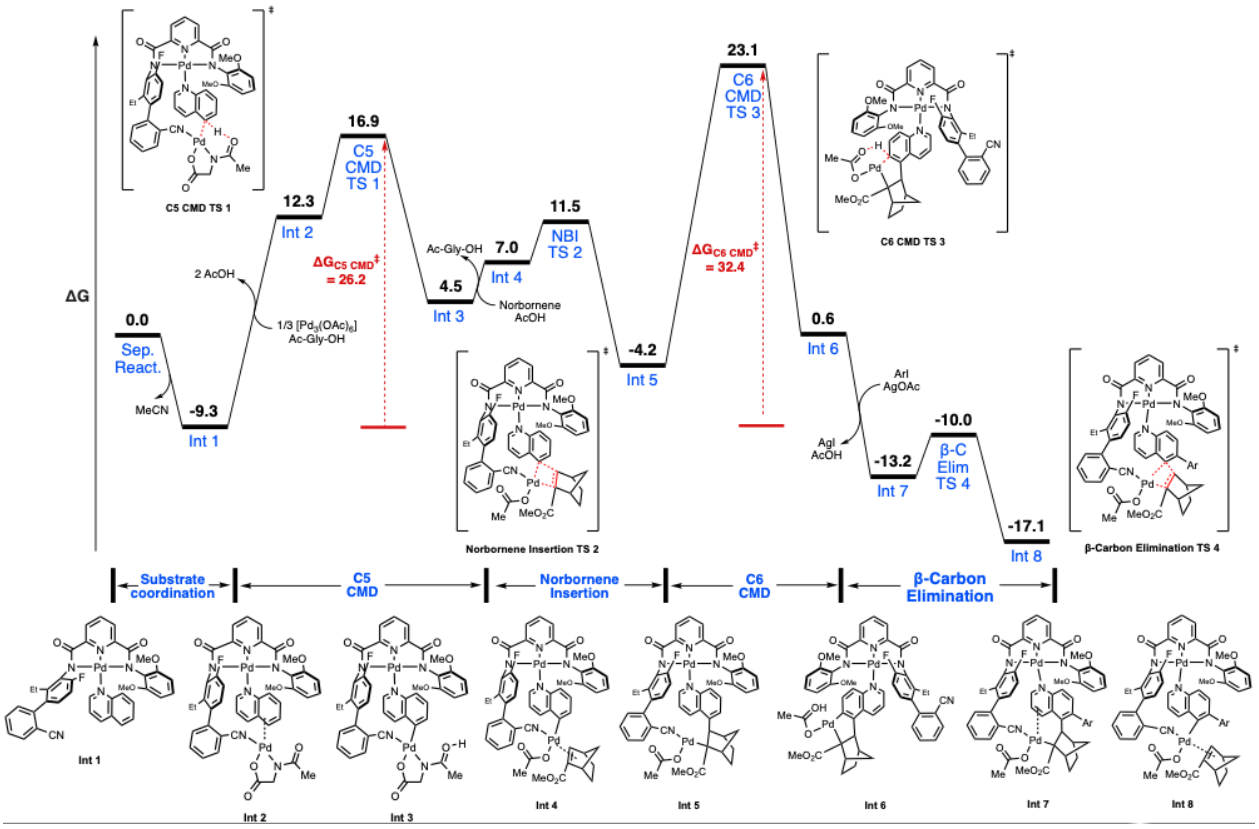

Figure 5.3. Free energy profile of Pd-catalyzed remote C6-arylation of quinoline.

To further test whether this strategy can be broadly used to differentiate remote, adjacent C–H bonds, we embarked on remote site-selective C–H arylation of other arenes bearing covalently attached U- shaped templates (Table 5.3). We found that tetrahydroisoquinoline can be arylated at the C7 position, which is also one bond further away compared to the previous C8 arylation using remote directing template alone (**4a**). The reaction conditions tolerated a range of substituents at different positions, including 1-methyl (**4b**), 3-carboxylate (**4c**), 5-ethyl (**4d**), 5-phenyl (**4e**), and 5-bromo (**4f**). Finally, para-arylation of phenylpropanoic acid derivatives[9] was also realized using this approach (**6a**, **6b**) (Table 5.4). Various aryl iodides containing mono or disubstitutions were compatible, giving moderate yields (**6c** to **6f**).

Table 5.3. Remote C7-arylation of tetrahydroisoquinolines.

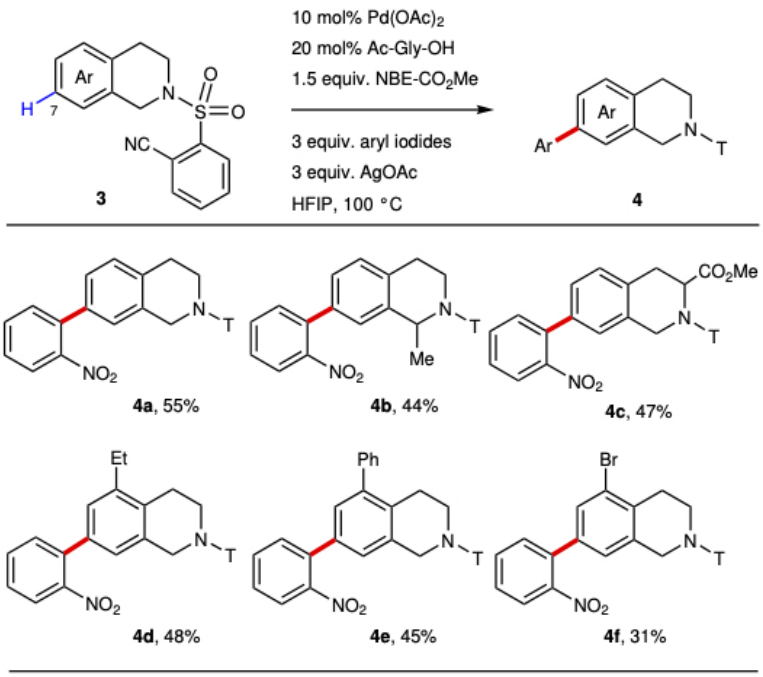

Table 5.4. Remote *para*-arylation of phenylpropanoic acid derivatives.

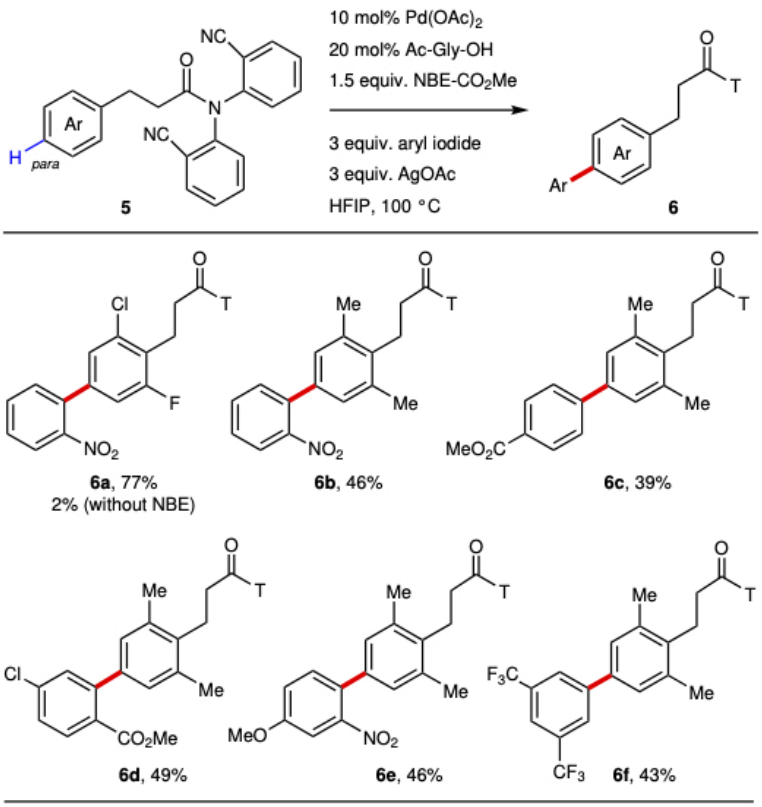

5.4 Conclusions

In summary, we have developed a new strategy to distinguish remote C–H bonds within one-bond distance. This new method, along with previously developed template chemistry, allows us to access two different remote C–H bonds with precise control. The established approach is generally applicable to a wide range of heterocycles as well as other classes of synthetically useful substrates. The delicate cooperation of a remote directing template, a transient mediator norbornene and MPAA ligand reveals great potential for developing unprecedented catalytic systems in C–H activation.

5.5 References

[1] Daugulis, O., Do, H.-Q. & Shabashov, D. *Acc. Chem. Res.* **2009**, *42*, 1074−1086.

[2] Lyons, T. W. & Sanford, M. S. *Chem. Rev.* **2010**, *110*, 1147−1169.

[3] Abrams, D. J., Provencher, P. A. & Sorensen, E. J. *Chem. Soc. Rev.* **2018**, *47*, 8925−8967.

[4] Li, J., Sarkar, S. D. & Ackermann, L. *Top. Organomet. Chem.* **2016**, *55*, 217−257.

[5] Breslow, R. *Acc. Chem. Res.* **1980**, *13*, 170−177.

[6] Das, S., Incarvito, C. D., Crabtree, R. H. & Brudvig, G. W. *Science* **2006**, *312*, 1941−1943.

[7] Phipps, R. J. & Gaunt, M. J. *Science* **2009**, *323*, 1593−1597.

[8] Saidi, O., et al. *J. Am. Chem. Soc.* **2011**, *133*, 19298−19301.

[9] Leow, D., Li, G., Mei, T.-S. & Yu, J.-Q. *Nature* **2012**, *486*, 518−522.

[10] Kuninobu, Y. Ida, H., Nishi, M. & Kanai, M. *Nat. Chem.* **2015**, *7*, 712−717.

[11] Bag, S., et al. *J. Am. Chem. Soc.* **2015**, *137*, 11888−11891.

[12] Okumura, S., et al. *J. Am. Chem. Soc.* **2016**, *138*, 14699−14704.

[13] Stephens, D. E. & Larionov, O. V. *Tetrahedron* **2015**, *71*, 8683−8716.

[14] Berman, A. M., Lewis, J. C., Bergman, R. G. & Ellman, J. A. *J. Am. Chem. Soc.* **2008**, *130*, 14926−14927.

[15] Takagi, J., Sato, K., Hartwig, J. F., Ishiyama, T. & Miyaura, N. *Tetrahedron Lett.* **2002**, *43*, 5649−5651.

[16] Ye, M., Gao, G.-L. & Yu, J.-Q. *J. Am. Chem. Soc*. **2011**, *133*, 6964−6967.

[17] Nakao, Y., Yamada, Y., Kashihara, N. & Hiyama, T. *J. Am. Chem. Soc.* **2010**, *132*, 13666−13668.

[18] Tsai, C.-C., et al. *J. Am. Chem. Soc.* **2010**, *132*, 11887−11889.

[19] Yamamoto, S., Saga, Y., Andou, T., Matsunaga, S. & Kanai, M. *Adv. Synth. Catal.* **2014**, *356*, 401−405.

[20] Kwak, J., Kim, M. & Chang, S. *J. Am. Chem. Soc.* **2011**, *133*, 3780−3783.

[21] Konishi, S., et al. *Chem. Asian J.* **2014**, *9*, 434−438.

[22] Zhang, Z., Tanaka, K. & Yu, J.-Q. *Nature* **2017**, *543*, 538−542.

[23] Wang, X.-C., et al. *Nature* **2015**, *519*, 334−338.

[24] Dong, Z., Wang, J. & Dong, G. *J. Am. Chem. Soc.* **2015**, *137*, 5887−5890.

[25] Shen, P.-X., Wang, X.-C., Wang, P., Zhu, R.-Y. & Yu, J.-Q *J. Am. Chem. Soc.* **2015**, *137*, 11574−11577.

[26] Ye, J. & Lautens, M. *Nat. Chem.* **2015**, *7*, 863−870.

[27] Della, Ca' N., Fontana, M., Motti, E. & Catellani, M. *Acc. Chem. Res*. **2016**, *49*, 1389−1400.

[28] Shi, H., Herron, A. N., Shao, Y., Shao, Q. & Yu, J.-Q. *Nature* **2018**, *558*, 581−586.

[29] Wang, P., et al. *Nature* **2017**, *551*, 489−493.

[30] Bracher, F. & Tremmel, T. *Arch. Pharm. Chem. Life Sci.* **2017**, *350*, e1600236.

Chapter 6. Cyclization by C(sp_3)–H Functionalization by a Transient Directing Group

6.1 Abstract

We report the development of a Pd(II)-catalyzed C(sp_3)–H cyclizative arylation of ketones with a transient directing group (TDG). Based on calculations, the oxidative addition step implicates a highly strained trigonal bipyramidal geometry around a Pd(IV) intermediate afforded by the bidendate transient directing group and the intramolecular arylation. As a consequence, the unproductive protodeiodination outcompetes the cyclizative arylation Pd(II/IV) pathway under standard conditions. The desired selectivity was achieved by prudent selection of the transient directing group and silver(I) source. The reaction is accelerated by the inclusion of stoichiometric quantities of trifluoroacetic acid, which benefits both the palladium catalysis, as well as the attachment of the transient directing group for the pivotal C(sp_3)–H palladation. Critically, the use of 2-pyridone ligand improves yields significantly and enables the arylative cyclization of both methyl and linear methylene C–H bonds. The reaction is showcased in a two-step synthesis of a substituted indane using 3-iodoanisole as the linchpin in a [3+2] cyclization concept featuring two C(sp_3)–H arylations.

6.2 Introduction

C(sp_3)–H functionalization by Pd(II) catalysis offers manifold opportunities to expedite synthesis of complex molecules.[1,2,3,4,5,6] Towards that end, our lab and others aim to develop strategic disconnections[7,8,9,10,11,12] that could be enabled by creative applications of C–H functionalization. In this way, we aim to develop a logic of C–H functionalization in synthesis. Advances in understanding of metal geometry effects, ligand acceleration/catalyst stabilization, palladium speciation, and control of supposed Pd(II/IV) oxidative addition pathways have been pivotal to the successful development and proliferation of palladium-catalyzed C–H functionalization reactions.[13,14,15,16,17] Crucial to the successful promulgation of C–H functionalization logic in synthesis is the avoidance of directing group auxiliaries, and the use of

Scheme 6.1. Directed C(sp3)–H arylation-cyclization reactions.

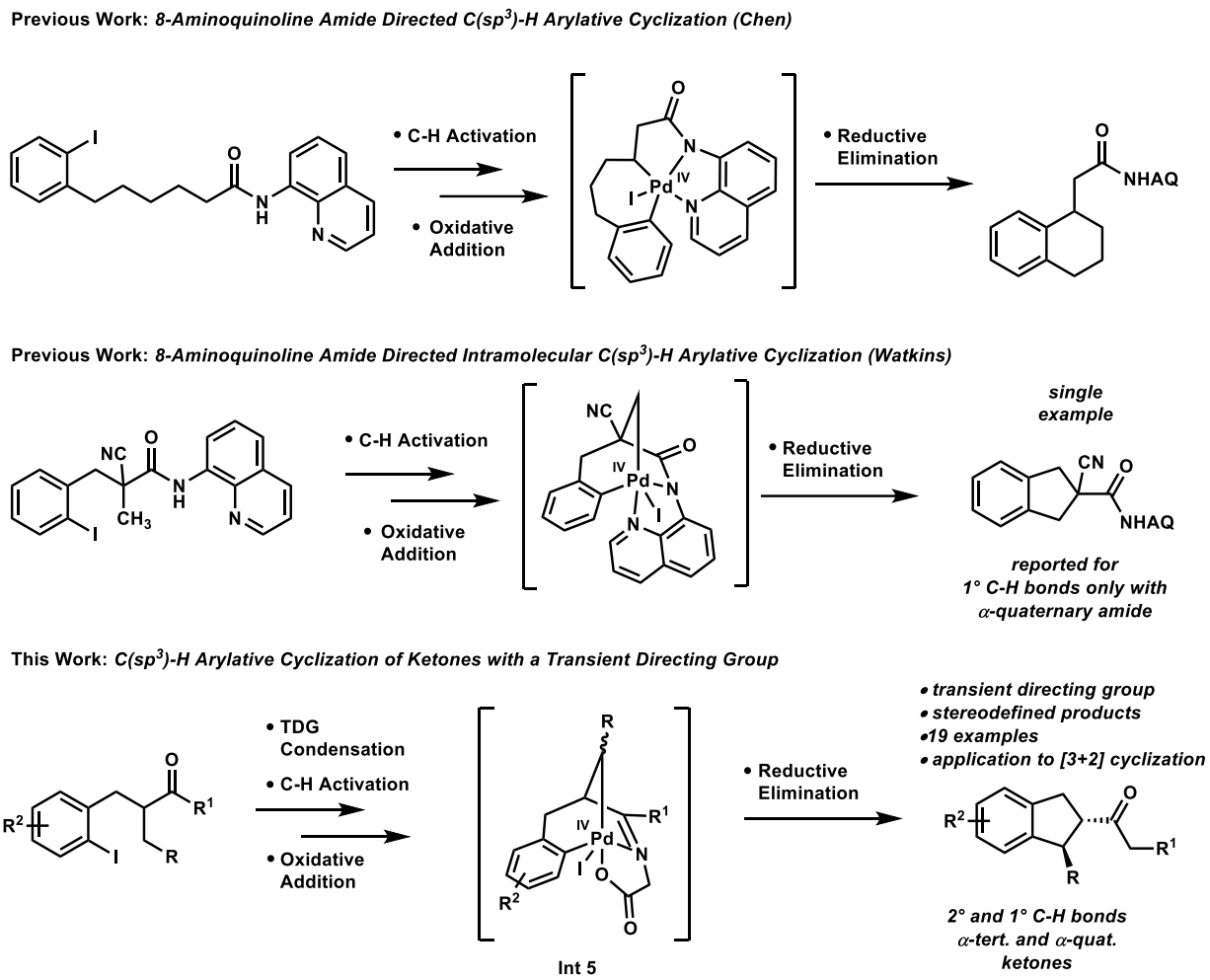

a transient directing group is a powerful strategy to this end. While highly attractive due to the opportunity for highly efficient synthesis, chemical transformations reliant on a transient directing group are stymied by the highly dynamic nature of the reaction. The use of transient directing groups has significant confounding effects on reaction development[18,19,20,21,22,23]: first, the free directing group moiety is often a very good ligand for palladium,[24] which can have a deleterious impact on reactivity; and secondly, the acidic environment employed to promote directing group/substrate condensation[25,26,27,28,29,30] typically precludes fine control of the ligand environment around palladium. Thirdly, most of the successful TDG strategies for harnessing Pd(II)-catalyzed C–H functionalization have resorted to bidentate directing groups, which can

saturate the Pd coordination sphere, effectively impeding the use of additional ligand(s) to modulate Pd reactivity. Specific to the cyclization reaction we present here, the combination of transient bidentate directing group and intramolecular arylation inevitably involves a highly strained bipyramidal Pd(IV) intermediate. Thus, the challenge was two-fold: retain conditions amenable to a transient directing group catalysis, while also taking consideration for the unique oxidative addition pathway required for intramolecular arylation. To date, all known ring-closure reactions that leverage C(sp_3)–H functionalization require an auxiliary directing group.

Previous developments in the field of directed palladium-catalyzed C(sp_3)–H arylation are shown in **Error! Reference source not found.**.[31,32] Both depicted strategies employ the 8-aminoquinoline amide (AQ) directing group, which requires additional steps for installation and removal. When utilizing the AQ directing group, removal typically requires exposure of the substrate to strong acids and/or multistep manipulations.[31,33] Chen has employed directing group auxiliaries to make cyclophane-braced peptide macrocycles, which highlights the potential for C(sp_3)–H arylation-cyclization reactions to impact the broader scientific community.[18,19] Comparing Chen's work to ours, the Pd(IV) intermediate (**Int 5**) invoked in our reaction manifold is significantly more strained and rigid, making the reaction more challenging to solve. The Watkins cyclization (**Error! Reference source not found.**), which is conceptually related to the reactions described herein, was a single example reported with little additional information regarding the scope of the reaction.[32] This article describes the first example of cyclization by C(sp_3)–H functionalization through the agency of a transient directing group. This work is a first step toward the broader aim of developing relay C(sp_3)–H functionalizations for chemical synthesis.

6.3 Results and Discussion

We desired a catalytic method to transform compound **1** to substituted indane **2** (**Error! Reference source not found.**). In the wake of the directing group formation by Schiff base formation, we anticipated that directed C(sp_3)–H bond activation would generate palladacycle

Int 4. A subsequent intramolecular oxidative addition of the C–I bond to the Pd(II) center of **Int 4** would

Scheme 6.2. Ring-formation through directed C(sp_3) –H functionalization raises questions of palladium(IV) geometry. TFA = trifluoroacetic acid; HFIP = hexafluoroisopropanol. Yields were determined by $_1$H NMR spectroscopy using 1,3,5-timethoxybenzene as internal standard.

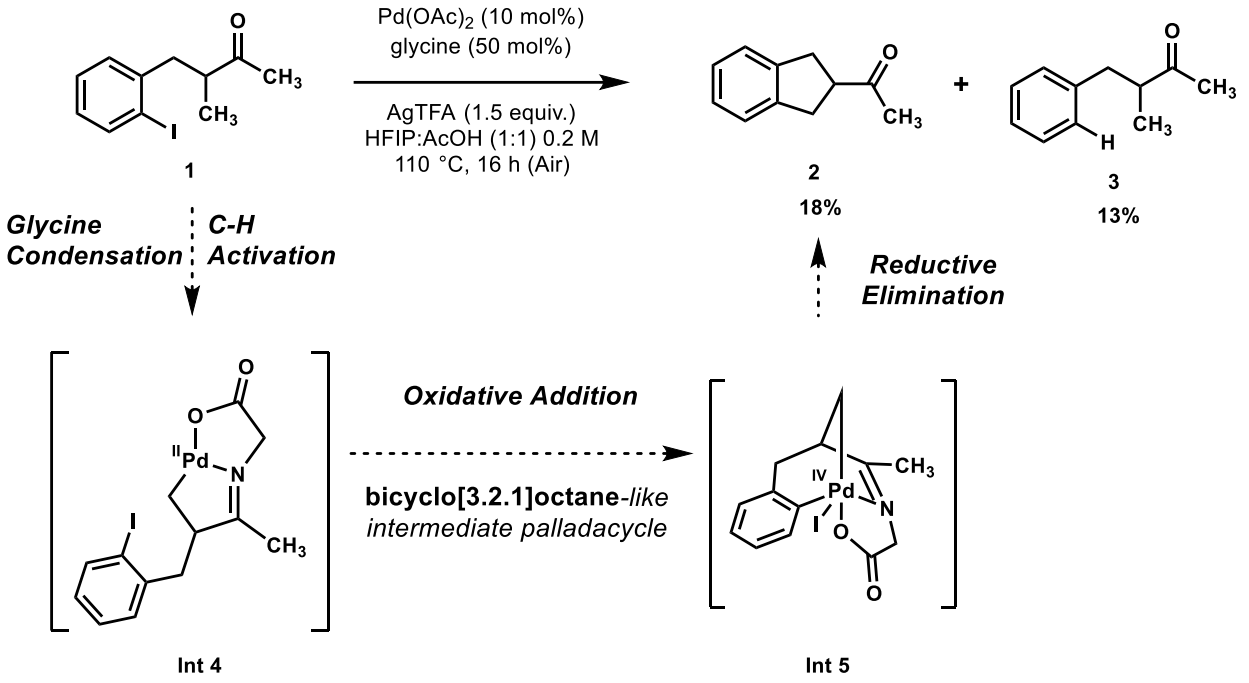

likely proceed through the intermediacy of an architecturally strained bicyclo[3.2.1]palladacycle **Int 5**. Reductive elimination of **Int 5** would finally form the five-membered ring of **2**. In fact, the direct cyclization of **1** to **2** may be achieved, albeit in low yield, under the conditions shown in **Error! Reference source not found.**. Since this reaction also afforded a comparable amount of compound **3**, we needed to confront several issues in an effort to improve the ratio of **2** to **3**. First and foremost, we needed to find a way to suppress the undesired, palladium-catalyzed protodeiodination (**1** $\mapsto$ **3**). In other words, superior selectivity of the Pd(II/IV) redox couple must be achieved. Unbound palladium(II) in solution could engage in non-productive protodeiodination, whereas directing group-bound palladium(II) proceeded through the desired

cyclization reaction. Preliminary calculations (**Error! Reference source not found.**) indicated that the productive aryl iodide-induced Pd(II/IV) oxidative addition would pass through a very high energy putative transition state **TS 2** to reach bicyclic Pd(IV) intermediate **Int 5**. The high energy of the Pd(II/IV) transition state was associated not only with the steric hindrance of the 2-substituted aryl iodide **1**, but also a high ring strain energy. Indeed, calculations indicated that the **TS 2** was of higher energy than the concerted metalation deprotonation (CMD) C–H activation transition state **TS 1**. Thus, providing conditions and coordination environments around palladium were essential to controlling selectivity between cyclization and protodeiodination.

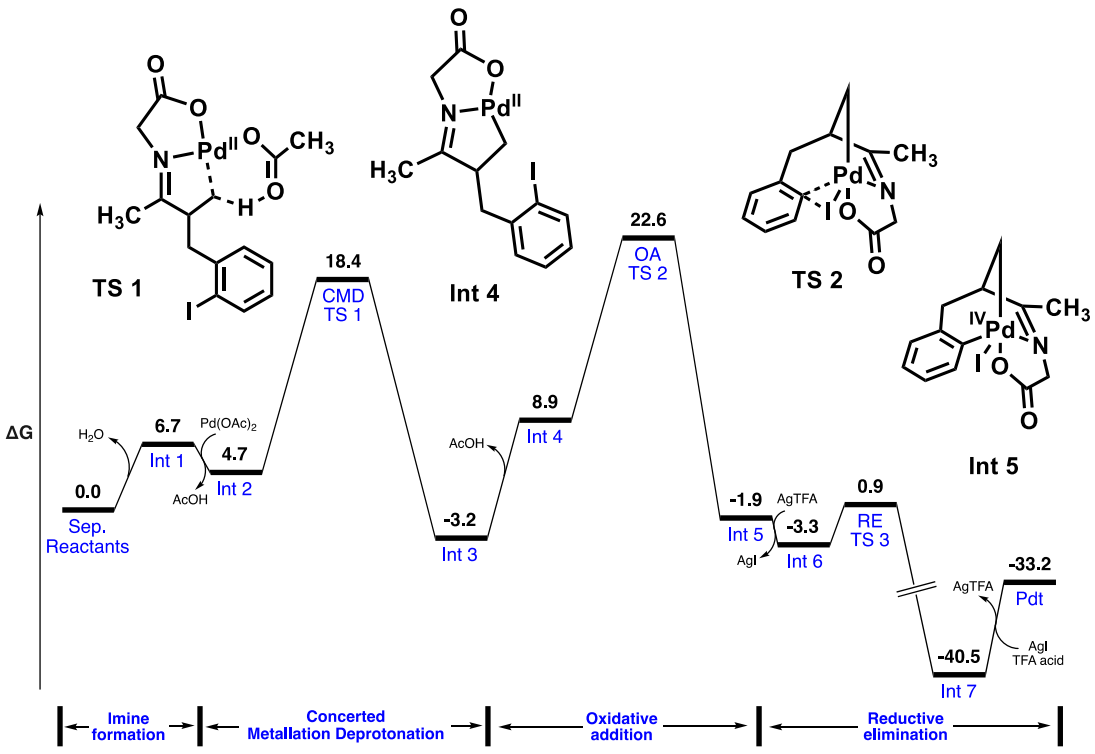

Figure 6.1. Calculated reaction coordinate diagram for C(sp_3)–H cyclizative arylation of ketones with a transient directing group (energies in kcal mol^{-1}).

Pd(IV) organometallic chemistry has been inextricably linked with the massive growth in palladium catalyzed C–H functionalization.[34] Controlled access to this rarified and reactive palladium oxidation state has been key to the success of a significant portion of palladium

catalyzed C–H functionalization reactions. The palladium(IV) complexes that have been characterized and described thus far have nearly all been octahedral.[34, 35] Calculations suggested that the intramolecular oxidative addition of the C–I bond in **Int 4** to Pd(II) would generate the topologically unique **Int 5** with a rare trigonal bipyramidal coordination geometry at the metal center, consideration for this outcome was leveraged in our efforts to optimize the formation of indane **2**. Our study of the direct cyclization of **1** to **2** was sustained by the hope that higher efficiencies might be possible by modulating the coordination geometry of the putative Pd(IV) intermediate preceding product **2**.

Our initial thoughts toward reaction optimization suggested that we could modulate the geometry at Pd(IV) in **Int 5** by changing the nature of the transient directing group. Our results shown in **Error! Reference source not found.** are consistent with several theories in transient directing group chemistry. In this case, AcOH is considered to be the catalyst for the transient imine formation.[25] We observed generally superior reactivity with the alkyl amine TDGs (**TDG1**-**TDG7**), suggesting that the aniline TDGs (**TDG8**-**TDG13**) have insufficient reactivity in condensations with ketones. Lack of reactivity in pendant pyridine directing groups (**TDG6**-**TDG7**) indicate that a **LX** type ligand as directing group is preferred in Pd-catalyzed TDG C–H functionalization. As clearly indicated in **Error! Reference source not found.**, the loading of TDG significantly impacts overall palladium reactivity, as more chelate-bound palladium seems to attenuate both protodeiodination reactivity and desired C–H functionalization chemistry. Based on a glycine (**TDG1**) stoichiometry screen, we reason that increased glycine loading decreases overall reactivity, while decreased glycine loading allows unbound [Pd] to participate in protodeiodination.

Table 6.1. Effect of transient directing group identity and stoichiometry.

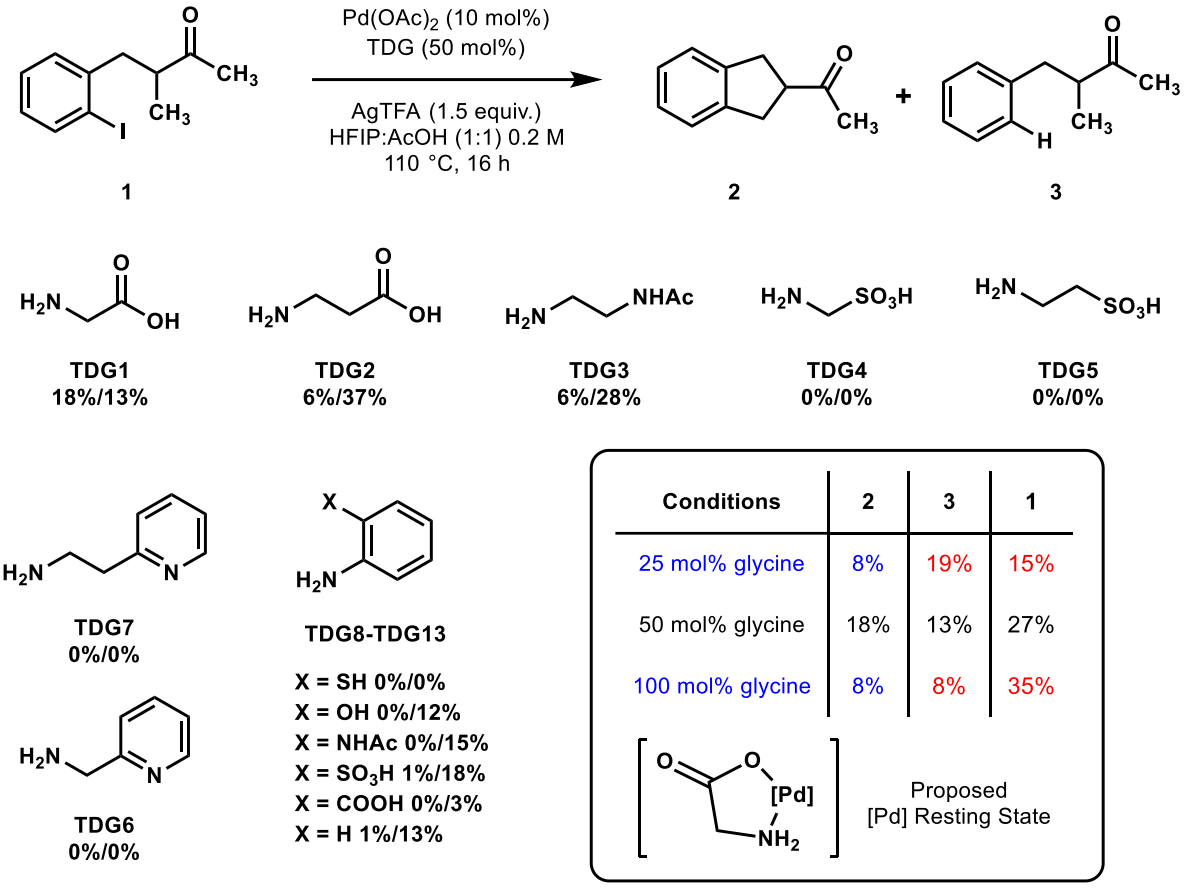

After carefully examining the role of each reagent and its impact on the reaction, we discovered that the Ag(I) salt is the likely culprit in promoting unproductive protodeiodination (**Error! Reference source not found.**), although $Pd(OAc)_2$ is, of course, ultimately responsible for the side reaction as evidenced by the control reaction. As AgTFA stoichiometry was decreased, we observed a steady decline in protodeiodination while the yield of desired product remained steady at ~20% yield. In many reported intermolecular TDG C–H arylation conditions,[25,26] several equivalents of the aryl iodide are employed, which to some degree may compensate for protodeiodination and homo-coupling of the excess iodoarenes. In an intramolecular C–H arylation reaction, there is an inherent limitation of the 1:1 stoichiometry; thus, if any protodeiodination or homocoupling occurs, the mass balance suffers considerably.

We thus wondered if modification of the Ag(I) counterion might temper some of this unwanted reactivity.

Table 6.2. Protodeiodination controlled by AgTFA. Discovery of Ag_3PO_4 and TFA effect on C(sp_3)–H arylative cyclization.

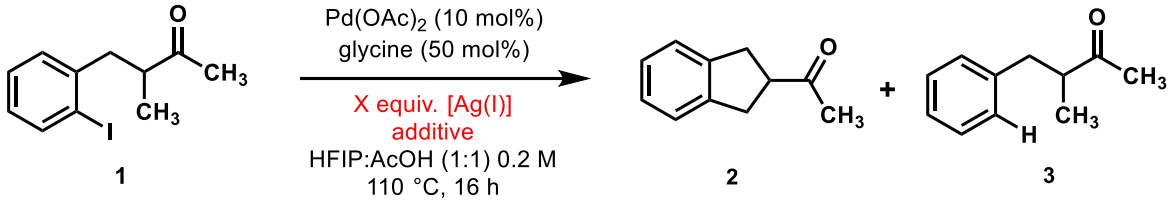

equiv. AgTFA	2	3	1
1.5 equiv.	18%	13%	27%
0.9 equiv.	20%	6%	29%
0.7 equiv.	21%	4%	37%
0.5 equiv.	19%	**trace**	44%
omit $Pd(OAc)_2$[a]	0%	0%	95%

[a]with1.5 equiv. AgTFA

equiv. Ag_3PO_4	equiv. TFA	2	3	1
0.7 equiv.	--	38%	3%	24%
1.5 equiv.	--	**43%**	6%	13%
4.5 equiv.	--	35%	8%	28%
1.5 equiv.	1.5 equiv.	**52%**	13%	30%
1.5 equiv.	4.8 equiv.	24%	34%	0%
1.5 equiv.	19.2 equiv.	4%	45%	0%

Since the Ag source plays a role in promoting the undesirable protodeiodination pathway, we screened several Ag sources. As reported in the supporting information, Ag(I) salts commonly employed in palladium-catalyzed C–H arylations furnished significantly lower yields of the desired product. In the reaction shown in **Error! Reference source not found.**, when we employed 0.5 equivalents Ag_3PO_4, the yield improved significantly, from 20% to 43%, while protodeiodination remained around 6%. We considered that this might be indicative of a Pd/Ag couple being responsible for selectivity in Pd(II/IV) catalysis. AgTFA is thought to be a highly reactive silver source, due in part to its high solubility in organic solvents, while Ag_3PO_4 is essentially insoluble. From these results, it seems likely that the Ag(I) concentration has a strong influence on the product distribution. In addition, we also considered whether the

introduced phosphate ion could accelerate the reaction though coordination of the palladium metal center.[36,37,38]

Our aim was to understand how the AgTFA/Ag_3PO_4 reagent change promoted desired reactivity, and so we explored how each aspect of this reagent change affected the reaction. Initially, we theorized that phosphate could be acting as a ligand at palladium. As shown in the supporting information, screening the identity and equivalents of phosphate additives resulted in either a reduction in reaction efficiency or no change, indicating that phosphate may not be key to the yield enhancement. When the trifluoroacetate ion was reintroduced to the reaction as trifluoroacetic acid (**Error! Reference source not found.**), we found that this reagent could exert broad control over the palladium reactivity. With addition of 1-2 equivalents of TFA, the desired C–H arylation yield increased by ~10%, with a concomitant small increase in protodeiodination. When TFA was increased beyond this loading, up to 30% of solvent (19 equiv.), protodeiodination was enhanced to 45% yield, while the desired arylation process became non-competitive. TFA seems to have broad impact on the profile of palladium catalysis occurring in solution. The impact of TFA on the reaction is significant in several ways. Upon physical examination of the reactions, the solubility of otherwise insoluble silver phosphate increases as TFA is increased; thus, TFA may control a slow infusion of AgTFA into the solution upon reaction with Ag_3PO_4. However, this does not account for instances where a large excess of TFA is present, under which conditions the palladium catalysis is almost entirely shunted to protodeiodination. This phenomenon indicates that either the high acidity or a direct trifluoroacetate-palladium interaction controls some reactivity pathway. Upon closer examination of this result, calculations showed that productive silver-mediated iodide abstraction from the trigonal bipyramidal intermediate **Int 5** led to an octahedral TFA bound Pd complex **Int 6** (**Error! Reference source not found.**). This calculation suggests that TFA may facilitate the reorganization at Pd to the more favorable octahedral geometry. Use of $Pd(TFA)_2$ as Pd source

showed no improvement on the reaction efficiency, and use of other strong acids like haloacetic acids or others in place of TFA as additive also furnished no benefit.

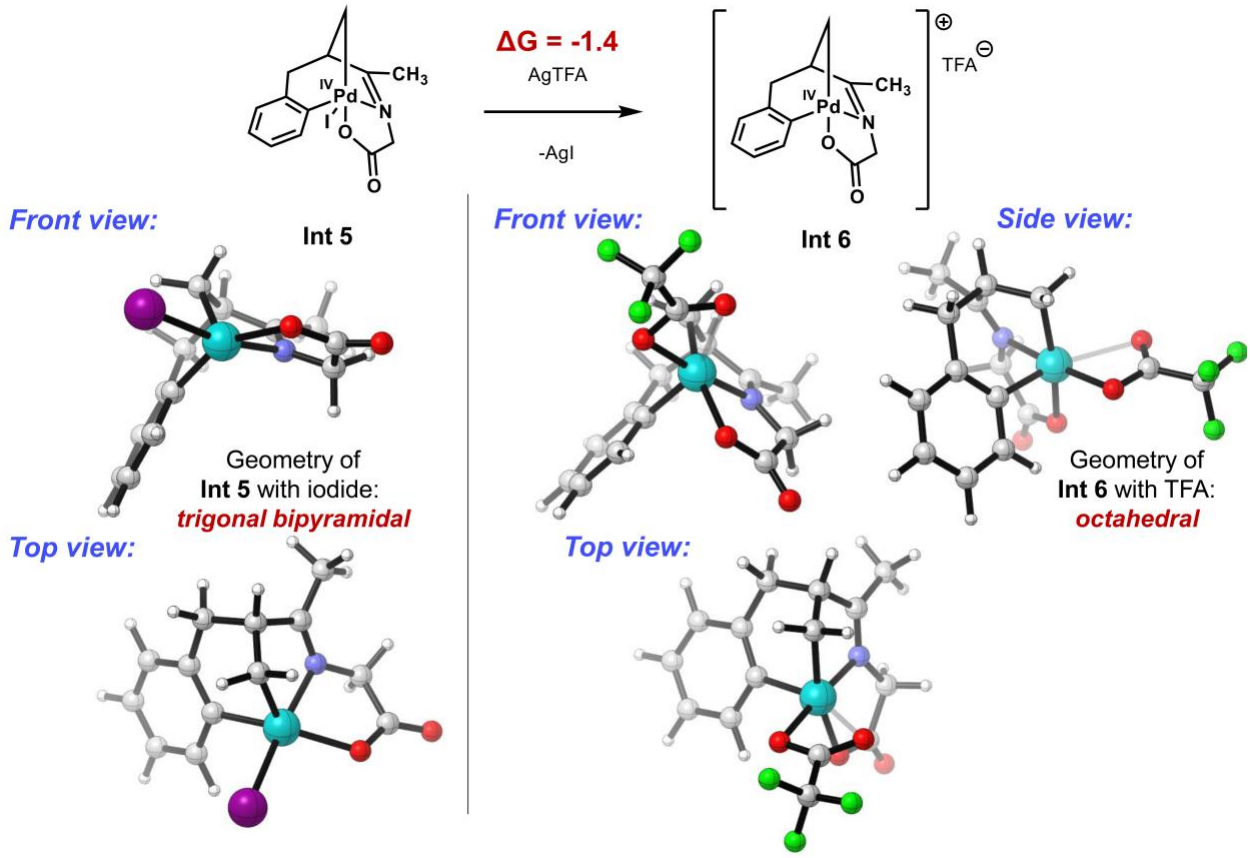

Figure 6.2. Calculated structures of Int 5 and Int 6. TFA = trifluoroacetate.

To examine how this new cyclization reaction is impacted by C–H bond type, we investigated intramolecular arylations of linear methylene C–H bonds. We also anticipated that the palladium geometry may have implications on either the stereochemical or regiochemical outcome of this reaction. Linear methylene C–H activation by CMD is thought to proceed through a higher-energy transition state, and often fails under conditions reported for functionalization of methyl and cyclic methylene C–H bonds.[26] After extensive screening of conditions, we found that an increased glycine loading, increased temperature, and omission of TFA led to a 52% yield of substituted indane **5** with 5:1 dr for the reaction outlined in **Error! Reference source not found.**. Omission of TFA, reduced AcOH loading, and increased glycine

loading indicated that reduced acidity of the solvent medium improved reaction yield. More broadly, our observations indicate that at higher temperatures, strongly acidic conditions promote unselective palladium reactivity pathways leading to protodeiodination and general substrate degradation. Thus, increased glycine loading (broad reactivity attenuator) and increased temperature (broad reactivity promoter) are inversely related and must be balanced to afford the highest yield of desired product. Contrary to previous reports,[26] use of β-alanine as the TDG furnished no detectable cyclization product; this observation was surprising since calculations revealed that the β-alanine-derived 6,5 palladacycle is less strained than the glycine-derived 5,5 palladacycle. As shown in the supporting information, the substrate is easily prepared in a single, scalable step from commercially available starting materials, and thus this method for transforming an unactivated methylene C–H bond provides direct access to stereochemically defined, disubstituted indanes. While Dyker,[39,40] Fagnou,[41] Cramer,[42] Baudoin,[43] and others[10] have developed palladium(0/II) catalyzed C(sp^3)–H arylation reactions that afford benzo-fused frameworks, it seems, at the time of writing, that the nature of the Pd(0/II) redox frameworks employed in these reactions limit the gamut of reactivity to methyl and cyclic methylene C(sp^3)–H bonds due to kinetically competitive β-hydride elimination in linear methylene C(sp^3)–H functionalization.[44,45,46] Furthermore, Baudoin has established that the C(sp^3)–H bond in the β position of enolizable ketones will not undergo efficient C–H functionalization in the Pd(0/II) redox framework, specifically precluding the acetyl indane compounds described herein as potential product classes derived from that chemistry.[47]

The high levels of diastereoselectivity in this reaction are uncharacteristic of C(sp^3)–H arylative cyclizations. Reports of auxiliary-directed palladium catalyzed C–H arylation-cyclization from the Chen laboratory generally exhibit the low or no diastereoselectivity.[19,31] Based on calculations showing that the oxidative addition step in the proposed catalytic pathway has the highest energy barrier, we reasoned that the relative stereochemical relationship reflected in

compound **5** might be arising from a well-ordered and rigid Pd(II/IV) transition state analogous to **TS 2** (**Error! Reference source not found.**).

Table 6.3. Optimization of arylative cyclization of linear methylene C(sp_3)–H bonds in AcOH co-solvent mixtures.

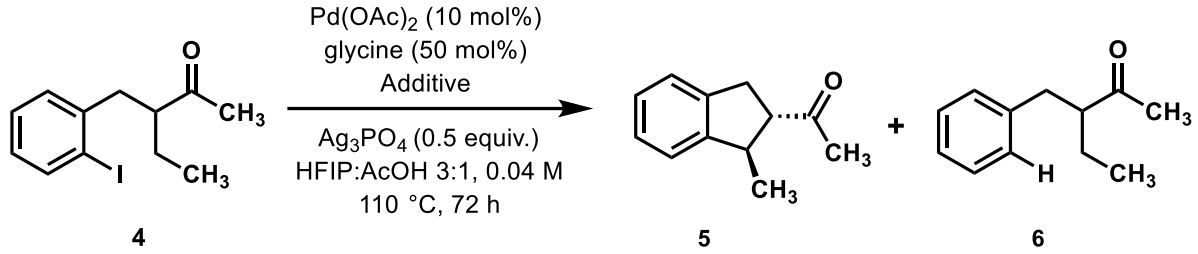

Condition	Additive	5	dr	6	4
110 °C, 36 h	TFA 1.25 equiv.	20%	8:1	7%	64%
120 °C, 72 h	TFA 1.25 equiv.	38%	8:1	10%	51%
glycine (1 equiv) 140 °C, 72 h in 5:1 HFIP:AcOH	--	**52%**	5:1	10%	37%
β-alanine[a] (**TDG2**) 120 °C, 72 h	TFA 1.25 equiv.	0%	nd	20%	80%

[a]50 mol% replaces glycine as TDG

Conditions we thought relevant to the unique Pd(II/IV) oxidative addition process of this system have been optimized: the insoluble nature of Ag_3PO_4 reduced off-cycle protodeiodination, and the presence of trifluoroacetic acid promoted desired iodide abstraction and facilitated geometric relaxation at the Pd(IV) metal center. However, we had not addressed any apparent improvement of the C–H palladation step purported to be [Pd_{II}-OAc] mediated CMD. Indeed, the previous report[26] of intermolecular ketone-TDG-directed linear methylene C(sp_3)–H arylation report no substrates with α-branched substrates, indicating that this substrate class is very challenging for C(sp_3)–H activation, regardless of strained Pd(IV) pathways. The use of 2-pyridone in place of acetate as the purported CMD ligand has enabled

significant improvement in several Pd catalyzed C–H functionalization reactions.[48,49,50,51,52,53,54] In theory, the 2-pyridone ligand is a superior CMD alternative to acetate and can be electronically tuned by substitution of the pyridone ring. We elected to study 2-pyridones specifically because this particular TDG-catalyzed reaction manifold employs a bidentate directing group, which saturates the coordination sphere of palladium(II) and precludes the use of some other ligand classes.[55] Not only is the pyridone ligand implicated in the C–H CMD step of catalysis, but prior reaction profile analysis suggests that the ligand also reduces decomposition of the Pd catalyst.[56] In reported examples of palladium-catalyzed ketone TDG C–H functionalization, AcOH is employed as a significant portion of the solvent medium in order to catalyze the difficult TDG-substrate condensation step. It has been reported that ketone substrates require an exogeneous acid catalyst to form the TDG-imines,[25,26] whereas acid catalysis for aldehyde and amine condensations is generally not needed,[53,57] presumably due to the increased ease with which aldehyde-derived imines form and hydrolyze. This can loom as a significant challenge in reaction design for ketones, since AcOH outcompetes binding to Pd(II) and precludes the effectiveness of exogeneous ligands through competition. Indeed, when 2-pyridones are included in the reaction with even low loadings of AcOH (5% v/v), the reaction efficiency drops as delineated in the supporting information. However, our observation that small quantities of TFA have a modest improving effect on the reaction (**Error! Reference source not found.**) inspired the concept that TFA alone could be the TDG acid catalyst, and the smaller requisite quantities required could enable the use of ligands like 2-pyridone.

Remarkably, we observed an appreciable improvement in reaction efficiency with the application of 2-pyridone ligands and 1.5 equivalents TFA in neat HFIP (**Error! Reference source not found.**). The electronics of the 2-pyridone have a significant impact on the reaction efficiency. Substitution of the 3-position with electron-withdrawing groups shows a modest yield. The yield improves when the 5-position bears an electron-withdrawing group, and an apparent

additive effect is observed with significant yield improvements when the 3- and 5-positions are both electron-deficient to

Table 6.4. Discovering conditions compatible to use of ligand.

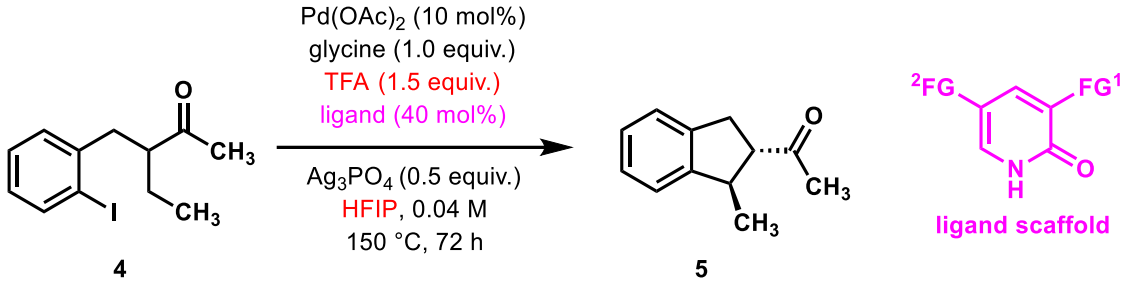

Ligand	FG^1	FG^2	Yield	dr
L1	NO_2	-	44%	9:1
L2	F	-	35%	9:1
L3	CN	-	39%	7:1
L4	-	NO_2	59%	8:1
L5	-	CF_3	45%	7:1
L6	-	Cl	46%	7:1
L7	NO_2	F	68%	9:1
L8	NO_2	Cl	71%	8:1
L9	NO_2	NO_2	71%	9:1
L10	NO_2	CF_3	67%	9:1

Condition[a,b]	Yield
36 h	69%
130 °C	46%
omit pyridone	2%
omit TFA	3%
60% ligand	80%
80% ligand	**83%**
omit $Pd(OAc)_2$[c]	0%
omit glycine[c]	0%
omit Ag_3PO_4[c]	17%

[a]using **L9** [b]all 9:1-8:1 dr
[c]using 80 mol% **L9**

furnish the desired carbocycle in ~70% yield. Looking more closely at these new ligand conditions in **Error! Reference source not found.**, the cyclization process still runs at similar efficiency when the reaction time is shortened to 36 hours; however, elevated temperatures are still required. Under the new ligand conditions, TFA becomes essential to reactivity, because it is now thought to be the lone catalyst for imine formation/hydrolysis. Higher ligand loading of 80 mol% significantly enhances the yield to 83%, possibly due to the dilute conditions employed for

this type of intramolecular cyclization and the dynamic palladium/ligand environment. Control experiments indicate that palladium and glycine are essential for reactivity, while some reactivity (17% yield) is still observed when Ag_3PO_4 is omitted.

Table 6.5. Scope of reaction. Yields based on mass of isolated material after purification; performed on 0.1 mmol scale unless otherwise noted.

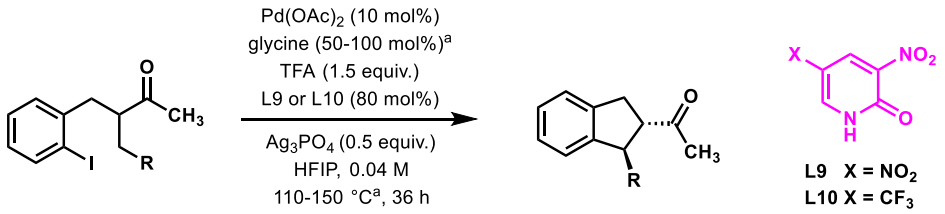

Linear Methylene Arylation Products

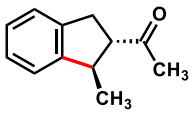

5
86% (L9) 8.5:1 dr

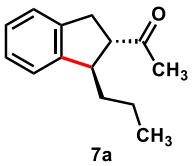

7a
72% (L10) 10.5:1 dr
68% (L9)
86% (L9, 1 mmol scale)

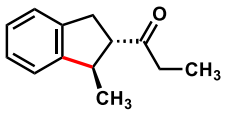

7b
45% (L9) 8.7:1 dr
42% (L10)

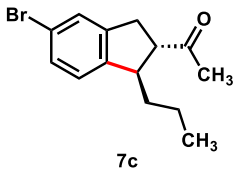

7c
93% (L9) 13:1 dr

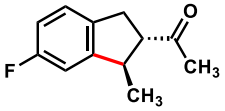

7d
53% (L10) 10:1 dr
45% (L9)

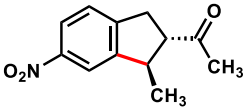

7e
45% (L9) 6.6:1 dr

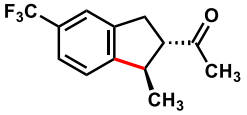

7f
71% (L10) 11:1 dr
67% (L9)

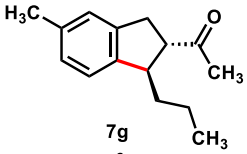

7g
83%[c] (L9)

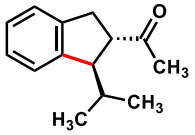

7h
38%[c] (L9)

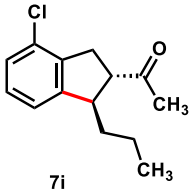

7i
91%[c] (L10)
87% (L9)

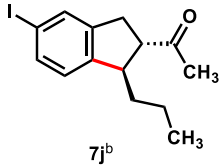

7j[b]
27%[c] (L9)

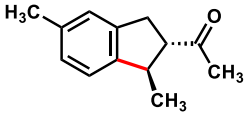

7k
69% (L9) 10:1 dr

Methyl Arylation Products

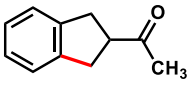

2
71% (L10)
63% (L9)

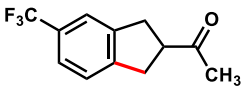

8a
70% (L9)

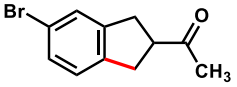

8b
50% (L9)

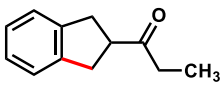

8c
80% (L10)
69% (L9)

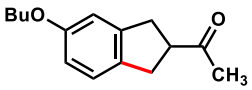

8d
60% (in 3:1 HFIP:AcOH)
(12%) (L9)

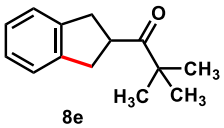

8e
0% (L10)
0% (L9)

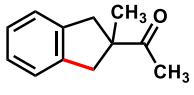

8f
40% (L9)[d]

[a]100 mol% glycine, 150 °C for methylene C-H arylation; 50 mol% glycine, 110 °C for methyl C-H arylation [b]major product
[c]single diastereomer isolated [d]reaction performed at 150 °C with 100 mol% glycine

Gratifyingly, these conditions are generally broad in scope (**Error! Reference source not found.**), and the 2-pyridone ligand effect is still apparent in the 1° C–H bond substrate: the

simple acetylindane **2** is formed in 71% yield when **L10** is used as ligand. Our optimized conditions are shown in **Error! Reference source not found.** along with isolated yields of the products. The reaction yield generally benefits from a longer alkyl group on which the C–H bond is functionalized (**7a**, **7c**, **7g**, **7i**), which we attribute to greater stability of product towards further reactivity with palladium due to increased steric hindrance. Reactivity is diminished by steric repulsion when the alkyl chain of interest is branched vicinal to the position of C–H functionalization (**7h**). Small increases in steric bulk on the distal side of the ketone is allowed, but a concomitant drop in yield is observed (**7b**). The *tert*-butyl ketone substrate **8e** furnishes no product, which is consistent with the theory that the transient directing group is operative on the ketone through condensation. Steric influence vicinal to the directing methyl ketone is apparent in the synthesis of quaternary ketone **8f**. Fluoroindanes are accessible, as well as aryl bromo- and chloroindanes, which could be amenable to subsequent cross-coupling reactions. The yield for these bromo- and chloroindanes can exceed 90% (**7c**, **7i**). There is some reduction in reaction efficiency when the arene is substituted *meta* to the iodide (**7d**, **7e**), though substitution at the *para* and *meta(prime)* positions are tolerated. The reaction furnishes very little product with electron-rich aryl iodides, but when the ligand is switched for AcOH most of the reactivity is recovered (**8d**). The reaction gives a high yield of 83% when scaled to 1 mmol (**7a**).

As a larger goal, we sought to couple directed intermolecular C–H arylation with the intramolecular C–H annulation reaction developed in the first part of this report as part of a new [3+2] ring forming reaction (Reaction (1), **Error! Reference source not found.**). The different outcomes of Reactions (1) and (2) in **Error! Reference source not found.** highlight the salient differences between the reaction pathways of inter- and intramolecular Pd(II) catalyzed C(sp_3)–H arylation. As we slowly developed conditions more conducive to the high energy Pd(II/IV) oxidative addition process required for ring-closure, the intermolecular C(sp_3)–H arylation step became less favorable. As shown in **Error! Reference source not found.**, the one-pot [3+2] C–H arylation reaction between 3-methyl-2-butanone and 1,2-diiodobenzene (**10**)

afforded low yields of the desired acetylindane **2** (Reaction (1)). Several phenomena negatively influence the outcome of this reaction. Under typical palladium-catalyzed C–H functionalization conditions, 1,2-Diiodobenzene (**10**) is unstable and readily undergoes protodeiodination. As a result, significant quantities of iodobenzene in solution react preferentially to form the dead-end phenyl substituted butanone product **3**. 1,2-diiodobenzene (**10**) is also a relatively hindered aryl iodide coupling partner, and so the steric hindrance projected by the *ortho*-iodo functionality slows the first arylation step (**9** to **1**).[58] Compound **1** also undergoes protodeiodination, competing with the final ring-closing event. We postulate that both of these protodeiodination events occur through a Pd(II/IV) pathway.

Scheme 6.3. Understanding reactivity pathways of the [3+2] double C(sp3)–H arylation.

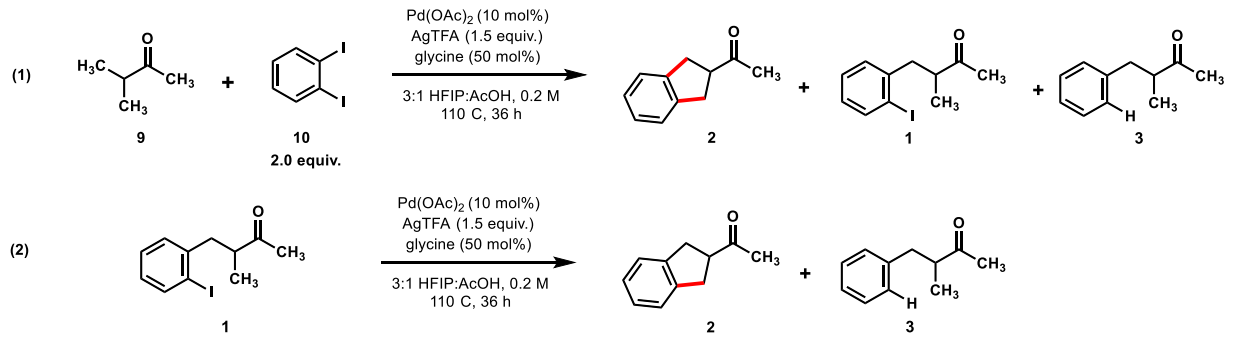

Condition	Reaction (1) Yield 2/3/1	Reaction (2) Yield 2/3
As Shown	5%/7%/14%	18%/13%
Ag_3PO_4 (0.5 equiv.)[a]	trace	43%/6%
Ag_3PO_4 (0.5 equiv.)[a] 1.5 equiv. TFA	5% (yield of 2)	52%/13%
Ag_3PO_4 (0.5 equiv.)[a] 1.5 equiv. TFA[b] in neat HFIP L9 (80 mol%)[b]	trace	70%/10%

[a]replaces AgTFA [b]additive

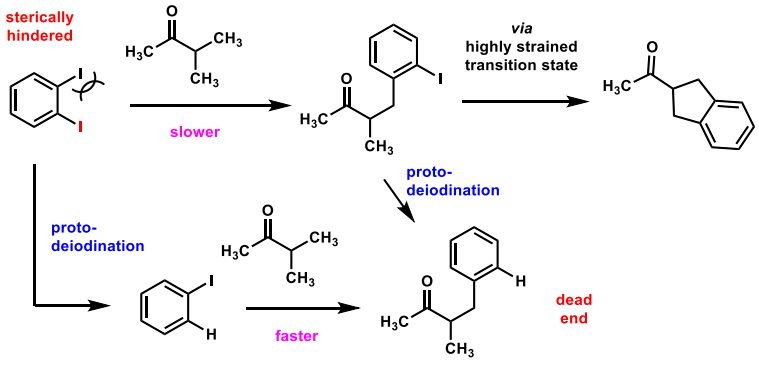

We thus reenvisioned the proposed [3+2] double C(sp3)–H functionalization arylative cyclization. After the intermolecular C(sp3)–H arylation depicted in **Error! Reference source not found.** between 3-iodoanisole (**11**) and ketone **12**, we took advantage of a curious property of substituted phenyl ethers: regardless of steric hindrance, the silver(I) mediated iodination of

the benzene ring occurs exclusively *para* to the ether electron donating group.[59] As such, a telescoped process was devised: after the intermolecular C(sp_3)–H arylation of ketone **12** was complete, addition of I_2 and AgOAc to the room-temperature reaction mixture furnishes the desired aryl iodide intermediate **13**. After isolation, ring closure using conditions developed for electron-rich arenes completed the cyclization sequence in two reaction vessels, furnishing the desired indane **14** in 35% yield. While the aryl ether substrate promotes the requisite arene iodination, electron-rich iodoarenes are less reactive as Pd(II) ↦ Pd(IV) oxidants, and for this reason the yields are somewhat lower.

Scheme 6.4. A two-pot procedure for ring construction by iterative C–H arylation, iodination, arylation. Isolated yields; [a]performed on 0.4 mmol scale; [b]performed on 0.2 mmol scale [c]performed on 0.1 mmol scale. TFA = trifluoroacetic acid; HFIP = hexafluoroisopropanol.

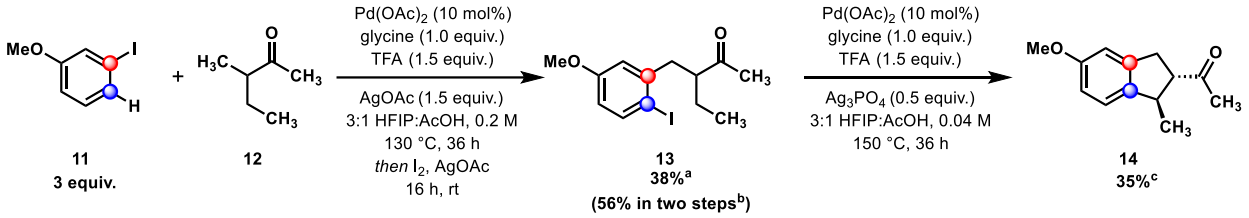

6.4 Conclusion

In conclusion, a C(sp_3)–H arylative cyclization of ketones has been developed featuring a transient directing group strategy and the use of 2-pyridone ligands to enhance reaction efficiencies. The reaction is effective for intramolecular arylations of unactivated methyl and linear methylene C(sp_3)–H bonds and can proceed with high margins of diastereoselectivity. Controlling the Pd(II/IV) pathways between C(sp_3)–H arylation and protodeiodination was essential to the successful reaction development, and this was determined through co-product analysis. Based on calculations, this ring annulation reaction process is proposed to proceed through an unusual trigonal bipyramidal Pd(IV) intermediate, which reorganizes to a favored octahedral geometry upon silver(I)-mediated iodide abstraction and TFA coordination. The ring closure reaction described herein was applied to complete a stepwise [3+2] double C(sp_3)–H

arylation, which takes advantage of intermolecular C(sp_3)–H arylation to strategically relay C–H functionalization events.

6.5 References

[1] Abrams, D. J.; Provencher, P. A.; Sorensen, E. J. *Chem. Soc. Rev.* **2018**, *47* (23), 8925–8967.

[2] Gutekunst, W. R.; Baran, P. S. *Chem. Soc. Rev.* **2011**, *40* (4), 1845–2040.

[3] Yakura, T.; Nambu, H. *Tetrahedron Lett.* **2018**, *59* (3), 188–202.

[4] Brady, P. B.; Bhat, V. *European J. Org. Chem.* **2017**, *2017* (35), 5179–5190.

[5] McMurray, L.; O'Hara, F.; Gaunt, M. J. *Chem. Soc. Rev.* **2011**, *40* (4), 1885.

[6] Yamaguchi, J.; Yamaguchi, A. D.; Itami, K. *Angew. Chem. Int. Ed.* **2012**, *51* (36), 8960–9009.

[7] Bedell, T. A.; Hone, G. A. B.; Valette, D.; Yu, J. Q.; Davies, H. M. L.; Sorensen, E. J. *Angew. Chem. Int. Ed.* **2016**, *55* (29), 8270–8274.

[8] Siler, D. A.; Mighion, J. D.; Sorensen, E. J. *Angew. Chem. Int. Ed.* **2014**, *53* (21), 5332–5335.

[9] Zhu, R. Y.; Liu, L. Y.; Yu, J. Q. *J. Am. Chem. Soc.* **2017**, *139* (36), 12394–12397.

[10] He, J.; Wasa, M.; Chan, K. S. L.; Shao, Q.; Yu, J. Q. *Chem. Rev.* **2017**, *117* (13), 8754–8786.

[11] Chen, X.-Y.; Ozturk, S.; Sorensen, E. J. *Org. Lett.* **2017**, *19* (5), 1140–1143.

[12] Ting, C. P.; Maimone, T. J. *Angew. Chem. Int. Ed.* **2014**, *53* (12), 3115–3119.

[13] Engle, K. M.; Mei, T.-S.; Wasa, M.; Yu, J.-Q. *Acc. Chem. Res.* **2012**, *45* (6), 788–802.

[14] Park, H.; Verma, P.; Hong, K.; Yu, J. *Nat. Chem.* **2018**, *10* (7), 755–762.

[15] Zhu, R. Y.; Li, Z. Q.; Park, H. S.; Senanayake, C. H.; Yu, J. Q. *J. Am. Chem. Soc.* **2018**, *140* (10), 3564–3568.

[16] Zhuang, Z.; Yu, J.-Q. *Nature* **2020**, *577* (7792), 656–659.

[17] Engle, K. M.; Yu, J. *J. Org. Chem.* **2013**, *78* (18), 8927–8955.

[18] Li, B.; Li, X.; Han, B.; Chen, Z.; Zhang, X.; He, G.; Chen, G. *J. Am. Chem. Soc.* **2019**, *141* (23), 9401–9407.

[19] Zhang, X.; Lu, G.; Sun, M.; Mahankali, M.; Ma, Y.; Zhang, M.; Hua, W.; Hu, Y.; Wang, Q.; Chen, J.; He, G.; Qi, X.; Shen, W.; Liu, P.; Chen, G. *Nat. Chem.* **2018**, *10* (5), 540–548.

[20] Zhu, R. Y.; Liu, L. Y.; Park, H. S.; Hong, K.; Wu, Y.; Senanayake, C. H.; Yu, J. Q. *J. Am. Chem. Soc.* **2017**, *139* (45), 16080–16083.

[21] Gandeepan, P.; Ackermann, L. *Chem* **2018**, *4* (2), 199–222.

[22] Chen, X. Y.; Sorensen, E. J. *Chem. Sci.* **2018**, *9* (48), 8951–8956.

[23] Chen, X. Y.; Sorensen, E. J. *J. Am. Chem. Soc.* **2018**, *140* (8), 2789–2792.

[24] Navarro, R.; García, J.; Urriolabeitia, E. P.; Cativiela, C.; Diaz-de-Villegas, M. D. *J. Organomet. Chem.* **1995**, *490* (1–2), 35–43.

[25] Zhang, F. L. F.-L. F. L.; Hong, K.; Li, T.-J. T. J.; Park, H.; Yu, J. Q. J.-Q. *Science* **2016**, *351* (6270), 252–256.

[26] Hong, K.; Park, H.; Yu, J.-Q. *ACS Catal.* **2017**, 6938–6941.

[27] Wang, J.; Dong, C.; Wu, L.; Xu, M.; Lin, J.; Wei, K. *Adv. Synth. Catal.* **2018**, *360* (19), 3709–3715.

[28] Yang, K.; Li, Q.; Liu, Y.; Li, G.; Ge, H. *J. Am. Chem. Soc.* **2016**, *138* (39), 12775–12778.

[29] St John-Campbell, S.; White, A. J. P.; Bull, J. A. *Chem. Sci.* **2017**, *8* (7), 4840–4847.

[30] Ma, F.; Lei, M.; Hu, L. *Org. Lett.* **2016**, *18* (11), 2708–2711.

[31] Feng, Y.; Wang, Y.; Landgraf, B.; Liu, S.; Chen, G. *Org. Lett.* **2010**, *12* (15), 3414–3417.

[32] Reddy, M. D.; Watkins, E. B. *J. Org. Chem.* **2015**, *80* (22), 11447–11459.

[33] Wu, W.; Yi, J.; Xu, H.; Li, S.; Yuan, R. *Molecules* **2019**, *24*, 1234.

[34] Sehnal, P.; Taylor, R. J. K.; Fairlamb, I. J. S. *Chem. Rev.* **2010**, *110* (2), 824–889.

[35] Maleckis, A.; Sanford, M. S. *Organometallics* **2011**, *30* (24), 6617–6627.

[36] Pohorilets, I.; Tracey, M. P.; LeClaire, M. J.; Moore, E. M.; Lu, G.; Liu, P.; Koide, K. *ACS Catal.* **2019**, *9* (12), 11720–11733.

[37] Dânoun, K.; Essamlali, Y.; Amadine, O.; Tabit, R.; Fihri, A.; Len, C.; Zahouily, M. *Appl. Organomet. Chem.* **2018**, *32* (4), e4232.

[38] Adrio, L. A.; Nguyen, B. N.; Guilera, G.; Livingston, A. G.; Hii, K. K. (Mimi). *Catal. Sci. Technol.* **2012**, *2* (2), 316–323.

[39] Dyker, G. *Angew. Chemie Int. Ed. English* **1992**, *31* (8), 1023–1025.

[40] Dyker, G. *Angew. Chemie Int. Ed. English* **1994**, *33* (1), 103–105.

[41] Campeau, L.-C.; Parisien, M.; Leblanc, M.; Fagnou, K. *J. Am. Chem. Soc.* **2004**, *126* (30), 9186–9187.

[42] Saget, T.; Lemouzy, S. J.; Cramer, N. *Angew. Chem. Int. Ed.* **2012**, *51* (9), 2238–2242.

[43] Holstein, P. M.; Vogler, M.; Larini, P.; Pilet, G.; Clot, E.; Baudoin, O. *ACS Catal.* **2015**, *5* (7), 4300–4308.

[44] Sofack-Kreutzer, J.; Martin, N.; Renaudat, A.; Jazzar, R.; Baudoin, O. *Angew. Chem. Int. Ed.* **2012**, *51* (41), 10399–10402.

[45] Kefalidis, C. E.; Davi, M.; Holstein, P. M.; Clot, E.; Baudoin, O. *J. Org. Chem.* **2014**, *79* (24), 11903–11910.

[46] Hitce, J.; Baudoin, O. *Adv. Synth. Catal.* **2007**, *349* (11–12), 2054–2060.

[47] Janody, S.; Jazzar, R.; Comte, A.; Holstein, P. M.; Vors, J.-P.; Ford, M. J.; Baudoin, O. *Chem. - A Eur. J.* **2014**, *20* (35), 11084–11090.

[48] Wang, P.; Verma, P.; Xia, G.; Shi, J.; Qiao, J. X.; Tao, S.; Cheng, P. T. W.; Poss, M. A.; Farmer, M. E.; Yeung, K. S.; Yu, J. Q. *Nature* **2017**, *551* (7681), 489–493.

[49] Chen, X.; Wu, Y.; Zhou, J.; Wang, P.; Yu, J. *Org. Lett.* **2019**, *21* (5), 1426–1429.

[50] Wang, P.; Farmer, M. E.; Huo, X.; Jain, P.; Shen, P.; Ishoey, M.; Bradner, J. E.; Wisniewski, S. R.; Eastgate, M. D.; Yu, J. *J. Am. Chem. Soc.* **2016**, *138* (29), 9269–9276.

[51] Zhu, R.-Y.; Li, Z.; Park, H. S.; Senanayake, C. H.; Yu, J. *J. Am. Chem. Soc.* **2018**, *140* (10), 3564–3568.

[52] Farmer, M. E.; Wang, P.; Shi, H.; Yu, J. *ACS Catal.* **2018**, *8* (8), 7362–7367.

[53] Chen, Y.; Wang, Z.; Wu, Y.; Wisniewski, S. R.; Qiao, J. X.; Ewing, W. R.; Eastgate, M. D.; Yu, J. *J. Am. Chem. Soc.* **2018**, *140* (51), 17884–17894.

[54] Liu, L.; Yeung, K.; Yu, J. *Chem. - A Eur. J.* **2019**, *25* (9), 2199–2202.

[55] Engle, K. M.; Wang, D.-H.; Yu, J.-Q. *J. Am. Chem. Soc.* **2010**, *132* (40), 14137–14151.

[56] Wang, P.; Verma, P.; Xia, G.; Shi, J.; Qiao, J. X.; Tao, S.; Cheng, P. T. W.; Poss, M. A.; Farmer, M. E.; Yeung, K.; Yu, J. *Nature* **2017**, *551* (7681), 489–493.

[57] Liu, X.; Park, H.; Hu, J.-H.; Hu, Y.; Zhang, Q.-L.; Wang, B.; Sun, B.; Yeung, K.; Zhang, F.; Yu, J. *J. Am. Chem. Soc.* **2017**, *139* (2), 888–896.

[58] Mu, D.; Gao, F.; Chen, G.; He, G. *ACS Catal.* **2017**, *7* (3), 1880–1885.

[59] Carson, J. R.; Almond, H. R.; Brannan, M. D.; Carmosin, R. J.; Flaim, S. F.; Gill, A.; Gleason, M. M.; Keely, S. L.; Ludovici, D. W.; Pitis, P. M.; Rebarchak, M. C.; Villani, F. J. *J. Med. Chem.* **1988**, *31* (3), 630–636.

Chapter 7. Computational Exploration of a Pd(II)-Catalyzed γ-C–H Arylation where Stereoselectivity Arises from Attractive Aryl–Aryl Interactions

7.1 Abstract

The enantioselective Pd(II)-catalyzed γ-C–H arylation of picolinamides with a chiral BINOL phosphate ligand was explored using density functional theory (DFT). Enantioselectivity arises from attractive aryl–aryl interactions between the pseudo-equatorial phenyl substituent of the substrate and the chiral BINOL phosphate ligand.

7.2 Introduction

Transition-metal catalysis is a powerful tool for aliphatic C–H functionalization.[1] While a number of enantioselective Pd(II)-catalyzed C–H desymmetrization processes have been reported by the Jin-Quan Yu group, there are few chiral ligands for asymmetric oxidative C–H functionalization with Pd(II) catalysts.[2] Chiral phosphines are incompatible with the reaction conditions needed for oxidative Pd(II)-catalyzed C–H functionalization.[3] Scheme 7.1 shows three examples of new classes of anionic chiral ligands that have been developed for Pd(II) catalysts that enantioselective C–H bond activations.

Yu *et al.* described a highly selective enantiotopic methylene C–H arylation in thioamide derivatives (Scheme 7.1a).[4] Gaunt *et al.* used a BINOL-phosphoric acid derivative to enable Pd-catalyzed enantioselective C–H amination of aliphatic amines to form aziridines (Scheme 7.1b). However, the role of the ligand has yet to be explained in either case.[5] Duan *et al.* used a BINOL-derived phosphoric acid and amide as ligands for aminoquinoline-directed benzylic β-C–H arylation of 3-arylpropanamides (Scheme 7.1c).[6]

Scheme 7.2 depicts a highly enantioselective picolinamide auxiliary-directed benzylic C–H arylation of 3-arylpropylamines that Gang He and Gong Chen *et al.* have reported recently.[7] This reaction requires (*R*)-BINOL phosphoric acid, Cs_2CO_3, and solvent-free conditions to produce the (*S*)-enantiomer of the product with up to 97% *e.e*. It has been known that Cs_2CO_3 is

Scheme 7.1. Examples of Enantioselective Pd(II)-catalyzed C–H Activation Using Phosphine Ligands

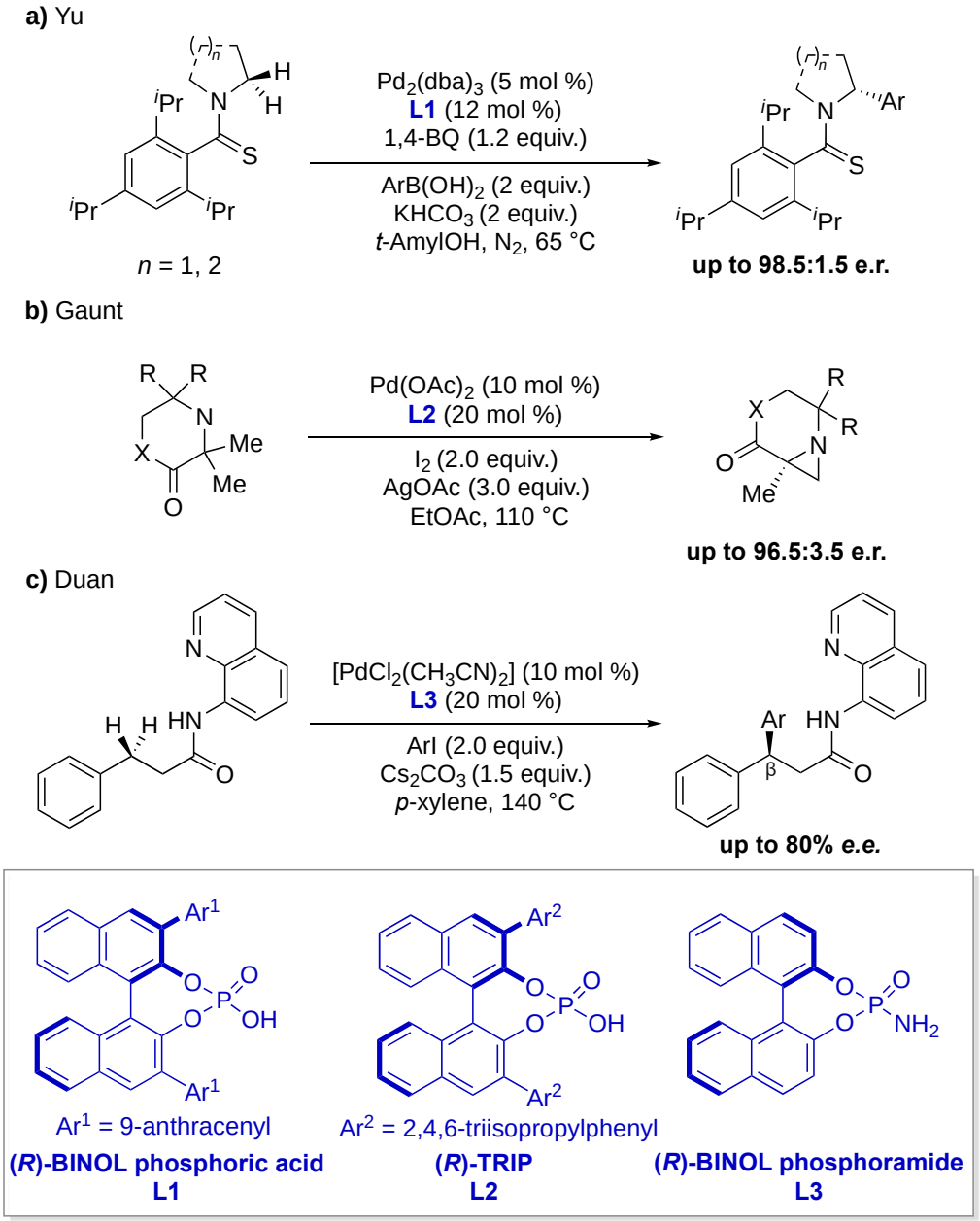

a highly soluble salt, which is essential since such reaction conditions are neat. We have investigated the role of the chiral ligand in controlling stereoselectivity. The experimentalists found the C–H activation step to be the rate- and stereoselectivity-determining step of the C–H aryl- ation. Two different transition state models, A and B, were proposed as possible key

concerted metallation deprotonation (CMD) C–H activation steps, involving either one **L** ligand or two **L** ligands bound by Cs^+ (Scheme 7.3). Based on observations of a non-linear correlation between *e.e.* of **L** and *e.e.* of the product, it was proposed that multiple BINOL phosphate ligands might participate in the transition state.[7]

Scheme 7.2. The He and Chen Enantioselective Pd-catalyzed Chiral Phosphate-mediated benzylic C–H Arylation Directed by a Picolinamide Auxiliary Group

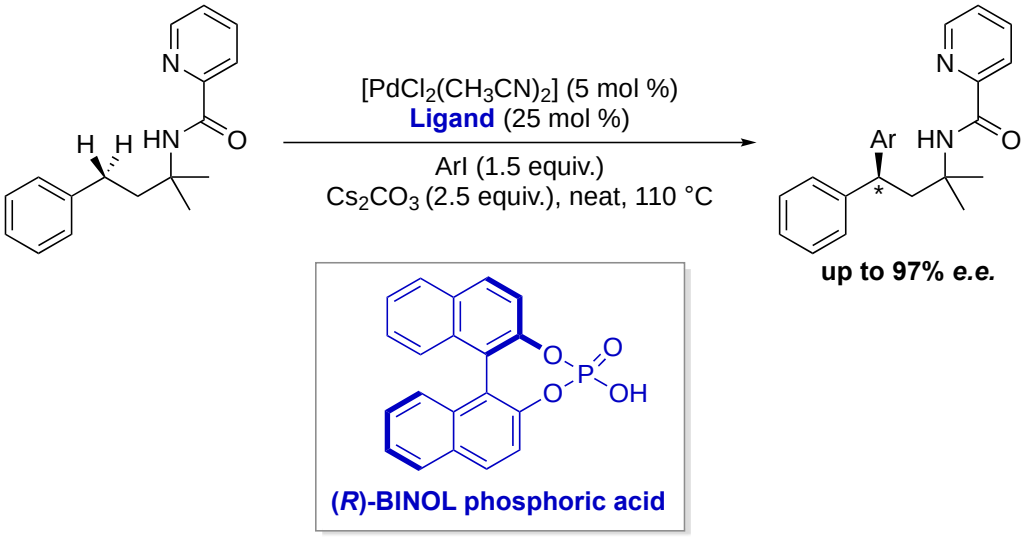

Scheme 7.3. Proposed Transition State Models for the Enantioselective C–H Palladation

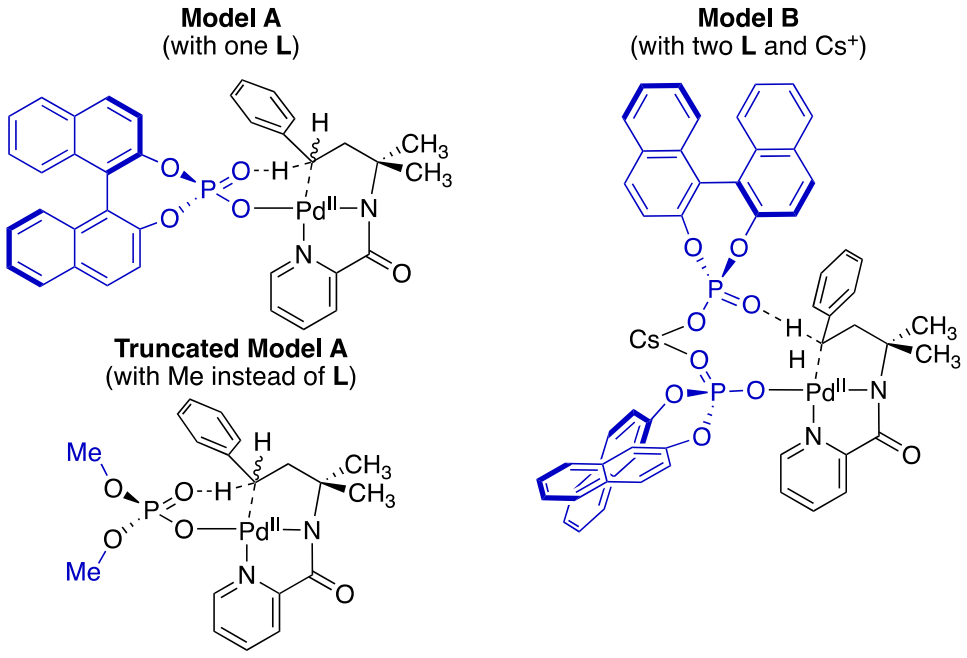

7.3 Results and Discussion

We used computations to differentiate between the two models and to elucidate the origins of enantioselectivity. In the two models developed, the role of the BINOL phosphate ligand differs at the transition state. In Model A, one phosphate ligand is responsible for both the metal coordination and hydrogen abstraction. However, in Model B one phosphate ligand coordinates as an anion to Pd, while the other phosphate ligand acts as an internal base for the hydrogen abstraction during the CMD step; here the phosphates are ion-paired to Cs^+. We also studied a truncated Model A without BINOL to establish the favored geometry of the transition state.

Quantum mechanical calculations were performed with Gaussian 09.[8] For Model A, geometries were optimized in the gas phase using the B3LYP[9] functional with the 6-31G(d)[10] basis set for all non-metal atoms and the LANL2DZ +f (1.472)[11] basis set with effective core potential (ECP) for Pd. Single point corrections were calculated using Truhlar's M06[12] functional with the 6-311++G(d,p)[13] basis set for all non-metal atoms and the SDD[14] effective core potential for Pd.

For Model B, ground state and transition state geometries were calculated using ONIOM(B3LYP[9]/6-31G(d)[10]-LANL2DZ[11]:UFF[15]) which enables optimizations of organometallic compounds with bulky ligands.[16] The BINOL ligands were calculated at the MM level while all the other atoms were calculated at the QM level. SCF (electronic) energies were obtained by single-point calculations using M06[13] functional with the 6-311++G(d,p) basis set for all non-metal atoms and the SDD[14] effective core potential for Pd. Vibrational frequencies were computed at the QM:MM level to determine if the optimized structures are minima or saddle points on the potential energy surface corresponding to minima and transition state geometries, respectively. The reported free energies include zero-point energies and thermal corrections calculated at 298.15 K and 1 atm. Molecular structures are illustrated with CYLview.[17]

We studied the proposed catalytic cycle shown in Scheme 7.4. The computed barriers for each major step can be found in Supporting Information. The cycle starts with an activated Pd catalyst **A** as a bisligated species binding to the picolinamide substrate via N–H bond cleavage to form **B**. The γ-carbon of the substrate coordinates to Pd to form reactant complex **C**. Then, C–H activation occurs via CMD to form **D**. The neutral chiral phosphate ligand exchanges with MeCN to form **E**. Oxidative addition of iodotoluene occurs to form the Pd(IV) complex **F**, followed by reductive elimination **G** to form the arylated product. Computationally, it was found that the C– H activation step is the rate- and stereodetermining step, in accordance with experimental observations.

Scheme 7.4. Proposed catalytic cycle for Pd-catalyzed C–H arylation of picolinamides

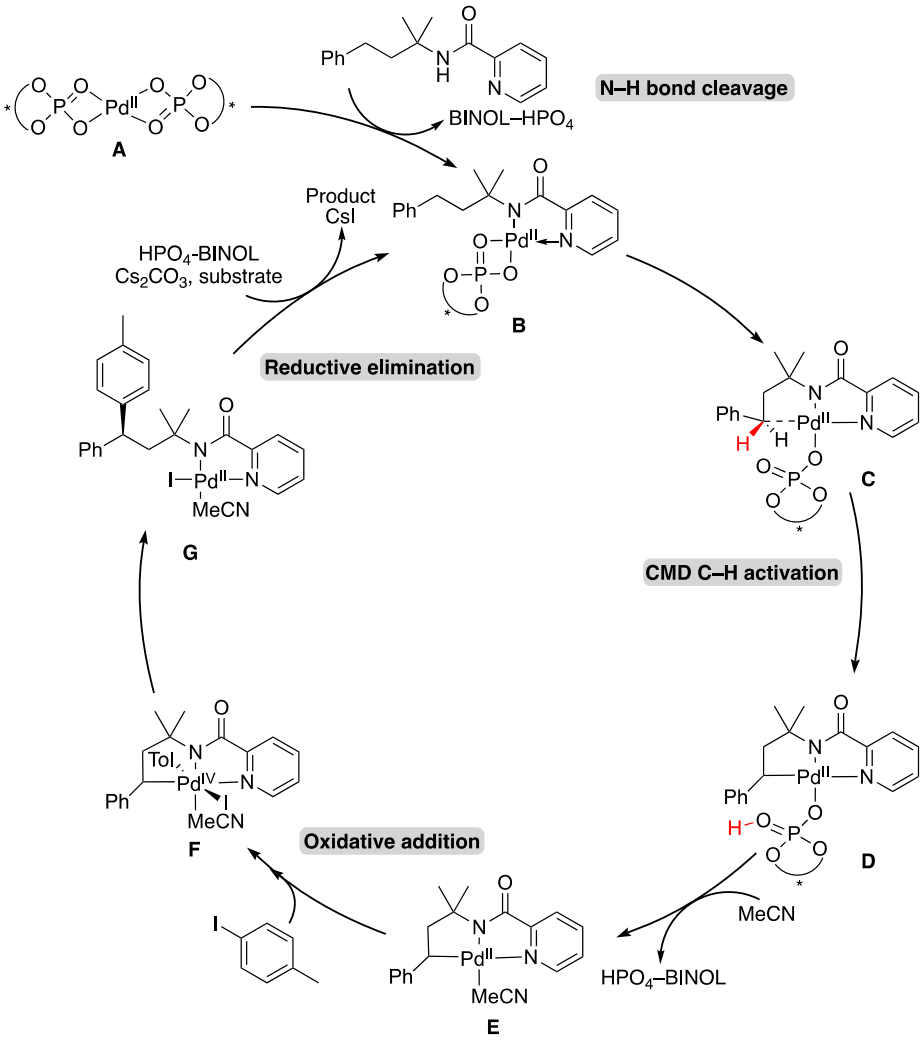

We first studied a simple model system, truncated Model A, in which the BINOL phosphate ligand in Model A is truncated to methyl substituents. The transition states for CMD are shown in Figure 7.1. The preferred conformation of the dimethyl phosphate is chiral, but the small methyl groups have minimal effect, so the (*S*) and (*R*) pseudo-equatorial TSs have slightly different energies. In **OMe TS(*S*)-2a** and **OMe TS(*R*)-4a**, there is a 1,3-diaxial interaction between the phenyl group and the closest methyl group, as seen in the Newman projection along the C_1–C_2 bond. This steric clash causes **OMe TS(*S*)-2a** to be 1.4 kcal mol^{-1} and **OMe TS(*R*)-4a** to be 1.5 kcal mol^{-1} higher in energy than **OMe TS(*S*)-1a**. The TS structure is lower in energy when the phenyl substituent is in the pseudo-equatorial position. We then used this information to build Model A with one chiral BINOL phosphate ligand and a phenyl substituent at

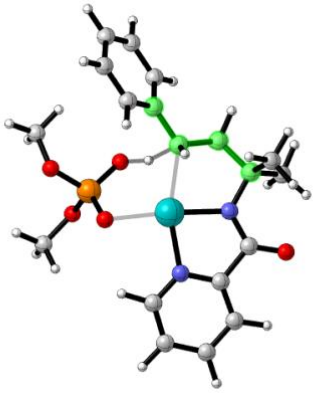

OMe TS(*S*)-1a: $\Delta\Delta G^{\ddagger} = 0.0$

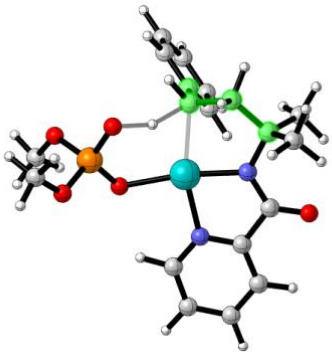

OMe TS(*S*)-2a: $\Delta\Delta G^{\ddagger} = 1.4$

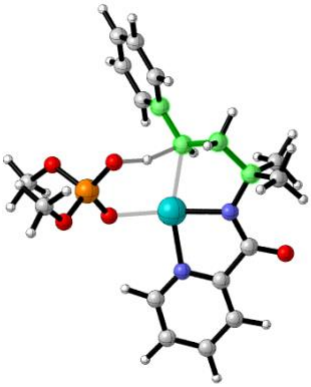

OMe TS(*R*)-3a: $\Delta\Delta G^{\ddagger} = 0.1$

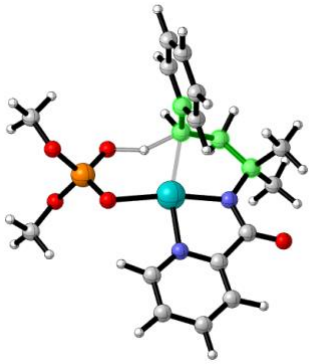

OMe TS(*R*)-4a: $\Delta\Delta G^{\ddagger} = 1.5$

Figure 7.1. Conformers of CMD transition states of truncated Model A where BINOL is replaced with methyl groups. Free energies are in units of kcal mol^{-1}.

the pseudo-equatorial position.

Figure 7.2 shows the two lowest energy TS structures of Model A with one chiral phosphate BINOL ligand, **TS(*S*)-1a** and **TS(*R*)-2a**. The BINOL phosphate ligand, shown in blue in Figure 7.2 defines a plane, C_a–C_b–P. In **TS(*S*)-1a**, C_a–C_b–P is approximately coplanar with the square-planar Pd complex. However, in **TS(*R*)-2a** the C_a–C_b–P plane is rotated 90° about the C_2 axis and is perpendicular to the square-planar Pd complex. The binding mode of the BINOL phosphate ligand to Pd produces interactions that affect the enantioselectivity of the reaction.

The five-membered palladacycle, highlighted in blue on the right structure in Figure 7.2 puckers either above or below the palladacycle to form two different envelope conformations. Notably, both structures avoid steric clashes between the phenyl ring and methyl substituent by

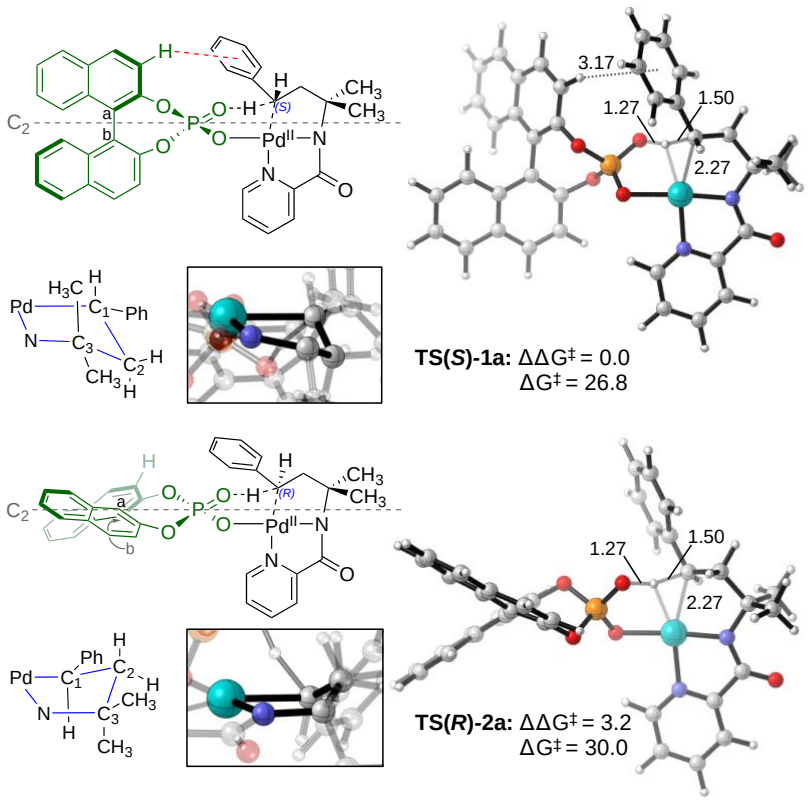

Figure 7.2. Optimized geometries of lowest energy transition states TS(*S*)-1a and TS(*R*)-2a for Model A involving one BINOL phosphate ligand.

having the phenyl ring in the pseudo-equatorial position. **TS(*R*)-2a** is 3.2 kcal mol^{-1} higher in energy than **TS(*S*)-1a**.

We surmise this energy difference is due to T-shaped interaction between the phenyl ring and the naphthyl substituent of the (*R*)-BINOL phosphate ligand. Experimentally, Chen *et al.* obtained 97% *e.e.* ($\Delta\Delta G^{\ddagger}$ = 2.8 kcal mol^{-1} at 110 ºC) in favor of the (*S*)-enantiomer from this reaction, which is in reasonable agreement with our computed results of $\Delta\Delta G^{\ddagger}$ = 3.2 kcal mol^{-1}. According to previous calculations, a C–H–π distance of 3.17 Å provides about 2.5 kcal mol^{-1} of stabilization in a benzene dimer.[18] **TS(*R*)-2a** does not have such C–H–π interactions because the ligand is bound perpendicular to the square- planar Pd complex. We analyzed the edge-to-face aryl–aryl interaction by measuring the distance from the center of one benzene ring to the center of the second benzene ring (Figure 7.3). This distance of 5.47 Å gives 2 kcal mol^{-1} stabilization for calculations on benzene dimers.[19] Both the C–H–π and edge-to-face aryl–aryl interaction is absent in the **TS(*R*)-2a**, the binding mode of the phosphate ligand is essential to the enantioselectivity.

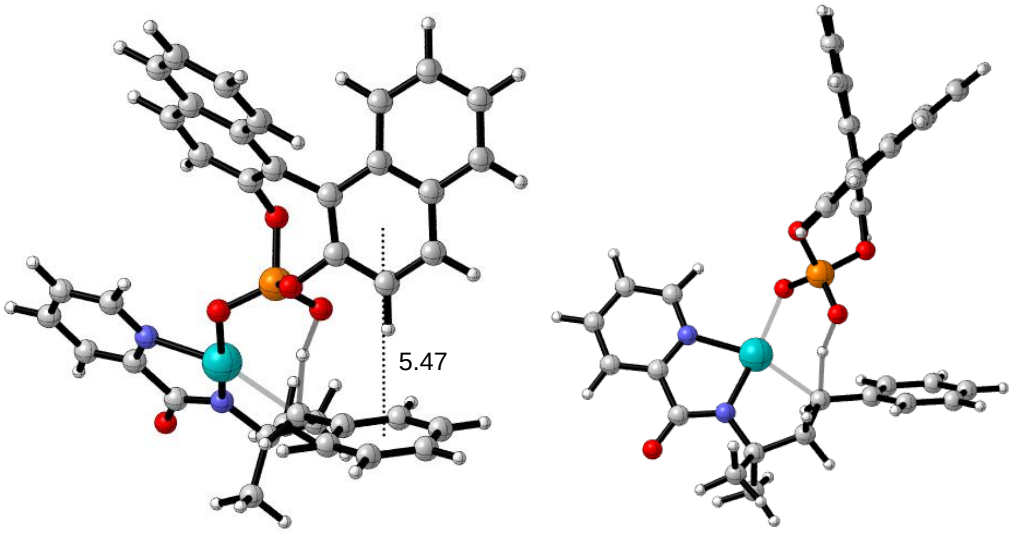

TS(*S*)-1a: $\Delta\Delta G^{\ddagger}$ = 0.0 **TS(*R*)-2a:** $\Delta\Delta G^{\ddagger}$ = 3.2

Enantioselectivity due to attractive aryl–aryl interaction

Figure 7.3 Edge-to-face aryl–aryl interaction in TS(*S*)-1a.

Model B consists of two phosphate ligands bound by Cs^+. Details of the conformational analysis for the Cs-complex and the chiral catalyst are present in the Supporting Information. Figure 7.4 shows the lowest energy TS structures from Model B. Unlike Model A, **TS(*R*)-b** is only 0.8 kcal mol^{-1} higher in energy than **TS(*S*)-b**; Model B does not reproduce the experimentally observed level of selectivities of 97% *e.e*. In both **TS(*S*)-b** and **TS(*R*)-b**, the C_a–C_b–P plane of the ligand that participates in the H-abstraction is in the same plane of the ligand coordinated to Pd is rotated such that it is perpendicular to the square-planar Pd-complex. The orientation square-planar Pd-complex; the C_a–C_b–P plane of the of both BINOL ligands around the phenyl ring increases the possibility for arene–arene interactions. All other ligand binding mode combinations that were explored with less arene–arene interaction gave higher energy transition states. This arises because the lowest-energy complexes both exhibit 5-membered palladacycles that minimize the possibility for steric clashes, since the phenyl substituent is in the pseudo-equatorial position. In both **TS(*S*)-b** and **TS(*R*)-b**, the phenyl ring is positioned between both BINOL ligands, allowing for π–π interactions to occur between the phenyl ring and the aromatic portions of the ligands. TS structures that did not exhibit such arene–arene interactions with the ligands were at least 3.0 kcal mol^{-1} higher in energy. The addition of another BINOL phosphate ligand in Model B allows for more stabilizing arene–arene interactions, which reduces the enantioselectivity.

In our mechanism, Cs^+ does not affect the CMD rate-determining TS, but the non-linear correlation between *e.e.* of **L** and *e.e.* of the product may arise from a BINOL phosphate ligand dimeric species bound by Cs^+ that is present off-cycle. This complex dissociates to form a monoligated species, serving as the activated catalyst **A**, as shown in our proposed mechanism. Since the reaction is run neat, Cs^+ may have additional non-catalytic roles.

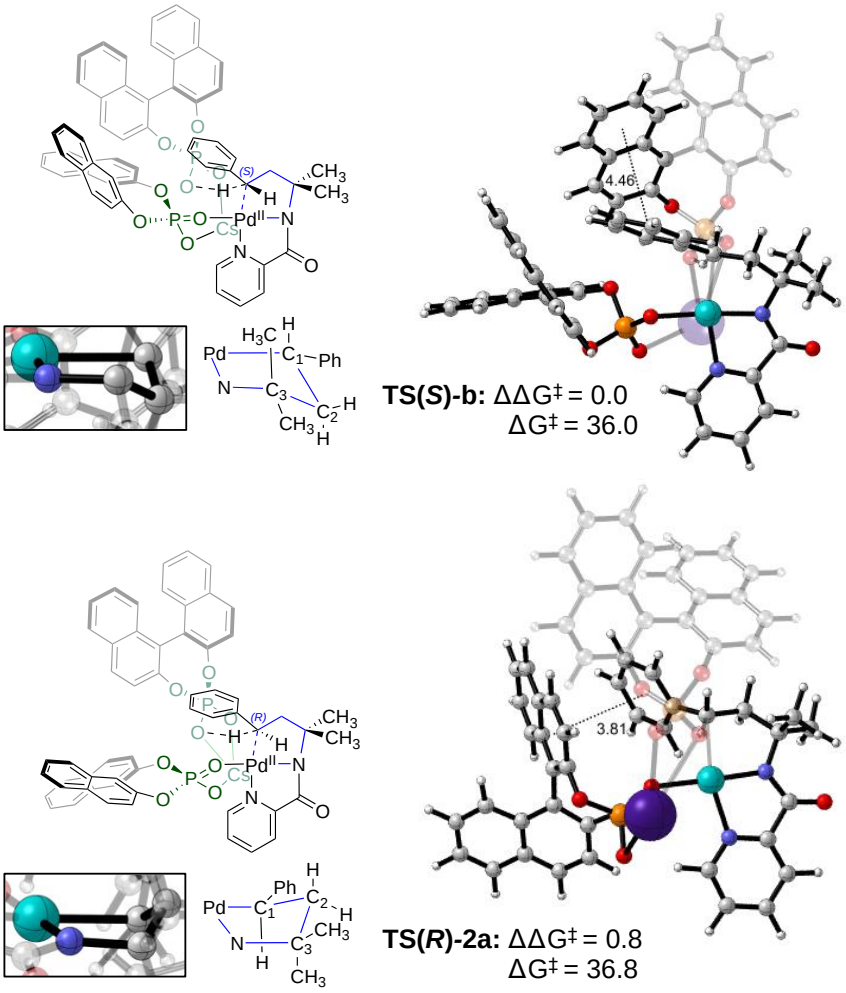

Figure 7.4. Optimized geometries of lowest energy transition states TS(*S*)-b and TS(*R*)-b for Model B involving two BINOL phosphate ligands.

7.4 Conclusions

We have elucidated the origins of the enantioselective palladium-catalyzed benzylic C–H arylation reaction of picolinamide-derivatized alkyl amines with aryl iodide.[8] The transition state involves a pseudo-equatorial position of the phenyl substituent on the 5-membered palladacycle. When the ligand is positioned to abstract the H leading to the (*S*) product, there are stabilizing arene–arene interactions. The computed activation free energies ($\Delta\Delta G_{‡}$) are consistent with experimental *e.e.*'s. Model A, proposed by Chen *et al.*, with one phosphate ligand, predicts the correct enantioselectivity, while Model B, with two phosphate ligands bound

by Cs^+, predicts enantioselectivity that is much smaller than found experimentally. We anticipate that chiral catalysts with stabilizing arene–arene interactions can tune the enantioselectivity of C–H activation processes.

7.5 References

[1] Yu, J.-Q.; Giri, R.; Chen, X. *Org. Biomol. Chem.* **2006**, *4*, 4041.

[2] Engle, K. M., Yu, J.-Q. *J. Org. Chem.* **2013**, *78*, 8927–8955.

[3] a) Anas, S.; Cordi, A.; Kagan, H. B. *Chem. Commun.* **2011**, *47*, 11483; b) Martin, N.; Pierre, C.; Davi, M.; Jazzar, R.; Baudoin, *O. Chem. - Eur. J.* **2012**, *18*, 4480; c) Saget, T.; Lemouzy, S.; Cramer, N. *Angew. Chem., Int. Ed*. **2012**, *51*, 2238; d) Yang, L.; Lucotti, A.; Tommasini, M.; Chalifoux, W. A. *J. Am. Chem. Soc*. **2016**, *138*, 9137; e) Saget, T.; Cramer, N. *Angew. Chem., Int. Ed.* **2012**, *51*, 12842; f) Pedroni, J.; Donets, P. A.; Cramer, N. *Chem. Sci*. **2015**, *6*, 5164; g) Nakanishi, M.; Katayev, D.; Besnard, C.; Kundig, E. P. *Angew. Chem., Int. Ed*. **2011**, *50*, 7438.

[4] Jain, P.; Verma, P.; Xia, G.; Yu, J.-Q. *Nat. Chem*. **2016**, *353*, 1023.

[5] Smalley, A. P.; Cuthbertson, J. D.; Gaunt, M. J. *J. Am. Chem. Soc.* **2017**, *139*, 1412.

[6] Yan, S.-B.; Zhang, S.; Duan, W.-L. *Org. Lett*. **2015**, *17*, 2458.

[7] Wang, H.; Tong, H.-R.; He, G.; Chen, G. *Angew. Chem., Int. Ed*. **2016**, *55*, 15387−15387.

[8] Frisch, M. J.; Trucks, G. W.; Schlegel, H. B.; Scuseria, G. E.; Robb, M. A.; Cheeseman, J. R.; Scalmani, G.; Barone, V.; Mennucci, B.; Petersson, G. A.; Nakatsuji, H.; Caricato, M.; Li, X.; Hratchian, H. P.; Izmaylov, A. F.; Bloino, J.; Zheng, G.; Sonnenberg, J. L.; Hada, M.; Ehara, M.; Toyota, K.; Fukuda, R.; Hasegawa, J.; Ishida, M.; Nakajima, T.; Honda, Y.; Kitao, O.; Nakai, H.; Vreven, T.; Montgomery, J. A.; Peralta, J. E.; Ogliaro, F.; Bearpark, M.; Heyd, J. J.; Brothers, E.; Kudin, K. N.; Staroverov, V. N.; Kobayashi, R.; Normand, J.; Raghavachari, K.; Rendell, A.; Burant, J. C.; Iyengar, S. S.; Tomasi, J.; Cossi, M.; Rega, N.; Millam, J. M.; Klene, M.; Knox, J. E.; Cross, J. B.; Bakken, V.; Adamo, C.; Jaramillo, J.; Gomperts, R.; Stratmann, R. E.; Yazyev, O.; Austin, A. J.; Cammi, R.; Pomelli, C.; Ochterski, J. W.; Martin, R. L.; Morokuma, K.;

Zakrzewski, V. G.; Voth, G. A.; Salvador, P.; Dannenberg, J. J.; Dapprich, S.; Daniels, A. D.; Farkas; Foresman, J. B.; Ortiz, J. V.; Cioslowski, J.; Fox, D. J. *Gaussian 09*; Gaussian Inc.: Wallingford, CT, 2009.

[9] (a) A. D. Becke. *J. Chem. Phys.* **1993**, *98*, 5648–5652. (b) C. Lee, W. Yang, R. G. Parr. *Phys. Rev. B.* **1988**, *37*, 785–789. (c) A. D. Becke. *J. Chem. Phys*. **1993**, *98*, 1372–1377. (d) P. J. Stephens, F. J. Devlin, C. F. Chabalowski, M. J. Frisch. *J. Phys. Chem*. **1994**, *98*, 11623–11627.

[10] (a) R. Ditchfield, W. J. Hehre, J. A. Pople. *J. Chem. Phys.* **1971**, *54*, 724–728. (b) W. J. Hehre, R. Ditchfield, J. A. Pople. *J. Chem. Phys.* **1971***, 54*, 2257–2261.

[11] (a) P. J. Hay, W. R. Wadt. *J. Chem. Phys.* **1985**, *82*, 299–310. (b) L. E. Roy, P. J. Hay, R. L. Martin. *J. Chem. Theory Comput.* **2008**, *4*, 1029–1031. (c) A. W. Ehlers, M. Böhme, S. Dapprich, A. Gobbi, A. Höllwarth, V. Jonas, K. F. Köhler, R. Stegmann, A. Veldkamp, G. Frenking. *Chem. Phys. Lett.* **1993**, *208*, 111–114.

[12] Zhao, Y.; Truhlar, D. G. *Theor. Chem. Acc*. **2008**, *120*, 215.

[13] A. V. Marenich, C. J. Cramer, D. G. Truhlar. *J. Phys. Chem. B.* **2009**, *113*, 6378–6396.

[14] (a) M. Dolg, U. Wedig, H. Stoll, H. Preuss. *J. Chem. Phys.* **1987**, *86*, 866–872. (b) D. Andrae, U. Häußermann, M. Dolg, H. Stoll, H. Preu. *Theor. Chem. Acc.* **1990**, *77*, 123–141.

[15] (a) Morokuma, K. *et al. Chem. Rev*. **2015**, *115*, 5678−5796. (b) Dapprich, S., Komáromi, I., Byun, K. S., Morokuma, K. & Frisch, M. J. *J. Mol. Struct. (Theochem)*. **1999**, 462, 1–21. (c) Svensson, M. *et al. J. Phys. Chem.* **1996**, *100*, 19357–19363.

[16] Vreven, T. *et al. J. Chem. Theory and Comput.* **2006**, 2, 815–826.

[17] Legault, C. Y. CYLview, 1.0b; Université de Sherbrooke, 2009 (http://www.cylview.org)

[18] Tsuzuki, S.; Honda, K.; Uchimaru, T.; Mikami, M. *The Journal of Chemical Physics.* **2005**. *122*, 144323.

[19] Wheeler, S. E.; Houk, K. N. *Molecular Physics*, **2009**, *107***,** 749–760.